Sea Grant College Program

MIT-T-85-005 C2

ON THE RATIONAL SELECTION OF STRENGTHENING CRITERIA FOR NAVIGATION IN ICE

P.C. Xirouchakis

MITSG 85-32TN

March 1985

Massachusetts Institute
of Technology
Cambridge, Massachusetts
02139

ON THE RATIONAL SELECTION OF STRENGTHENING CRITERIA FOR NAVIGATION IN ICE

P.C. Xirouchakis

MITSG 85-32TN

March 1985

Sea Grant College Program
Massachusetts Institute of Technology
Cambridge, Massachusetts 02139

Grant No.: NA81AA-D-00069
Project No.: R/T-6

Copies of this report may be ordered from

Sea Grant Information Center
MIT Sea Grant College Program
Room E38-320
Massachusetts Institute of Technology
77 Massachusetts Ave.
Cambridge, MA 02139

price: $7.00

TABLE OF CONTENTS

ABSTRACT

Methods are briefly summarized to predict the maximum ice sheet pressure exerted on the walls of the side shell structure of an Ice-Transiting Vessel. Furthermore simple structural idealizations are employed to define stiffness criteria while numerical procedures are developed to define strengthening criteria for Ice Navigation. Structural models based on the theory of beams on elastic foundation are used to define stiffness criteria. Elastic-Plastic frame buckling criteria are also developed using a generalized Shanley model and a numerical solution procedure. Furthermore, approximate methods for frame buckling are suggested. Stiffness criteria are of importance in interpreting field test data so that the imposed ice forces can be evaluated. The lower bound theorem of limit analysis is used to determine the collapse pressure of the grillage structure. From this information strengthening criteria can be defined by evaluating ice damage records. Recommendations for future work are given.

NOTATION

Symbols which are not given in this list are defined in the text.

A	cross-sectional area	$= BH$
$\bar{A}$	non-dimensional parameter	$= \int_A k_s \, dA/A$
B	width of cross-section	
E	Young's modulus of elasticity	
H	height of cross-section	
I	cross-sectional moment of inertia	$= \frac{1}{12}BH^3$
$\bar{I}$	non-dimensional parameter	$= \int_A k_s \eta^2 dA/I$
K	mid-section (additional) curvature	
K_{el}	curvature corresponding to first yield	$= f_y/(EH/2)$
K_0	mid-section curvature due to imperfection	
L	length of column	
M	mid-section bending moment	
M_{el}	first yield moment	$= fyW_{el}$
M_{pl}	fully plastic moment	$= \frac{3}{2} M_{el}$
P	axial force	
P_c	elastic buckling load of model	$= \frac{\gamma EI}{\xi L^2}$
P_E	column Euler load	$= \frac{\eta^2 EI}{L^2}$
P_{pl}	fully plastic axial force	$= Af_y$
R	radius of arc which beam bends into	
$\bar{S}$	non-dimensional parameter	$= \int_A k_s \eta dA/W_{el}$
W_{el}	elastic section modulus	$= \frac{1}{6}BH^2$
e	non-dimensional parameter	$= \varepsilon_a/\varepsilon_y$
e_R	non-dimensional parameter	$= \varepsilon_R/\varepsilon_y$
f_y	yield stress	
k	non-dimensional parameter	$= \frac{EIK}{M_{el}}$

k_0	non-dimensional parameter	$= \frac{E I K_0}{M_{el}}$
k_s	ratio of current tangent modulus of each fiber to the Young's modulus	
m	non-dimensional parameter	$= M/M_{el}$
p	non-dimensional parameter	$= P/P_{pl}$
p_c	non-dimensional parameter	$= P_c/P_{pl}$
p_{el}	value of p corresponding to first yield	
u	relative axial displacement	
w_o	transverse displacement due to initial imperfection	$= L\theta_0/2$
δ	non-dimensional parameter	$= u/L\varepsilon_y$
ε_a	axial strain of the centroid	
ε_b	axial strain due to bending	
ε_{max}	maximum strain	
ε_R	axial strain of the straight segments of the Shanley model	
ε_x	strain in x (axial) direction	
ε_y	initial yield strain	$= f_y/E$
ζ	non-dimensional parameter	$= \varepsilon_{max}/\varepsilon_y$
θ	additional rotation	
θ_0	initial rotation due to imperfection	
ξ	parameter which determines the extension of the rotational spring in the Shanley model	$= 4/\pi^2$
σ_a	stress due to axial force	
σ_b	stress due to bending moment	
σ_x	stress in x (axial) direction	
η	transverse distance from centroid	
η_{cy}, η_{ty}	distance from centroidal axis to the fibers that have reached the yield stress in compression or tension respectively	
η_y	distance form centroidal axis to the fibers	

that have reached the yield stress (applies in the pure bending case)

$\bar{\eta}$ distance from the centroidal axis to the neutral axis (applies when both bending moment and axial forces are present)

ϕ central angle of the arc that the beam bends into

1. INTRODUCTION

The object of the present report is to present, in a summary form, the work performed on the project: "On the Rational Selection of Strengthening Criteria for Navigation in Ice."

In Section 2 methods to predict the maximum ice pressure in the case of ice compression are briefly described. The possible failure modes of an ice sheet under compression are considered in order to predict the maximum ice pressure exerted on the hull structure. Relevant references to the estimation of the maximum ice pressure due to interactions with other important ice features are given in section 8.1. Furthermore, the present work reports procedures for the calculation of upper bounds to the ice loading due to interactions with vertical and sloping wide stuctures.

In Section 3 methods are described to define the stiffness criteria for the structural design of Ice-Transiting Vessels. The definition of suitable stiffness criteria is useful in the estimation of the working stresses. Furthermore, stiffness criteria are of importance in interpreting field test data so that the imposed ice forces can be evaluated.

In Section 4 methods are described to predict the ultimate strength of transversely loaded rectangular grids subjected to ice loading. At present existing strengthening requirements are derived from evaluating ice damage records on the basis of a clamped-clamped beam model of the side plating betwen two frames. However, the actual structure consists of a grillage of intersecting beams together with the associated plating. Thus strengthening criteria should be defined by evaluating ice damage records on the basis of calculations of the collapse pressure of the grillage structure. All possible collapse mechanisms of the grillage structure should be considered and not merely the clamped-clamped beam mode. This is very important since even the strictest of the existing strengthening requirements are not always on the conservative side as evidenced recently by the extensive hull damage suffered by two Canadian vessels (an Icebreaker and an Ice-Transiting vessel).

Structural Criteria

Methods to obtain structural criteria for ice navigation are given for the basic structural elements of the side structures: plates, stringers, frames and the grillage assembly. Plate criteria were suggested in References (60), (62), (63) and (41). These give very useful practical suggestions for plate damage due to ice loading. So, our research proposal did not plan on any additional work on plate damage. Granted that there are always refinements and extensions that one may want to pursue. Some of the discussion to Reference (41) addresses these questions.

Structural criteria for stringers are presented in section 3.1 and in Reference (82). This is part of the work done following our research proposal. A relatively simple structural model is suggested and maximum bending moments and corresponding stresses are calculated. From these expressions stiffness criteria for stringers are developed. In addition to this work, we did work on the load carrying capacity of the stringers as they form part of the grillage assembly. This is important since the ultimate stength of each stringer is beyond the first yield capacity. This work is reported in section 4 and in References (25) and (26).

Structural criteria for transverse frames are presented in sections 3.1, 3.2 and in Reference (82). First yield criteria are reported in section 3.1 while ultimate criteria are reported in 3.2. For higher strength steels first yield criteria are more appropriate since their ultimate strength is of the elastic type. In section 3.2 the criteria are developed for a rectangular section frame while in Reference (84) we report work on an ideal I section.

The criteria for frames are very important. As reported in Reference (41) structural damage due to ice loading has always been associated with frame buckling or crippling of its web. This work that we did, with regard to frame criteria, we believe is an important contribution. This is so since this frame buckling mode was not extensively considered previously in the published ice damage literature. We are considering the axial compressive loading case since this is the worst loading case on the frame. This gives a conservative estimate of the frame capacity in comparison to the

lateral loading case. This is so since in the latter case tensile stresses are also developed in addition to the compressive stresses in part of the cross-section. This then gives higher capacities.

So, we developed first a numerical model following a Shanley idealization of the elastic-plastic frame column buckling. The experimental evidence reported in Reference (81) show that this deformation mechanism gives a reasonable estimate of the load capacity for the lateral torsional buckling mode. We carried this analysis and we present results for the maximum load that the column can carry. We also obtained results for the post-buckling path. Geometric imperfections are included in this analysis.

In addition to this numerical analysis we did develop an approximate and much simpler method of analysis that gives very close predictions to the numerical model. This we report in section 3.2 under the heading: Approximate Moment-Curvature Relations. We present the comparison of the two methods in Figures 22, 24, 26 and 27, for columns of three different slenderness ratios and some values of the initial imperfection.

The crippling mode of collapse of the web of the frame was previously addressed in References (39) and (67). The theoretical results presented in Reference (67) give good predictions of this mode of collapse for higher web depth to thickness ratios. This comes out of the comparison of these theoretical predictions with relevant experiments reported in Reference (39). For lower web depth to thickness ratios the elastic-plastic column analysis gives reasonable predictions when compared to the experimental results. So as reported in Reference (39) when the web depth to thickness ratio is lower than about $0.4\sqrt{E/f_y}$ (where E is the Young's modulus and f_y the yield stress in compression) then our previously described column analysis is valid.

Structural criteria for the grillage assembly can be obtained using the methods we are reporting in section 4. We adopted to ice loading a limit analysis computer program. We list the program in reference (25) and we handed out a tape copy of this program to the American Bureau of Shipping, sponsor of this work.

More details of the work done on this project are reported in the

following References: (14), (22), (25), (26), (36), (38), (40), (44), (83) and (84). We are also reporting in section 8.2 quite a few references on torsional buckling and tripping.

Summary of Work Done Following our Research Proposal

Task Breakdown

The research work we are reporting is now indexed according to the Research Plan described in our proposal. The work planned according to the six Task breakdown is completed and we intend now to briefly summarize how this was done according to each Task.

Task I Construct Theoretical Model

The theoretical model is constructed to develop stiffness and strengthening criteria and is briefly summarized in sections 3.1 and 4 respectively. In section 3.2 we report the theoretical model for frame stiffness criteria which is discussed under Task II.

I.1 Estimate the Structural Foundation Modulus

The general functional relation is given by eq. (21) of this report. The details of this analysis are presented in Reference (26), equations (20) to (46). The non-dimensional structural foundation modulus is given as a function of four non-dimensional parameters which depend upon the location of the ice load application, the geometry of the longitudinal stringers and the geometry of the transverse framing.

I.2 Calculate the Load Carried by the Transverse Bulkheads

The longitudinal side-skin stringer is idealized as a beam on an elastic foundation (with the foundation modulus provided by the transverse framing stiffness) acted upon a uniformly distributed load per unit length due to ice and concentrated loads at the transverse bulkheads. The details of this work are presented in References (26) and (82), equations (14), (15) and Figure 5.

I.3 Calculate the Bending Stress in the Longitudinal Side-Skin Stringers

Following the same theoretical model we are obtaining the maximum bending moment and the corresponding stress developed in the longitudinal side-skin stringer. The details of this work are presented in References (26) and (82) section: numerical example.

I.4 Calculate the Bending Stress in the Transverse Frames

Following the same theoretical model we are obtaining the maximum bending moment and the corresponding stress developed in the transverse frame. The details of this work are presented in References (26) and (82) section: numerical example.

I.5 Develop a Procedure for Tripping Bracket Design

This work is reported in section 3.2 of this report for a rectangular section, while we report the corresponding work for an ideal I section in Reference (84). The procedure we developed gives expressions for the necessary frame unsupported length so that frame buckling will be prevented. This unsupported length provides a basis for spacing the tripping brackets. Reference (60) gives details on various tripping bracket arrangements. More details on the work we performed on Task I are reported in Reference (25), (36), (38) and (40).

Task II Consider Transverse Frame Possible Collapse Mechanisms

The first yield, elastic-plastic buckling and ultimate plastic collapse mechanisms are considered and reported in sections 3.1, 3.2 and 4 respectively. In section 4 various ultimate plastic transverse frame collapse mechanisms are studied depending on the location and extent of ice pressure loading. The numerical tool to do this is developed and more details can be found in Reference (25).

Task III Exercise Theoretical Model

Particular numerical examples are given throughout our work reported in References (14), (25), (26), (36), (38), (40), (44) and (84). In the present report we present numerical results in Figures

15 to 27 and 30 to 32. In section 9 we give the titles of each figure.

Task IV List Assumptions

The basic assumptions of the theoretical model are discussed in section 3.1 p. 20, section 3.2 p. 21 and section 4.1 p. 64. In section 6 we suggest some recommendations for future work. From the structural viewpoint these mainly include the coupling of the local collapses mechanisms to the grillage collapse mode. Furthermore fracture-tearing criteria must be developed.

Task V Compare with Classification Societies Requirements

The results obtained are compared in some particular cases with the previously established requirements. In this report we present some of these results and comparisons. With regard to the elastic-plastic frame buckling mechanisms we present some of our results and the comparison with previous first yield criteria in Figures 21 and 27. The relevant discussion of these comparisons is presented in section 3.2. With regard to the grillage collapse mechanisms we present in this report some of our results and the comparisons with Reference's (60) three hinge mechanism in Figures 30 to 32. The relevant discussion of these comparisons is presented in section 4.3.

Task VI Review Published, Full-Scale Experimental Data

Figure 33 from Reference (9) presents this review. In Reference (22) we presented an overview of icebreaking impact pressures, while in Reference (14) we considered the non-uniform ice pressure distribution due to the coupling with the structural wall stiffness.

2. PREDICTION OF MAXIMUM ICE PRESSURE

Methods are presented to predict the maximum ice pressure exerted on the walls of the side shell structure. The approach taken is to evaluate the maximum force necessary to fail the ice feature under consideration. A rigid structure is studied such that its deformation does not affect the magnitude of the ice forces developed.

Structures with vertical and sloping sides are considered. Maximum ice pressures predicted for vertical sided structures may be applicable for the structural design of the side shell structure amidships. Correspondingly, predictions derived for sloping structures can be useful for the structural design of the fore and aft part of the ship. The present report is mainly concerned with the prediction of the maximum ice pressure for wide structures. Interactions with uniform ice sheets are only considered.

2.1 ICE TYPES

The prediction of the maximum ice pressure exerted against the walls of the ship structure depends upon the type of ice under consideration. A classification of river and lake ice based on its formation, structure and texture has been presented in Reference (13). This report is mainly concerned with polycrystalline sea ice types.

The basic ice unit is a single crystal of ice. An ideal crystal has oxygen atoms of the water molecules arranged in such a fashion to give rise to hexagonal symmetry about the c-axis. Molecules lie close to a set of parallel planes, which are the basal planes of the crystal. The basal plane is the sole demonstrated glide plane of the lattice. Shear applied parallel to this plane gives a strain rate about two orders of magnitude higher than that resulting from shear normal to the basal plane. There is no significant preference in the glide direction.

The mechanical properties of the polycrystalline ice depend strongly on the anisotropy of the monocrystal. When the c-axes of the constituent crystals are randomly oriented the polycrystalline ice can be considered isotropic. However, when subjected to prolonged deviatoric loading, recrystallization can take place and as a consequence the crystal orientation ceases to be random. Strain softening of the bulk ice results from the development of preferred orientations of the c-axes.

An ice type which is of importance for ocean engineering applications is S2 ice (13). It is characterized by random orientation of the c-axes in horizontal planes (columnar grained) and average grain size of the order of 5mm.

2.2 MECHANICAL PROPERTIES OF SEA ICE

The prediction of the maximum ice pressure exerted against the walls of the ship structure depends upon the mechanical properties of the particular type of ice under consideration. The mechanical properties of ice depend upon the ice temperature, crystal structure, direction of loading, rate of load application, degree of confinement, sample size, and the presence of impurities such as salts and air.

The brine volume of sea ice is a function of the salinity and the temperature of the ice, it is related to its strength. The brine volume ν_b is defined by

$$\nu_b = b_r \frac{\rho_I}{\rho_b} \tag{1}$$

where b_r is the brine content by weight, ρ_I is the density of sea ice and ρ_b is the density of the brine. The following approximate equation has been presented in reference (3)

$$\nu_b = S \left(\frac{49.185}{\theta} + 0.532 \right) \tag{2}$$

to compute the brine volume ν_b in parts per thousand when the salinity S of the ice in parts per thousand and the absolute value of the ice temperature θ in °C are known. Equation (2) can be used in the range of θ from -0.5° to -22.9°C. The volume of brine for ice temperatures between -0.1° and -0.4°C can be evaluated from the table presented in Reference (1). Reference to the table must be made for temperatures below -22.9°C.

In order to predict the maximum ice pressure exerted against the walls of the ship structure it is usually necessary to know the following mechanical properties of ice: the Young's modulus E_I, the uniaxial compressive strength σ_c, the shear strength τ_s and the flexural strength σ_f. Test data on the mechanical properties of sea ice are presented in References (18), (21), (24) etc.

The Young's modulus of ice E_I can be evaluated from (21)

$$E_I = (771 - 63.2\sqrt{\nu_b})10^3 \tag{3}$$

where E_I is expressed in p.s.i. and ν_b in parts per thousand. This equation was derived on the basis of laboratory and field sea ice beam test data. Strains were measured in the laboratory with extensometers bonded to the underside of simply supported beams subjected to two-point loadings. Field beam test data were based on measured transverse deflections.

The uniaxial compressive stength σ_c (in the horizontal direction) can be evaluated from (21)

$$\sigma_c = 825 - 60.1\sqrt{\nu_b} \tag{4}$$

where σ_c is expressed in p.s.i. and ν_b in parts per thousand.

Data for the evaluation of the shear strength of ice τ_s are summarized in reference (18). Only a small number of shear strength test data are reported in the literature, since it is extremely difficult to obtain pure shear strength test results.

The flexural strength of sea ice σ_f can be evaluated from (21)

$$\sigma_f = 139.1 - 8.82\sqrt{\nu_b} \tag{5}$$

where σ_f is expressed in p.s.i. and ν_b in parts per thousand.

2.3 ICE FEATURES

Important ice features include sheet ice, ridges, rubble, fragmented covers, brash ice and ice islands. A terminology of relevant terms often used to describe various ice formations is included in Appendix A. The interaction of these ice features with fixed and moving structures is an important research area of concern to Naval Architects and Ocean Engineers. More work is needed to better understand the mechanical behavior and the interaction of these ice aggregates with ocean engineering structures. Important aspects of the problem include the determination of the mechanical properties of ice sheets and of the bulk properties of large ice masses. Additional field observations, analytical investigations, and

laboratory model studies are needed to better understand the properties of various ice formations.

An accumulation of sea ice will either be called FAST ICE or PACK ICE. Pack ice is any accumulation of sea ice other than fast ice, no matter what form it takes or how it is disposed.

Depending on whether an ice feature has been unaffected by deformation or has been deformed the terms LEVEL ICE or DEFORMED ICE should be used. Important deformation processes include HUMMOCKING, RIDGING, and RAFTING.

The pressure process by which sea ice is forced upwards into hillocks of broken ice is called hummocking.

The pressure process by which sea ice is forced into ridges is called ridging.

Ice movement results in lateral changes in ice thicknesses and characteristics in almost any area of sea ice. Ice break up of an initially continuous piece of sea ice results in movement away from the shore. This occurs with crack formation. If a crack opens to a sufficient extent an open water area is created which is referred to as a LEAD. Crack formation does not always mean that a lead will develop. This is due to the possibility for crack refreezing. In the case of closing of the leads the thin ice in the leads is broken and pushed into a variety of piles, so-called pressure ridges. In general, there are two primary types of pressure ridges: p-ridges caused by closures essentially normal to the lead and s-ridges (so-called shear ridges) produced by motion parallel to the lead.

Massive low-salinity MULTIYEAR PRESSURE RIDGES can be created through freezing processes bonding the ice blocks together.

The pressure process whereby one piece of ice overrides another is called rafting.

In many cases ice deformation does not result in the creation of discrete ridges. Instead the complete ice sheet is converted into a chaotic terrain of ice blocks which is called RUBBLE FIELD.

Brash ice fields are obtained when accumulations of floating ice are formed from fragments (not more than 2m(6')) across the wreckage of other forms of ice.

Ice islands, icebergs, bergy bits and growlers can pose

significant hazards in locations where they occur. They should be considered as ice features in the sea and not sea ice in a strict sense. They can be a problem to offshore operations in the eastern Arctic and in particular in the region between Greenland and Canada. The icebergs of the Arctic Ocean are called ICE ISLANDS. An ICEBERG is a massive piece of land formed ice of greatly varying shape and size, showing more than 5m(16') above sea level. Icebergs in heights above sea level of 450' have been observed in Canadian and Greenland Arctic waters. In general, the size of an iceberg is comparable to the size of a ship.

A BERGY BIT is a large piece of floating glacier ice, generally showing less than 5m(16') above sea level but more than 1m (3') and of 100 to 300m^2 (109 to 328 square yards) in area. In general, the size of a bergy bit is comparable to the size of a small cottage.

A GROWLER is a smaller piece of ice than a bergy bit, extending less than 1m (3') above the sea surface and with an area of about 20m^2 (65 ft^2). In general, the size of a growler is comparable to the size of a piano.

The most needed information on ice islands is improved observational data on their number, location, and size distribution. This would allow estimates to be made of the encounter probabilities between such features and offshore structures.

2.4 VERTICAL SIDED STRUCTURES

The possible failure modes of a linear elastic ice sheet under compression are considered in order to predict the maximum ice pressure exerted on the hull structure. The presentation is restricted to wide structures only.

The maximum ice crushing pressure q/h can be estimated using the equation proposed by Korzhavin (8)

$$q = ImK\sigma_c h \qquad (6)$$

where q is the ice load per unit length,

h is the ice thickness,

I is the indentation factor which depends on the geometry of the indentor, the ice thickness and boundary

conditions; I is nominally equal to 2.5 for a narrow structure while it is equal to 1.0 for a wide structure,

m is the shape factor; m is equal to 1.0 for a flat face while it is equal to 0.9 for a round face,

K is the contact factor; K is equal to 1.0 for perfect contact while it might reach higher values for frozen in conditions.

and σ_c is the ice strength in compression. The main difficulty in using equation (6) is in the selection of a suitable value for σ_c. This is so since ice strength is a function of temperature, salinity, crystal orientation, strain rate, degree of confinement and other factors (such as the size of the ice piece).

The dependence of σ_c on temperature and salinity can be estimated from equations (2) and (4). The expression given by equation (4) refers to the uniaxial compressive strength in the horizontal direction. A similar equation is suggested in Reference (21) to obtain the uniaxial compressive strength in the vertical direction.

The uniaxial compressive strength of ice strongly depends on the strain rate. This is so since the mode of failure is a function of the strain rate. At very low strain rates, ice tends to flow or creep at low stresses and as a consequence a ductile failure results. Few visible surface failures are present during this process of deformation at low strain rates. A brittle failure is obtained at higher strain rates. Now ice fails by flaking or shattering. A typical set of strength σ_c versus strain rate $\dot{\varepsilon}$ data for columnar ice is shown in Figure 1. It should be cautioned that higher values for σ_c should be used when plain strain conditions prevail and/or when the confined ice strength is more appropriate. Furthermore it should be noted that in general higher values are obtaind for σ_c from small-scale laboratory tests than from field tests.

The process of crushing against a very wide structure can lead to the non-simultaneous ice failure across the structural width. A lower average ice pressure results for a wide structure than for a narrow structure. In the case of non-simultaneous failure the ice width is subdivided into different regions which are at various stages of failure. A statistical approach was employed in Reference (10) to

estimate the influence of the structural width on the magnitude of the design ice pressure.

The elastic buckling load per unit length of the intact ice sheet is (19)

$$q = \rho g \ell_c^2 \left[1 + \frac{3.32}{\frac{2b}{\ell_c}\left(1 + \frac{b}{2\ell_c}\right)} \right] \qquad (7a)$$

where ρ is the mass density of sea water,

g is the gravity acceleration,

b is the width of ice loading,

$$\ell_c = (D_I/\rho g)^{1/4} \quad \text{is the characteristic length of the ice plate} \qquad (7b)$$

$$D_I = E_I h^3/12(1 - \nu_I^2) \quad \text{is the flexural rigidity of the ice plate} \qquad (7c)$$

and E_I, ν_I are the Young's modulus and Poisson's Ratio of the ice plate respectively

The maximum ice load per unit length developed when cracking of the ice sheet occurs due to shear stresses is given by (15)

$$q = \pi \tau_s h \qquad (8)$$

where τ_s is the ultimate shearing strength of ice.

When a floating ice plate is subjected to compression (by a flat indentor pressing against its free edge) radial cracks emanate from the loaded region at a certain load level. When the load magnitude is further increased more radial cracks are created which may finally lead to the buckling of the cracked region. The elastic buckling load per unit length (for a semi-infinite floating ice sheet loaded uniformly at the contact surface) of the cracked ice plate is given by (5)

$$q = n(\rho g D_I)^{1/2} \qquad (9)$$

where n is a parameter that depends on the boundary conditions. For hinged or fixed boundary conditions n = 2, while n = 1 for a free edge. The effective values of E_I and ν_I will depend upon the characteristics of the pre-cracked plate and consequently they should be determined from the same test data on which n is estimated (6).

It should be cautioned that the critical value of ice pressure when a thin floating ice plate becomes unstable is not necessarily the lowest bifurcation pressure (7). The buckling load can be lower than the lowest bifurcation pressure. In this regard the post-buckling behavior needs to be examined, taking into consideration the possibility of lift-off of the ice cover from the water foundation (7).

Figure 2 presents the dependence of ice pressure p on ice thickness as well as failure mode according to equations (6) up to (9) and for I = 1, m = 1, K = $1/\sqrt{2}$, σ_c = 284 p.s.i., τ_s = 43 p.s.i., ρg = 62.4 lb/ft^3 $E_I = 5.7*10^4$ p.s.i., ν_I = 0.34 and n = 1. It should be noted that the elastic buckling load per unit length of the intact ice sheet (given by Equation (7)) depends upon the so-called aspect ratio 2b/h, i.e. the ratio of the load width to the ice thickness. It is clear that as the aspect ratio tends to infinity the corresponding ice load curve approaches the curve governed by the elastic buckling load of the cracked ice sheet, as it should.

2.5 SLOPING STRUCTURES

The two-dimensional system shown in Figure 3 is considered. Initially, local crushing occurs of the upper face of the ice sheet in contact with the sloping structure. This results in the development of the interaction force N which is normal to the sloping surface. Furthermore a frictional force μN is developed (where μ is the friction coefficient of ice moving against the sloping surface) due to the ice movement.

These forces can be represented by the statically equivalent vertical and horizontal forces V ahd H respectively which are acting at the center of the crushed area. The magnitude of the forces V and H are such that they will cause ice failure in bending.*

The ice sheet is modelled as a plate resting on a liquid

* An unlimited driving force is assumed

foundation. The effect of H on the bending failure of ice is ignored. This is expected to be a reasonable approximation except for very steep structures. The load V necessary to cause ice sheet failure is the lateral load on the structure.

The statically equivalent vertical and horizontal forces V and H respectively, are given by

$$V = N\cos\bar{\alpha} - \mu N\sin\bar{\alpha}$$
$$H = N\sin\bar{\alpha} + \mu N\cos\alpha \qquad (10a,b)$$

where $\bar{\alpha}$ is the slope of the structure with the horizontal (Figure 3). Elminating N from equations (10)

$$H = V\left(\frac{\sin\bar{\alpha} + \mu\cos\bar{\alpha}}{\cos\bar{\alpha} - \mu\sin\bar{\alpha}}\right) \qquad (11)$$

Ice sheet failure in bending is considered to occur when the maximum tensile stress in the ice plate reaches the flexural strength of ice σ_f

$$\sigma_f = 6M_f/bh^2 \qquad (12)$$

where M_f is the maximum bending moment developed in the ice plate, b is the width of the ice plate and h is the ice thickness.

The maximum bending moment M_f is

$$M_f = \ell_c V e^{-\pi/4} \qquad (13)$$

where ℓ_c is the characteristic length of the ice plate (given by equation (7b)). Equation (13) is obtained from the linear elastic response of a semi-infinite ice plate resting on a liquid foundation and subjected to an edge line load of magnitude V.

Combining equations (12) and (13)

$$V/b = 0.36555\ \sigma_f h^2/\ell_c \qquad (14)$$

Equations (11) and (14) give

$$H/b = 0.36555 \frac{\sigma_f h^2}{\ell_c} \left(\frac{\sin\bar{\alpha} + \mu\cos\bar{\alpha}}{\cos\bar{\alpha} - \mu\sin\bar{\alpha}} \right) \qquad (15)$$

Equations (10a) and (14)

$$q = N/b = 0.36555\ \sigma_f h^2/\ell_c (\cos\bar{\alpha} - \mu\sin\bar{\alpha}) \qquad (16)$$

where q is the maximum ice load per unit length (acting normal to the sloping surface) in the case of the bending mode of ice failure. In the simple two-dimensional theory presented above, the length of the transverse crack is equal to the width of the structure.

3. STIFFNESS CRITERIA

The determination of stiffness criteria is of interest for the structural design of Ice-Transiting Vessels. Criteria are needed for the selection of the stiffness of side shell plating, transverse framing and longitudinal side-skin stiffening. The definition of suitable stiffness criteria is useful in the estimation of the working stresses. Furthermore, stiffness criteria are of importance in interpreting field test data so that the imposed ice forces can be evaluated. Criteria must be defined for the fore, aft and midship section of an Ice-Transiting Vessel. The problem is further complicated due to the presence of the strengthened ice-belt region. Structural design procedures are needed to evaluate the relative merit of a strengthened vessel design versus a design without an ice-belt zone. Numerical analysis procedures are available today and they can be utilized in order to obtain the response of ship structures to prescribed loading conditions. However, simple structural design procedures must also be developed to aid the designer in the initial phases of his work. The basis of these procedures is the formulation of a simple structural idealization while retaining the essential characteristics that influence the response. The benefit of this approach is the definition of explicit (though approximate) stiffness criteria that certainly are very useful in evaluating the relative merit of various alternative solutions. Furthermore, the uncertainty

that exists in the determination of the ice forcing functions further increases the usefulness of simplified structural analysis procedures.

A simple structural analysis method was recently suggested in the literature (82) to predict the load carried by the transverse bulkheads or deep transverse web frames, the maximum bending moments developed in the longitudinal stringer in the way of ice loading and in the transverse frames, which result from ice compression on an ice-transiting vessel. The system of framing considered was a combination of transverse and longitudinal framing. The possible ice sheet failure modes were considered to predict the maximum magnitude of ice pressure on the side shell wall structure. The longitudinal side-skin stringer in the ice loaded region was considered as a beam on an elastic foundation where the foundation modulus is provided by the stiffness of the transverse frames. The linear elastic static response of the side shell structure for the midship region was obtained. It was shown that the structural response depends upon the non-dimensional transverse bulkhead spacing that characterizes the strengthening for navigation in ice. The effect of the presence of several longitudinal stringers was approximately taken into account by the dependence of the effective breadth on the longitudinal stringer spacing. The case of non-uniform longitudinal stringer spacing was also discussed. In the present investigation the effect of the stiffness of the adjacent longitudinal stringers will be considered in the determination of the modulus K_{TF} of the imaginary continuous elastic foundation. The present analysis is useful for the investigation of the effects of load sharing. In Reference (82) the longitudinal side-skin stringer in the ice loaded region was considered as a beam on an elastic foundation where the foundation modulus K_{TF} is provided by the transverse framing bending stiffness EI_{TF}. Additionally, in the present investigation, each transverse frame is considered as a beam on an elastic foundation where the foundation modulus K_L is provided by the longitudinal stringer bending stiffness EI_L. In order to simplify the analysis a uniform spacing s_L and a constant bending stiffness EI_L is assumed for each longitudinal stringer. A similar procedure as employed in reference (82) provides the following relation

$$K_L = 171.73\ EL_L/s_L L^3 \qquad (17)$$

where L is the transverse bulkhead or deep transverse web frame spacing. The details of the derivation of equation (17) are presented in the Appendix B. Equation (17) is valid for closely spaced longitudinal stringers where the discrete elastic supports can be replaced by an imaginary continuous elastic foundation with elastic modulus K_L. This condition is satisfied if

$$s_L < 0.207L\ (I_{TF}/I_L)^{1/3} \qquad (18)$$

which is derived on the basis of the requirement that at least four of the supports are within the characteristic wavelength $\pi/(K_L/4EI_{TF})^{1/4}$ of the deflection line (11). The characteristic length $1/\lambda$ is defined by

$$\lambda = (K_L/4EI_{TF})^{1/4} \qquad (19)$$

and it depends on the flexural rigidity of the transverse frame EI_{TF} and the elasticity of the supporting medium K_L. The characteristic length is an important factor influencing the shape of the deflected beam. The beam response in this case displays the features of damped waves and consequently λ is sometimes called the damping factor (11).

In the present investigation the term elastic foundation is used for a Winkler support. Thus the beam under consideration is taken as resting on a kind of spring mattress, the infinitesimal springs forming a continuum, but acting independently of each other.

In the case that equation (18) is not satisfied then each longitudinal stringer should be considered as a separate elastic spring. In the special case of an infinite beam and uniform stiffener spacing the procedure presented in reference (82) could be used to obtain the beam response. Thus the presence of uniformly spaced transverse bulkheads was taken into consideration in deterimining the longitudinal side-skin stringer (in the way of the ice loading) response. However, the procedure must be modified to allow non-zero

deflections at the location of the stringers.

3.1 LONGITUDINAL SIDE-SKIN STRINGER FOUNDATION MODULUS PREDICTION

The structural geometry considered consists of a beam grillage (longitudinal stringers and transverse frames) delimited by deck and bottom plating and supported by two consecutive transverse bulkheads (Figure 4).

At first the stiffness of an isolated transverse frame is sought. The transverse frame is modelled as a beam of length T resting on an elastic foundation with modulus K_L. The ice force P is applied at a distance from the main deck.

The aim of the present analysis is to obtain some information on the following functional relation

$$K_{TF} = F(E,\ I_{TF},\ K_L,\ a,\ T,\ s_{TF}) \tag{20}$$

where s_{TF} is the transverse frame spacing. Equation (20) can be expressed in the following non-dimensional form

$$K_{TF}/E = f(a/T,\ K_L/E,\ s_{TF}/T,\ TI_{TF}/[a(T-a)]^{5/2}) \tag{21}$$

The parameter a/T characterizes the location of the ice load application. The parameter K_L/E depends upon the geometry of the longitudinal stringers. The parameters s_{TF}/T, $TI_{TF}/[a(T-a)]^{5/2}$ are functions of the geometry of the transverse framing (and the location of the ice load in the case of the non-dimensional moment of inertia parameter). The influence of the boundary conditions can be explicitly considered by a suitable modification of the parameter $TI_{TF}/[a(T-a)]^{5/2}$. In the present investigation the geometric mean is considered of the resulting deflections under the load application for simply supported and fixed boundary conditions at the ends of the transverse frames.

In Reference (26) two methods were described for obtaining the form of function f in equation (21). Thus the direct method and the method of superposition were discussed in Reference (26). The effects of load sharing were also discussed in Reference (26).

3.2 ELASTIC-PLASTIC BUCKLING CRITERIA

Euler was the first to derive a column formula and prove theoretically that there is a criterion for column strength which is independent of crushing or yielding of the material. For a simply supported ideal column subjected to an axial compressive force Euler's elastic buckling load P_E is given by:

$$P_E = \pi^2 EI/L^2 \tag{22}$$

in which L is the column length, E is Young's modulus for the material, and I is the moment of inertia of the column cross-section.

The Euler formula above is applicable to different elastic columns provided that the right-hand side of the above equation is multiplied by an appropriate constant coefficient, corresponding to different end conditions. It is seen from eq. (1) that the critical stress, which is obtained by dividing the axial force by the cross-sectional area is independent of the yield stress. For L sufficiently large the critical stress will be smaller than the yield stress, and thus buckling will occur before yielding. For a very short column, however, the behavior and strength is determined almost entirely by yielding and the plastic properties of the material.

When the column is of an intermediate length, yielding of the material will precede the elastic stability limit resulting in a requirement for plastic stability analysis.

This plastification of the cross-section causes material non-linearity during the buckling, and when we in addition know that the response of a beam-column is geometric non-linear even for a purely elastic material, it is obvious that the elastic-plastic buckling behavior of beam-columns of this intermediate length can be extremely complicated to analyze.

Yet another complicating factor is the dependence on the loading history. This is due to strain reversal for large deflections when the tensile stress due to bending exceeds the compressive stress due to the compressive axial force. Where strain reversal occurs, the stress-strain relationship is governed by Young's modulus E, while the relationship otherwise is governed by the instantaneous tangent

modulus. Where and when the strain reversal occurs is dependent on the relative magnitudes of the bending moment and the axial force, or in other words the loading history.

A large number of the members used in todays framed structures are of such an intermediate length range that plasticity will have an influence on the buckling behavior. Because of the mentioned complexities involved due to both geometry and material non-linearities as well as load history dependence, the exact solution of an elastic-plastic buckling problem can be extremely complicated to obtain. For this reason it is highly desirable to be able to obtain appropriate solutions of sufficient accuracy by using a simplified anlysis of the elastic plastic buckling problem.

One such simplified analysis method consists of idealizing the beam-column into a model composed of an elastic-plastic spring and two straight segments. The yield criterion adapted in the spring takes into account the reduced plastic bending moment capacity due to the simultaneous action of moment and compressive loads. This is called a generalized Shanely model idealization because it is a generalization of the model originally described by Shanley in Ref. (74).

The objective of this investigation is to study how well suited the generalized Shanley model is to predict the elastic-plastic buckling behavior of a real column. This is of large practical interest because of the large savings that can be obtained if this simplified model can be used to obtain solutions of acceptable accuracy, and thus eliminate the need for a time consuming and complicated exact solution.

The specific case of a simply supported column of rectangular cross-section is investigated here, but it is highly recommended that this work is extended to include other cross-sections and boundary conditions as well as the effect of lateral loads and end moments.

The reason why a simply supported column of rectangular cross-section will be used here to investigate the applicability of the generalized Shanley model, is that the exact solution can be obtained thus making it possible to compare the results from the Shanley model analysis with the exact solution.

For other cross-sections and boundary conditions, the exact solution can be much more complicated, so that the comparison needed to evaluate the Shanley model may be difficult to obtain. Complicating effects such as residual stresses, twisting of the cross-section, time dependent plasticity etc. are not considered in this investigation.

EXACT MOMENT-CURVATURE RELATIONS

The governing differential equation of a beam-column problem will always involve the quantity EI in its coefficients. Where E is the Young's modulus and I is the cross-sectional moment of inertia. This quantity can be considered as the slope of the moment curvature. In the elastic range this quantity EI is constant and therefore presents no difficulties.

In the plastic range, however, this quantity is not a constant due to the fact that the cross-section may be partly elastic and partly plastic. The elastic Young's modulus E will only apply in the elastic region or when we have strain reversal, otherwise the tangent modulus will apply. The tangent modulus is the tangent of the slope of the stress-strain relation after initial yielding, where the

stress-strain relation is not linear.

Thus in order to solve any beam-column problem where plasticity is involved, we must first obtain the non-linear moment-curvature relation. The moment-curvature relation is also dependent on the level of the axial force so what we are seeking is in reality a moment-curvature thrust relationship.

Pure Bending of Rectangular Section

The moment-curvature relation for a beam of rectangular cross-section undergoing pure bending deformations will be developed by considering a beam segment of length L and with rectangular cross-section (BxH) subjected to a pure bending moment M, as shown in Fig. 5. The beam material is assumed to have a bilinear stress-strain relation as shown in Fig. 6, with modulus $k_s E$ for stresses larger than the yield stress f_y. It is assumed that the beam cross-section remains unchanged during deformation.

The bending moment M is given by:

$$M = \int_A \sigma_x \eta dA = B \int_{-H/2}^{H/2} \sigma_x \eta \, d\eta = 2B \int_0^{H/2} \sigma_x \eta d\eta \qquad (23)$$

where σ_x is the bending stress developed a distance R from the centroid of the cross-section.

We are considering a member with a length which is much larger than the height. This means that shear deformations will be negligible, and we can thus use the assumption that plane sections remain plane. When this assumption is made, the beam segment in Fig. 5, will bend into a circular arc of radius R as shown in Fig. 7. The central angle ϕ and the curvature K is given by:

$$\phi = L/R \qquad (24)$$

$$K = 1/R \qquad (25)$$

The middle fiber does not change its length since it coincides with the neutral axis of the segment. A fiber which is a distance η away

from the neutral axis will have a length given by $(R + \eta)\phi$, and thus the axial strain ε_x will be given by:

$$\varepsilon_x = [(R + \eta)\phi - L]/L = \phi\eta/L = \eta/R = K\eta \tag{26}$$

Linear Elastic Behavior

When the bending moment M is sufficiently small the stresses will be everywhere elastic, and in this case we have:

$$\sigma_x = E\varepsilon_x = EK\eta \tag{27}$$

By using eqs. (23) and (27) we have:

$$M = B\int_{-H/2}^{H/2} EK\eta^2\, d\eta = \frac{1}{12} BH^3EK \tag{28}$$

This can also be written as:

$$M = IEK \tag{29}$$

where

$$I = \int_A \eta^2 dA = B\int_{-H/2}^{H/2} \eta^2 d\eta = \frac{1}{12} BH^3 \tag{30}$$

is the cross-sectional moment of inertia.

The maximum elastic bending moment M_{el} will occur when $|\sigma_x| = f_y$ at the outer fibers of the beam corresponding to $\eta = \pm H/2$. The moment M_{el} and curvature K_{el} in this case are:

$$M_{el} = f_y W_{el} \tag{31}$$

where W_{el} is the elastic section modulus given by:

$$W_{el} = I/\frac{H}{2} = \frac{1}{6} BH^2 \tag{32}$$

This gives us:

$$M_{el} = \frac{1}{6} BH^2 fy \tag{33}$$

From eq. (27) we will get:

$$K_{el} = f_y/(E\ H/2) \tag{34}$$

By using eqs. (28), (33) and (34) we get:

$$M / M_{el} = K/K_{el} \tag{35}$$

This is the moment-curvature relation in the elastic range for the pure bending case.

Elastic-Plastic Behavior

For a slender beam the assumption that plane sections remain plane is justified also in the plastic range.

The stress distribution in the elastic-plastic range is shown in Fig. 8, and this stress distribution can be written as:

$$\sigma_x = E\ \varepsilon_y\ \eta/\ \eta_y\ ; \qquad 0<\eta<\eta_y \tag{36}$$

$$\sigma_x = E\ \varepsilon_y + k_s E(\varepsilon_{max} - \varepsilon_y)\ \frac{\eta - \eta_y}{H/2 - \eta_y}\ ;\ \eta_y<\eta< \tag{37}$$

where:

$$\varepsilon_y = f_y/E \tag{38}$$

$$\eta_y = \frac{\varepsilon_y}{\varepsilon_{max}}\ \frac{H}{2} \tag{39}$$

The last relation follows from the fact that plane cross-sections remain plane also in the plastic range. ε_{max} is the maximum strain at the outer fibers of the beam cross-section, and η_y gives the distance from the centroid to the point where the yield stress is

reached.

The bending moment M is given by eq. (23), and by introducing eqs. (36) and (37) we obtain:

$$M = 2(M_1 + M_2) \tag{40}$$

where

$$M_1 = B\int_0^{\eta_y} E\,\varepsilon_y \frac{\eta}{\eta_y}\,\eta\,d\eta = \frac{1}{3} BE\,\varepsilon_y\,\eta_y^2 \tag{41}$$

and

$$M_2 = B\int_{\eta_y}^{H/2} [E\,\varepsilon_y + k_s E(\varepsilon_{max} - \varepsilon_y)\frac{\eta - \eta_y}{H/2 - \eta_y}]\,\eta\,d\eta \tag{42}$$

Resulting in:

$$M = BE\,\varepsilon_y[(\frac{H}{2})^2 - \frac{1}{3}\eta_y^2]$$

$$+ BEk_s(\varepsilon_{max} - \varepsilon_y)[\frac{2}{3}(\frac{H}{2})^3 + \frac{1}{3}\eta_y^3 - (\frac{H}{2})^2\eta_y]/(\frac{H}{2} - \eta_y) \tag{43}$$

If we introduce the parameter ζ defined as:

$$\zeta = \varepsilon_{max}/\varepsilon_y \tag{44}$$

Then eq. (39) can be written as:

$$\eta_y = \frac{1}{\zeta}\frac{H}{2} \tag{45}$$

By using eqs. (31), (32), (44) and (45) we obtain:

$$M/M_{el} = \left\{ (1-k_s) \left[2\left(\frac{\eta_y}{H}\right)^2 \eta_y - \frac{3}{2}\eta_y \right] + \frac{3}{4} H - \eta_y\left(\frac{\eta_y}{H}\right) - \frac{1}{2} K_s H \right.$$
$$\left. + k_s \zeta \left[\frac{1}{2} H + 2 \left(\frac{\eta_y}{H}\right)^2 \eta_y - \frac{3}{2}\eta_y \right] \right\} / \left(\frac{H}{2} - \eta_y\right) \qquad (46)$$

At η equals η_y, eq. (27) gives us:

$$f_y = EK\,\eta_y \qquad (47)$$

By introducing eq. (46) we can write eq. (47) as:

$$f_y = EK \frac{1}{\zeta} \frac{H}{2} \qquad (48)$$

By using eqs. (34) and (48) we will obtain:

$$\zeta = K/K_{el} \qquad (49)$$

and eq. (45) can then be written as:

$$\eta_y = \frac{K_{el}}{K} \frac{H}{2} \qquad (50)$$

By introducing eqs. (49) and (50) into eq. (46), we will finally get:

$$M/M_{el} = (1-k_s)\left[\frac{3}{2} - \frac{1}{2}\left(\frac{K_{el}}{K}\right)^2\right] + k_s \frac{K}{K_{el}} \qquad (51)$$

This is the general moment-curvature relation in the elastic-plastic range for a beam of rectangular cross-section subjected to pure bending.

When k_s=1, we are in the elastic range, and substituting this value of k_s into eq. (51) will give us:

$$M/M_{el} = K/K_{el} \qquad (52)$$

Eq. (52) is identical to eq. (14) as it should be.

Elastic-Perfectly Plastic Behavior

Elastic-perfectly plastic behavior corresponds to k_s=0, and by

substituting this value of k_s into eq. (51), we obtain:

$$M/M_{el} = \frac{3}{2} - \frac{1}{2}\left(\frac{K_{el}}{K}\right)^2 \tag{53}$$

This is the moment-curvature relation for the elastic-perfectly plastic case for a beam of rectangular cross-section subjected to pure bending.

Eq. (29) can be written as:

$$M_{el} = EI\ K_{el} \tag{54}$$

and by using this we can write the moment-curvature relation given by eq. (53) as:

$$M = EI\left[\frac{3}{2} - \frac{1}{2}\left(\frac{K_{el}}{K}\right)^2\right] K_{el} \tag{55}$$

The moment-curvature relation is presented in this form in Ref. [30].

In the limit as K/K_{el} goes to infinity the expression given by eq. (53) reduces to:

$$\lim_{K/K_{el} \to \infty} M/M_{el} = 3/2\ M_{pl}/M_{el} \tag{56}$$

M_{pl} is the fully plastic moment capacity of the cross-section when no axial force is acting.

Effects of Axial Compression

The moment-curvature relation for a beam of rectangular cross-section including the effects of axial compression will be developed by using the same assumptions as for the pure bending case, except for the effect of strain hardening which will be excluded.

When we are in the elastic region and both bending moment and axial compression are present, we will get a stress distribution as shown in Fig. 9. We notice that the neutral axis will not correspond to the centroidal axis of the cross-section, and we let $\bar{n}$ denote this

distance from the centroidal axis to the neutral axis.

As the loads are increased the compressive stress at the outermost fiber will reach the yield stress f_y, and any further increase in the loads will lead to the formation of a plastic region as shown in Fig. 10a). This condition with one plastic region will be called the primary plastic regime. We let η_{cy} denote the distance from the centroidal axis to the point where the stresses have reached the yield stress in compression. As the loads are still further increased, a second plastic region is formed at the outer surface where tensile stresses are acting as shown in Fig. 10b). This condition with two plastic regions will be called the secondary plastic regime. We let η_{ty} denote the distance from the centroidal axis to the point where the stresses have reached the yield stress in tension. Finally, the cross-section will become fully plastic as shown in Fig. 10c).

The instantaneous position of the neutral axis will depend on the relative magnitude of the bending stress and the direct axial compressive stress as the loads are increased. We need to know the instantaneous position of the neutral axis in order to find the moment-curvature relation, so this tells us that the exact solution cannot be obtained unless we know the loading history.

Linear Elastic Behavior

We have assumed that plane cross-sections remain plane, and by referring to Fig. 9 we find that the stress distribution σ_x is given by:

$$\sigma_x = E\,K\,(\eta - \bar{\eta}) \tag{57}$$

Where K is the curvature of the middle surface and $\bar{\eta}$ defines the position of the neutral axis. As shown in Fig. 9 this stress σ_x in the axial direction will consist of one contribution σ_a from the axial force P, and one contributon σ_b from the bending moment M. Thus:

$$\sigma_x = \sigma_a + \sigma_b \tag{58}$$

The stress σ_a can be written as:

$$\sigma_a = -P/A = -P/BH \tag{59}$$

The negative sign must be introduced because the axial force is compressive, while we define tensile stresses as positive. In the above equation A is the cross-sectional area, which in our case equals BxH. The bending stress σ_b can be written as:

$$\sigma_b = M\eta/I \tag{60}$$

and thus we obtain the following expression for σ_x:

$$\sigma_x = -P/A + M\eta/I \tag{61}$$

At the neutral axis σ_x is equal to zero, and plugging this into eq. (57) will give us $\eta = \bar{\eta}$ at the neutral axis, as it should. Using this and $\sigma_x = 0$ in eq. (61) will give us the following expression for the position $\bar{\eta}$ of the neutral axis:

$$\bar{\eta} = IP/AM \tag{62}$$

The fully plastic axial force P_{pl} can be written as:

$$P_{pl} = Af_y = BHf_y \tag{63}$$

From eqs. (31) and (32) we have:

$$1/M_{ek} = \frac{H}{2}/If_y \tag{64}$$

Dividing eq. (61) by f_y results in:

$$\sigma_x/f_y = -P/Af_y + M_\eta/If_y \tag{65}$$

When the compressive stress at the outermost fiber ($\eta = H/2$) reaches

the yield stress ($\sigma_x = -f_y$), the elastic interaction curve is obtained by using eqs. (63), (64) and (65) as:

$$P/P_{pl} + M/M_{el} = 1 \tag{66}$$

We are in the elastic range, and the moment-curvature relation given by eq. (35) is thus valid:

$$M/M_{el} = K/K_{el} \tag{67}$$

By using eqs. (62), (63) and (64) we can now obtain:

$$P/P_{pl} = 2M\bar{\eta}/M_{el}H \tag{68}$$

When first yield is reached, eqs. (66), (67) and (68) will give us:

$$\frac{M}{M_{el}} = \frac{H/2}{H/2 + \bar{\eta}} = \frac{K}{K_{el}} \tag{69}$$

Furthermore, when first yield is reached we will get the following by using eqs. (66) and (69):

$$\frac{P}{P_{pl}} = \frac{\bar{\eta}}{H/2 + \bar{\eta}} = \frac{K}{K_{el}} \frac{2}{H} \bar{\eta} \tag{70}$$

The stress distribution σ_x can be rewritten as:

$$\sigma_x = f_y(-P/P_{pl} + 2M\,\eta/M_{el}H) \tag{71}$$

Then by using eqs (69) and (70) we finally obtain the following expression for the stress distribution σ_x corresponding to the initial yield case:

$$\sigma_x = \frac{f_y}{H/2 + \bar{\eta}} (\eta - \bar{\eta}) \tag{72}$$

Elastic-Plastic Behavior in Primary Regime

The stress distribution in the primary plastic regime as shown in

Fig. 10a), can be expressed as:

$$\sigma_x = -f_y \qquad \text{when } -H/2 \leq \eta \leq -\eta_{cy} \tag{73}$$

$$\sigma_x = f_y \frac{\eta - \bar{\eta}}{\eta_{cy} + \bar{\eta}} \qquad \text{when } -\eta_{cy} \leq \eta \leq H/2 \tag{74}$$

The relation between the axial compressive force P and the stress σ_x is given by:

$$-P = \int_A \sigma_x dA = \int_{A\text{plastic}} \sigma_x \, dA_{\text{plastic}} + \int_{A\text{elastic}} \sigma_x \, dA_{\text{elastic}} \tag{75}$$

The negative sign is introduced because P is compressive while we consider tensile stresses as positive. By introducing the stress distribution given by eqs. (73) and (74), we can write eq. (75) as:

$$-P = B\int_{-H/2}^{-\eta_{cy}} -f_y d\eta + B\int_{-\eta_{cy}}^{H/2} f_y \frac{\eta - \bar{\eta}}{\eta_{cy} + \bar{\eta}} \, d\eta \tag{76}$$

Performing the integrations will give us the following result:

$$-P = \frac{B f_y}{\eta_{cy} + \bar{\eta}} \left[-\frac{1}{2}\eta_{cy}^2 + \frac{H}{2}\eta_{cy} + 2\bar{\eta}\frac{H}{2} - \frac{1}{8}H^2 \right. \tag{77}$$

By dividing eq. (77) through P_{pl} as given by eq. (63), we obtain:

$$\frac{P}{P_{pl}} = \frac{1}{\eta_{cy} + \bar{\eta}} \left[\frac{1}{2}\eta_{cy} + \bar{\eta} - \frac{1}{2}\left(\frac{\eta_{cy}}{H}\right)\eta_{cy} - \frac{1}{8}H \right] \tag{78}$$

The relation between the bending moment M and the stress σ_x is given by:

$$M = \int_A \sigma_x \eta \, dA = \int_{A\text{plastic}} \sigma_x \eta \, dA_{\text{plastic}} + \int_{A\text{elastic}} \sigma_x \eta \, dA_{\text{elastic}} \tag{79}$$

By introducing the stress distribution given by eq. (74), we can write eq. (79) as:

$$M = B\int_{-H/2}^{-\eta_{cy}} -f_y \eta \, d\eta + B\int_{-\eta_{cy}}^{H/2} f_y \frac{\eta - \bar{\eta}}{\eta_{cy} + \bar{\eta}} \eta \, d\eta \tag{80}$$

Performing the integrations will give us the following result:

$$M = \frac{B f_y}{\eta_{cy} + \bar{\eta}} \left[\frac{1}{24} H^3 + \frac{1}{8} H^2 \eta_{cy} - \frac{1}{6} \eta_{cy}^3\right] \tag{81}$$

By dividing the above equation with M_{el} as given by eq. (33), we obtain:

$$\frac{M}{M_{el}} = \frac{1}{\eta_{cy} + \bar{\eta}} \left[\frac{1}{4} H + \frac{3}{4} \eta_{cy} - \left(\frac{\eta_{cy}^2}{H}\right) \eta_{cy}\right] \tag{82}$$

Equation (57) applies in the elastic region so that:

$$\sigma_x = EK (\eta - \bar{\eta}) \qquad \text{when } -\eta_{cy} \leq \eta \leq H/2 \tag{83}$$

At $\eta = -\eta_{cy}$ the stress is $\sigma_x = -f_y$ and eq. (83) then gives:

$$f_y = EK (\eta_{cy} + \bar{\eta}) \tag{84}$$

By using eqs. (34) and (84) we can now obtain:

$$\frac{K}{K_{el}} = \frac{H/2}{\eta_{cy} + \bar{\eta}} \tag{85}$$

When η_{cy} is equal to H/2 we are in the fully elastic region. By plugging $\eta_{cy} = h/2$ into eqs. (78), (82) and (85) these equations reduce

to eqs. (70) and (69) respectively, as they should.

Finally, by using eq. (74) the yield stress is also reached in the outermost fiber $\eta = H/2$ where tensile stresses are acting when:

$$\eta_{cy} = \frac{H}{2} - 2\bar{\eta} \tag{86}$$

and this gives us a transition to the secondary plastic regime.

Elastic-Plastic Behavior in Secondary Regime

The stress distribution in the secondary plastic regime as shown in Fig. 10b), can be expressed as:

$$\sigma_x = -f_y \quad \text{when} \quad -\frac{H}{2} \leq \eta \leq -\eta_{cy} \tag{87}$$

$$\sigma_x = f_y \frac{\eta - \bar{\eta}}{\eta_{ty} - \bar{\eta}} \quad \text{when} \quad -\eta_{cy} \leq \eta \leq \eta_{ty} \tag{88}$$

$$\sigma_x = f_y \quad \text{when} \quad \eta_{ty} \leq \eta \leq H/2 \tag{89}$$

Since at $\eta = -\eta_{cy}$ the stress σ_x equals $-f_y$, it follows from eq. (88) that:

$$\eta_{ty} - \eta_{cy} = 2\bar{\eta} \tag{90}$$

The relation between the axial compressive force P and the stress σ_x is given by:

$$-P = \int_A \sigma_x dA = \int_{A_{1plastic}} \sigma_x dA_{1plastic} + \int_{A_{2plastic}} \sigma_x dA_{2plastic} + \int_{A_{elastic}} \sigma_x dA_{elastic} \tag{91}$$

The negative sign is introduced because P is compressive while we consider tensile stresses as positive. By introducing the stress

distribution given by eqs. (87), (88) and (89), we can write eq. (91) as:

$$-P = B\int_{-H/2}^{-\eta_{cy}} -f_y d\eta + B\int_{\eta_{ty}}^{H/2} f_y d\eta + B\int_{-\eta_{cy}}^{\eta_{ty}} f_y \frac{\eta - \bar{\eta}}{\eta_{ty} - \bar{\eta}} d\eta \qquad (92)$$

Performing the integrations will give us the following result:

$$P = \frac{B f_y}{\eta_{ty} - \bar{\eta}}\left[\frac{1}{2}\eta_{cy}^2 + \frac{1}{2}\eta_{ty}^2 - \eta_{cy}\eta_{ty} + 2\bar{\eta}\,\eta_{cy}\right] \qquad (93)$$

By dividing eq. (93) through by P_{pl} as given by eq. (63), we obtain:

$$\frac{P}{P_{pl}} = \frac{1}{\eta_{ty} - \eta}\left[\frac{1}{2}\left(\frac{\eta_{cy}}{H}\right)\eta_{cy} + \frac{1}{2}\left(\frac{\eta_{ty}}{H}\right)\eta_{ty} - \frac{1}{H}\eta_{cy}\eta_{ty} + \frac{2}{H}\bar{\eta}\,\eta_{cy}\right] \qquad (94)$$

The relation between the bending moment M and the stress σ_x is given by:

$$M = \int_A \sigma_x \eta dA = \int_{A_{1plastic}} \sigma_x \eta dA_{1plastic} + \int_{A_{2plastic}} \sigma_x \eta dA_{2plastic} + \int_{A_{elastic}} \sigma_x \eta dA_{elastic} \qquad (95)$$

By introducing the stress distribution as given by eqs. (87), (88), and (89) we can write eq. (95) as:

$$M = B\int_{-H/2}^{-\eta_{cy}} -f_y \eta d\eta + B\int_{\eta_{ty}}^{H/2} f_y \eta\, d\eta + B\int_{-\eta_{cy}}^{\eta_{ty}} f_y \frac{\eta - \bar{\eta}}{\eta_{ty} - \bar{\eta}} \eta\, d\eta \qquad (96)$$

Performing the integrations will give us the following result:

$$M = \frac{B f_y}{\eta_{ty} - \bar{\eta}}\left[\frac{1}{3}\eta_{cy}^3 + \eta_{cy}^2\bar{\eta} - \frac{1}{2}\eta_{cy}^2\eta_{ty} - \frac{1}{6}\eta_{ty}^3 + \frac{1}{4}H^2\eta_{ty} - \frac{1}{4}H^2\bar{\eta}\right] \qquad (97)$$

By dividing eq. (97) by M_{el} as given by eq. (33), we obtain:

$$\frac{M}{M_{el}} = \frac{1}{\eta_{ty} - \bar{\eta}} \left[2\left(\frac{\eta_{cy}}{H}\right)^2 \eta_{cy} + 6\left(\frac{\eta_{cy}}{H}\right)^2 \bar{\eta} - 3\left(\frac{\eta_{cy}}{H}\right)^2 \eta_{ty} - \left(\frac{\eta_{ty}}{H}\right)^2 \eta_{ty} + \frac{3}{2}\eta_{ty} - \frac{3}{2}\bar{\eta}\right] \tag{98}$$

In the present case we have elastic stress distribution for $-\eta_{cy} < \eta < \eta_{ty}$, and thus from eq. (57):

$$\sigma_x = EK(\eta - \bar{\eta}) \qquad \text{when } -\eta_{cy} \leq \eta \leq \eta_{ty} \tag{99}$$

At $\eta = \eta_{ty}$ the stress σ_x is f_y and thus eq. (99) will give us:

$$f_y = EK(\eta_{ty} - \bar{\eta}) \tag{100}$$

By using eqs. (34) and (100) we then obtain:

$$\frac{K}{K_{el}} = \frac{H/2}{\eta_{ty} - \bar{\eta}} \tag{101}$$

When η_{ty} is equal to H/2 we only have one plastic region, and this also corresponds to the case given by eq. (86). By plugging $\eta_{ty} = H/2$ and η_{cy} given by eq. (86) into eqs. (94), (98) and (101) these equations reduce to eqs. (78), (82), and (85) respectively, as they should.

Fully-Plastic State

The fully-plastic state with the stress distribution shown in Fig. 10c) occurs when:

$$\bar{\eta} = -\eta_{cy} = \eta_{ty} \tag{102}$$

Equation (94) can be rewritten as:

$$\frac{P}{P_{pl}} = \frac{\eta_{ty}}{H} - \frac{\eta_{cy}}{H} + \frac{1}{\eta_{ty} - \bar{\eta}}\left[\frac{1}{2}\frac{1}{H}\eta_{ty}^{2} - \frac{1}{H}\bar{\eta}\ \eta_{ty} - \frac{1}{2}\frac{1}{H}\eta_{cy}^{2}\right.$$

$$\left. - \frac{1}{H}\bar{\eta}\ \eta_{cy}\right] \qquad (103)$$

By taking the limit of eq. (103) as the state described by eq. (102) is approached, we obtain:

$$P/P_{pl} = 2\bar{\eta}/H \qquad (104)$$

This is because the numerator in the last term of eq. (103) goes to zero faster than the denominator.

Equation (98) can be rewritten as:

$$\frac{M}{M_{el}} = \frac{\frac{1}{4}H^{2} - \frac{1}{2}\eta_{cy}^{2} - \frac{1}{2}\eta_{ty}^{2}}{\frac{1}{6}H^{2}} + \frac{1}{\frac{1}{6}H^{2}(\eta_{ty} - \bar{\eta})}\left(\frac{1}{3}\eta_{ty}^{3} - \frac{1}{2}\bar{\eta}\ \eta_{ty}^{2}\right.$$

$$\left. + \frac{1}{3}\eta_{cy}^{3} + \frac{1}{2}\bar{\eta}\ \eta_{cy}^{2}\right) \qquad (105)$$

By taking the limit of eq. (105) as the state described by eq. (102) is approached, we obtain:

$$\frac{M}{M_{el}} = \frac{3}{2} - 6\left(\frac{\bar{\eta}}{H}\right)^{2} \qquad (106)$$

This is because the numerator in the last term of eq. (105) goes to zero faster than the denominator.

For the fully-plastic state described by eq. (102), the curvature given by eq. (101) approaches infinity as expected.

By eliminating $\bar{\eta}$ between eq. (104) and (106) we end up with :

$$\frac{M}{M_{el}} = \frac{3}{2}\left[1 - \frac{P}{(P_{pl})}^{2}\right] \qquad (107)$$

This is the fully-plastic interaction curve for a rectangular cross-section.

SHANLEY MODEL ANALYSIS

Assumptions

The objective of this chapter is to investigate the elastic-plastic behavior of a column of rectangular cross-section by using a Shanley model formulation. The bilinear stress-strain relationship shown in Fig. 6 is again assumed, and it is also assumed that the cross-section remains unchanged during deformation. The Shanley model formulation to be used in this analysis is a generalization of the model originally described by Shanley in Ref. (74).

In the generalized Shanley model as shown in Fig. 11, the initially straight, simply supported column, of length L is idealized by a model consisting of an elastic-plastic rotational spring and two non-flexural straight segments. The rotational stiffness of the elastic-plastic spring takes into account the reduction in stiffness due to partial yielding of the cross-section.

It is assumed that the curvature of the mid-section is constant over the length ξL, where ξ is a constant which is independent of the loading history and the slenderness of the column. The remaining portion of the column of length $(1-\xi)L$ remains straight. With the above assumptions, we can see from Fig. 12 that the relative rotation 2θ of the spring is given by:

$$2\theta = \xi LK \tag{108}$$

Where K is the curvature of the mid-section.

Governing Equations

The moment M at the mid-section is given by:

$$M = P\, w \tag{109}$$

whre P is the axial compressive force and w is the transverse displacement at mid-section. If θ_o is the initial stress free rotation and θ is the additional rotation, then for small rotations ($\sin\theta \tilde{=} \theta$):

$$w = \frac{1}{2} L(\theta + \theta_0) \tag{110}$$

Which together with eq. (109) will give us:

$$M = \frac{1}{2} PL(\theta + \theta_0) \tag{111}$$

The appropriate expressions for the cross-sectional moment of inertia I, the elastic section modulus W_{el}, the first yield bending moment M_{el}, and the fully plastic axial force P_{pl} for a rectangular section are already developed. These are given by eqs. (30), (32), (33), and (63) respectively. We also have the relation between moment and curvature in the elastic range as given by eq. (29).

By using eqs. (29), (108), and (111) we obtain the following expression for the elastic buckling load, without imperfections (θ_o=0), of the Shanley model. This buckling load is called P_c, and is given by:

$$P_c = 4EI/L^2\xi \tag{112}$$

In eq. (22) we described the Euler load P_E for a simply supported column of length L. When:

$$\xi = 4/\pi^2 \tag{113}$$

the load P_c is equal to P_E. We will use this value of the constant ξ because it will give the Shanley model the correct elastic buckling load.

The relation between the mid-section curvature K_0 due to imperfection and the rotation θ_0 due to imperfection is given from eq. (108) as:

$$2\theta_0 = \xi L K_0 \tag{114}$$

We can now introduce the following non-dimensional parameters m, p, p_c and k_0 given by:

$$m = M/M_{el} \tag{115}$$

$$p = P/P_{pl} \tag{116}$$

$$P_c = P_c/P_{pl} \tag{117}$$

$$k = EIK/M_{el} \tag{118}$$

$$k_0 = EIK_0/M_{el} \tag{119}$$

By using these non-dimensional parameters, we can rewrite eq. (111) in the following non-dimensional form.

$$m = p(k + k_0)/p_c \tag{120}$$

Since k_0 and P_c are constant, the incremental form of eq. (120), without neglecting higher order terms, is:

$$dm = [pdk + (k + k_0)dp + dpdk]/p_c \tag{121}$$

We have both bending moment and axial force acting, and for this reason the total axial strain ε_x will have a contribuiton ε_a from the axial force P and a contribution ε_b from the bending moment M, such that:

$$\varepsilon_x = \varepsilon_a + \varepsilon_b \tag{122}$$

The strain ε_a due to the axial force is constant over the cross-section, while the bending strain ε_b in a fibre at a distance η from the centroidal axis is given by eq. (26) such that:

$$\varepsilon_x = \varepsilon_a + K\eta \tag{123}$$

ε_x is here the total strain in the axial direction. K is the midsection curvature.

In incremental form we can write eq. (123) in the following way:

$$d\varepsilon_x = d\varepsilon_a + \eta dK \tag{124}$$

For our model with a bilinear stress-strain relationship, the incremental stress can be written as:

$$d\sigma_x = k_s E d\varepsilon_x \tag{125}$$

where $k_s=1$ when $\varepsilon_x < \varepsilon_y$, where ε_y is the strain corresponding to first yield as defined by eq. (38). Equations (124) and (125) give us:

$$d\sigma_x = k_s E(d\varepsilon_a + \eta dK) \tag{126}$$

In the Shanley model analysis it is most convenient to define the compressive axial force as positive and thus also compressive stresses as positive. With this definition the relationship between the incremental axial force dP and the incremental stress $d\sigma_x$ is given

by:

$$dP = \int_A d\sigma_x dA \tag{127}$$

Using eqs. (126) and (127), and the fact that $d\varepsilon_a$ and dK are constant over the cross-section, we obtain:

$$dP = Ed\varepsilon_a \int_A k_s dA + EdK \int_A ks\eta dA \tag{128}$$

By dividing the above equation by P_{pl} as given by eq. (63), we obtain:

$$\frac{dP}{P_{pl}} = \frac{Ed\varepsilon_a}{E\varepsilon_y A} \int_A k_s + \frac{EdK}{E\varepsilon_y A} \int_A k_s \eta dA \tag{129}$$

From eq. (118), we have that:

$$dK = M_{el}\, dk/EI \tag{130}$$

Let us introduce the non-dimensional parameter e defined as:

$$e = \varepsilon_a/\varepsilon_y \tag{131}$$

By introducing eqs. (33), (116), (130) and (131) into eq. (129) we obtain:

$$dp = de \int_A k_s\, dA/A + \frac{1}{3}\, dk \int_A k_s \eta\, dA/W_{el} \tag{132}$$

By introducing the non-dimensional parameters $\bar{A}$ and $\bar{S}$, defined by:

$$\bar{A} = \int_A k_s dA/A \tag{133}$$

$$\bar{S} = \int k_s \eta dA/W_{el} \tag{134}$$

we can write eq. (132) as:

$$dp = \bar{A}\, de + \frac{1}{3}\bar{S}\, dk \tag{135}$$

The relation between the incremental bending moment dM and the incremental stress $d\sigma_x$ is given by:

$$dM = \int_A d\sigma_x\, \eta dA \tag{136}$$

Using eqs. (126) and (136), and the fact that $d\,\varepsilon_a$ and dK are constant over the cross-section, we obtain:

$$dM = Ed\,\varepsilon_a \int_A k_s\, \eta dA + EdK \int_A k_s\, \eta^2 dA \tag{137}$$

By dividing eq. (137) by M_{el} as given by eq. (33), we will get:

$$\frac{dM}{M_{el}} = \frac{Ed\varepsilon_a}{f_y W_{el}} \int_A k_s \eta dA + \frac{EdK}{f_y W_{el}} \int_A k_s\, \eta^2 dA \tag{138}$$

By introducing eqs. (115), (130) and (131) into eq. (138), we obtain:

$$dm = de \int_A k_s\, \eta dA/W_{el} + dK \int_A k_s\, \eta^2 dA/I \tag{139}$$

Equation (139) can be rewritten as:

$$dm = \bar{S}\, de + \bar{I}\, dk \tag{140}$$

where $\bar{S}$ is defined by eq. (134) and $\bar{I}$ is defined as:

$$\bar{I} = \int_A k_s\, \eta^2 dA/I \tag{141}$$

By using eqs. (121) and (140) we will get:

$$\bar{S}\, de + \bar{I}\, dk = [pdk + (k + k_0)dp + dp\, dk]/p_c \tag{142}$$

By introducing eq. (135) for dp in eq. (142), we end up with:

$$de = \{|p+\tfrac{1}{3}\bar{S}(k+k_0) - p_c\bar{I}\ \ dk+\tfrac{1}{3}\bar{S}\ (dk)^2\}/\{\ p_c\bar{S}-(k+k_0)\bar{A}-\bar{A}dk\}$$

By introducing the three non-dimensional parameters C_1, C_2, and C_3 defined as:

$$C_1 = -[p+\tfrac{1}{3}(k+k_0)\bar{S}-p_c I]/[(k+k_0)\bar{A}-p_c\bar{S}] \tag{144}$$

$$C_2 = -[C_1\bar{A}+\tfrac{1}{3}\bar{S}]/[(k+k_0)\bar{A}-p_c\bar{S}] \tag{145}$$

$$C_3 = \bar{A}/[(k+k_0)\bar{A}-p_c\bar{S}] \tag{146}$$

we are able to write eq. (143) as:

$$de = C_1 dk + [C_2(dk)^2/(1+C_3 dk)] \tag{147}$$

Equations (114) and (126) will now give us:

$$dp = [C_1\bar{A} + \tfrac{1}{3}\bar{S}]dk + [C_2\bar{A}(dk)^2/(1+C_3 dk)] \tag{148}$$

Equations (147) and (148) give us expressions for de and dp repsectively as a function of dk.

When the loads are of such a magnitude that we are in the secondary plastic regime, and we define compressive stresses as positive, the expression for the non-dimensional parameter $\bar{A}$, as defined by eq. (133), will be:

$$\bar{A} = \int_A k_s dA/A = \frac{1}{B\cdot H}[B\int_{-H/2}^{-\eta_{ty}} k_s d\eta + B\int_{\eta_{cy}}^{H/2} k_s d\eta + B\int_{-\eta_{ty}}^{\eta_{cy}} d\eta] \tag{149}$$

Performing the integrations in the equation above will give us the

following result:

$$\bar{A} = \frac{1}{H}(1-k_s)\ (\eta_{ty} + \eta_{cy}) + k_s \tag{150}$$

The expression for the non-dimensional parameter $\bar{S}$, as defined by eq. (134) will be:

$$\bar{S} = \int_A k_s\ \eta dA/W_{el} = \frac{6}{BH^2}\left[B\int_{-H/2}^{-\eta_{ty}} k_s\ \eta d\eta + B\int_{\eta_{cy}}^{H/2} k_s \eta d\eta + B\int_{-\eta_{ty}}^{\eta_{cy}} \eta d\eta\right] \tag{151}$$

Performing the integrations in the eq. (151) will give us the following result:

$$\bar{S} = \frac{3}{H^2}[(1-k_s)\ (\eta_{cy}^{\ 2} - \eta_{ty}^{\ 2})] \tag{152}$$

Finally, the expression for the non-dimensional parameter $\bar{I}$, as defined by eq. (141) will be:

$$\bar{I} = \int_A k_s \eta^2 dA/I = \frac{12}{BH^3}\left[B\int_{-H/2}^{-\eta_{ty}} k_s \eta^2 d\eta + B\int_{\eta_{cy}}^{H/2} k_s \eta^2 d\eta + B\int_{-\eta_{ty}}^{\eta_{cy}} \eta^2 d\eta\right] \tag{153}$$

Performing the integrations in eq. (153) will give us the following result:

$$\bar{I} = \frac{4}{H^3}\ (1 - k_s)\ (\eta_{ty}^{\ 3} + \eta_{cy}^{\ 3}) + k_s \tag{154}$$

The expressions for $\bar{A}$, $\bar{S}$, and $\bar{I}$ in the primary plastic regime are obtained by simply substituting $\eta_{ty}=H/2$ into eqs. (150), (152) and (154) respectively. η_{ty} and η_{cy} have already been defined as the distance from the centroidal axis of the cross-section to the fibers that have reached the yield stress in tension and compression respectively. The entire cross-section is elastic when $\eta_{ty}= \eta_{cy}=H/2$. By plugging this into eqs. (150), (152) and (154) we obtain:

$$\bar{A}_{elastic} = \int_A dA/A = 1 \tag{155}$$

$$\overline{S}_{elastic} = \int_A \eta dA/W_{el} = 0 \tag{156}$$

$$\overline{I}_{elastic} = \int_A \eta^2 dA/I = 1 \tag{157}$$

as it should be.

When the column is subjected to an axial compressive force P, the relative axial displacement u will consist of three parts. First the membrane compression u_1 of the bending portion, given by:

$$u_1 = \xi L \varepsilon_a \tag{158}$$

Where ε_a is the axial strain of the centroid. Second the membrane compression u_2 of the straight segments:

$$u_2 = (1 - \xi)\, L\varepsilon_R \tag{159}$$

Where ε_R is the axial strain of the straight segments. The third component of the relative axial displacement is the axial component of the change in geometry, shown in Fig. 13, to be approximated by:

$$u_3 = \frac{1}{2} L\theta(\theta + 2\theta_0) \tag{160}$$

Thus the relative axial displacement u will be:

$$u = \xi L\varepsilon_a + (1 - \xi)L\varepsilon_R + \frac{1}{2} L\theta(\theta + 2\theta_0) \tag{161}$$

Equation (161) can be written in non-dimensional form by dividing by $L\,\varepsilon_y$, and by introducing the non-dimensional parameters δ and e_R, defined as:

$$\delta = u/L\varepsilon_y \tag{162}$$

$$e_R = \varepsilon_R/\varepsilon_y \tag{163}$$

Equation (161) can then be written in non-dimensional form as:

$$\delta = \xi e + (1 - \xi)e_R + \frac{1}{2}\frac{\theta}{\varepsilon_y}(\theta + 2\theta_0) \tag{164}$$

The last term in eq. (164) can be written in terms of p_c, K, and k_o as defined by eqs. (117), (118), and (119) respectively, in the following way:

$$\frac{1}{2}\frac{\theta}{\varepsilon_y}(\theta + 2\theta_0) = \xi k(k + 2k_0)/6\ p_c \tag{165}$$

Thus by introducing eq. (165) into eq. (164), we will finally obtain:

$$\delta = \xi e + (1 - \xi)e_R + \xi k(k + 2k_0)/6\ p_c \tag{166}$$

In incremental form, we can write eq. (166) as:

$$d\delta = \xi de + (1 - \xi)de_R + \xi dk[2(k + k_0) + dk]/6\ p_c$$

When $\varepsilon_R > \varepsilon_y$ the tangent modulus applies so that:

$$d\varepsilon_R = dP/Ak_sE \qquad \text{when } \varepsilon_R > \varepsilon_y \tag{167}$$

When $\varepsilon_R \leq \varepsilon_y$, Young's modulus applies so that:

$$d\varepsilon_R = dP/AE \qquad \varepsilon_R \leq \varepsilon_y \tag{168}$$

By dividing eq. (167) and (168) by ε_y, and using eqs. (38), (63), (116) and (163), we obtain:

$$de_R = dp/k_s \qquad \text{when } e_R > 1 \tag{169}$$

$$de_R = dp \qquad \text{when } e_R \leq 1 \tag{170}$$

Elastic Response

When the entire cross-section is elastic, we have from eqs. (155), (157) and (156) respectively, that $\bar{\bar{A}}=\bar{\bar{I}}=1$ and that $\bar{S}=0$. Thus in the elastic range, eq. (135), will reduce to:

$$p = e \tag{171}$$

Equation (140) will reduce to:

$$m = k \tag{172}$$

and finally, eq. (170) will reduce to:

$$e_R = p \tag{173}$$

Equations (120) and (172) will now give us:

$$k = \frac{p/p_c}{1-p/p_c}\, k_0 \tag{174}$$

The factor $(p/p_c)/(1-p/p_c)$ is the elastic amplification factor. By introducing eqs. (171), (173) and (174) in eq. (166), we get the result:

$$\delta = p + \frac{\xi p/p_c[2-p/p_c]}{6p_c(1 - p/p_c)^2}\, k_0^2 \tag{175}$$

First-Yield State

The first yield state is given by eq. (66), which can be written in non-dimensional form as:

$$m + p = 1 \tag{176}$$

Equations (172) and (174) will give us:

$$m = \frac{p/p_c}{1 - p/p_c} k_0 \tag{177}$$

Introducing eq. (177) for m in eq. (176) will now give us an expression that can be solved for p. This value of p will give us a value for the initial yield load p_{el}. First we obtain:

$$p^2 - (k_0 + p_c + 1)\, p + p_c = 0 \tag{178}$$

Solving eq. (178) for p will give us:

$$p = \frac{k_0 + p_c + 1 \pm \sqrt{(k_0 + p_c + 1)^2 - 4\, p_c}}{2} \tag{179}$$

First yield corresponds to the smallest value of p, so that:

$$p_{el} = \frac{(1 + p_c + k_0) - \sqrt{(1 + p_c + k_0)^2 - 4\, p_c}}{2} \tag{180}$$

By using eqs. (63), (112) and (117), we can obtain p_c as:

$$p_c = \frac{1}{3\xi}\left(\frac{E}{f_y}\right)\left(\frac{H}{L}\right)^2 \tag{181}$$

The transverse displacement w_0 is due to an initial imperfection θ_0 is given by:

$$w_0 = \frac{1}{2} L\theta_0 \tag{182}$$

The value of k_0 to be used in eq. (180) can be found from eq. (114), by introducing eqs. (119) and (182), with the result:

$$k_0 = 6\, p_c \, \frac{w_0}{L} \, \frac{L}{H} \tag{183}$$

Interaction Curves

The bending strain ε_b in eq. (122) has a maximum value when $\eta = H/2$. By using eq. (123) the maximum total strain ε_{max} can then be written as:

$$\varepsilon_{max} = \varepsilon_a + K \frac{H}{2} \tag{184}$$

By dividing the above equation by ε_y, and using eqs. (44), (118) and (131), we can write eq. (184) as:

$$\zeta = e + k \tag{185}$$

When deriving the expressions for the interaction curves, it is most convenient to use the same sign convention as used when deriving the exact moment-curvature relations, which means that tensile stresses will be considered as positive in this subchapter.

The bilinear stress-strain relation as shown in Fig. 6 is assumed and then the following will apply:

$$\sigma_x = E\,\varepsilon_x \quad ; \quad -\varepsilon_y \leq \varepsilon_x \leq \varepsilon_y \tag{186}$$

$$f_y = E\,\varepsilon_y \quad ; \quad \varepsilon_x = \varepsilon_y \tag{187}$$

$$\sigma_x = (1 - k_s)E\,\varepsilon_y + k_s E\,\varepsilon_x ;\ \varepsilon_x \geq \varepsilon_y \tag{188}$$

$$\sigma_x = -(1 - k_s)E\,\varepsilon_y + k_s E\,\varepsilon_x ;\ \varepsilon_x \leq -\varepsilon_y \tag{189}$$

The strain distribution over the cross-section in the secondary plastic regime is shown in Fig. 14a) and the corresponding stress distribution is shown in Fig. 14 b). Plane sections are assumed to remain plane also in the plastic region, so that the strain distribution over cross-section is linear. From Fig. 14a) we find that the maximum strain is compressive and thus negative. This is because the axial force P is compressive such that the strain ε_a due to this axial force is compressive. From Fig. 14a), we can also find the relation between the axial strain ε_x and η as:

$$\varepsilon_x = \frac{\varepsilon_{max} - \varepsilon_a}{H/2}\,\eta - \varepsilon_a \tag{190}$$

When $-\eta_{cy} \leq \eta \leq \eta_{ty}$, the stresses are elastic, so that eqs. (186) and (190) will give us:

$$\sigma_x = E\left[\frac{\varepsilon_{max} - \varepsilon_a}{H/2}\eta - \varepsilon_a\right]; \quad -\eta_{cy} \leq \eta \leq \eta_{ty} \tag{191}$$

In the plastic region corresponding to $\eta_{ty} \leq \eta \leq H/2$, eqs. (188) and (190) will give us:

$$\sigma_x = (1-k_s)E\varepsilon_y + k_s E\left[\frac{\varepsilon_{max} - \varepsilon_a}{H/2}\eta - \varepsilon_a\right]; \quad \eta_{ty} \leq \eta \leq H/2 \tag{192}$$

Finally in the plastic region corresponding to $-H/2 \leq \eta \leq \eta_{cy}$, eqs. (189) and (190) will give us:

$$\sigma_x = -(1-k_s)E\varepsilon_y + k_s E\left[\frac{\varepsilon_{max} - \varepsilon_a}{H/2}\eta - \varepsilon_a\right]; \quad -H/2 \leq \eta \leq -\eta_{cy} \tag{193}$$

The relation between the axial compressive force P and the stress σ_x is given by:

$$-P = \int_A \sigma_x dA = \int_{A_{1plastic}} \sigma_x dA_{1plastic} + \int_{A_{2plastic}} \sigma_x dA_{2plastic} + \int_{A_{elastic}} \sigma_x dA_{elastic} \tag{194}$$

The negative sign must be introduced because we here consider tensile stresses as positive, while P is compressive. Equations (192). (193) and (191) respectively, will now give us:

$$\int_{A_{1plastic}} \sigma_x dA_{1plastic} = B\int_{\eta_{ty}}^{H/2} \left\{(1-k_s)E\varepsilon_y + k_s E\left[\frac{\varepsilon_{max} - \varepsilon_a}{H/2}\eta - \varepsilon_a\right]\right\} d\eta \tag{195}$$

$$\int_{A_{2plastic}} \sigma_x dA_{2plastic} = B\int_{-H/2}^{-\eta_{cy}} \left\{-(1-k_s)E\varepsilon_y + k_s E\left[\frac{\varepsilon_{max} - \varepsilon_a}{H/2}\eta - \varepsilon_a\right]\right\} d\eta \tag{196}$$

$$\int_{A_{elastic}} \sigma_x dA_{elastic} = B\int_{-\eta_{cy}}^{\eta_{ty}} E\left[\frac{\varepsilon_{max} - \varepsilon_a}{H/2}\eta - \varepsilon_a\right] d\eta \tag{197}$$

By performing the integrations in eqs. (195) to (197) and substituting back into eq. (194), we obtain the following result:

$$P = B(1-k_s)E[\varepsilon_y(\eta_{ty} - \eta_{cy}) + \varepsilon_a(\eta_{cy} + \eta_{ty}) + \frac{\varepsilon_{max} - \varepsilon_a}{H}(\eta_{cy}^2 - \eta_{ty}^2)] + Bk_sE\varepsilon_aH \tag{198}$$

By dividing eq. (198) by P_{pl} given by eq. (63), and by using eqs. (44) and (131), we finally obtain:

$$\frac{P}{P_{pl}} = \{(1-k_s)\frac{1}{H}[(\eta_{cy}+\eta_{ty})+\frac{1}{H}(\eta_{ty}^2-\eta_{cy}^2)]+k_s\}e + (1-k_s)\frac{1}{H}[\eta_{ty}-\eta_{cy}+\frac{\zeta}{H}(\eta_{cy}^2-\eta_{ty}^2)] \tag{199}$$

The relation between the bending moment M and the stress σ_x is given by:

$$M = \int_A \sigma_x\eta dA = \int_{A_{1plastic}} \sigma_x\eta dA_{1plastic} + \int_{A_2} \sigma_x\eta dA_{2plastic} + \int_{A_{elastic}} \sigma_x\eta dA_{elastic} \tag{200}$$

Equations (192), (193) and (191) respectively, will now give us:

$$\int_{A_{1plastic}} \sigma_x\eta dA_{1plastic} = B\int_{\eta_{ty}}^{H/2}\{(1-k_s)E\varepsilon_y + k_sE[\frac{\varepsilon_{max} - \varepsilon_a}{H/2}\eta - \varepsilon_a]\}\eta d\eta \tag{201}$$

$$\int_{A_{2plastic}} \sigma_x\eta dA_{2plastic} = B\int_{-H/2}^{-\eta_{cy}}\{-(1-k_s)E\varepsilon_y + k_sE[\frac{\varepsilon_{max} - \varepsilon_a}{H/2}\eta - \varepsilon_a]\}\eta d\eta \tag{202}$$

$$\int_{A_{elastic}} \sigma_x\eta dA_{elastic} = B\int_{-\eta_{cy}}^{\eta_{ty}} E[\frac{\varepsilon_{max} - \varepsilon_a}{H/2}\eta - \varepsilon_a]\eta d\eta \tag{203}$$

By performing the integrations in eqs. (201) to (203), and substituting back into eq. (200), we obtain the following result:

$$M = BE\left\{(1-k_s)[\varepsilon_y(\frac{H^2}{4} - \frac{1}{2}\eta_{cy}^2 - \frac{1}{2}\eta_{ty}^2) + \varepsilon_a(\frac{1}{2}\eta_{cy}^2 - \frac{1}{2}\eta_{ty}^2) + \frac{\varepsilon_{max} - \varepsilon_a}{H/2}(\frac{1}{3}\eta_{ty}^3 + \frac{1}{3}\eta_{cy}^3)] + k_s \frac{\varepsilon_{max} - \varepsilon_a}{H/2}\frac{1}{12}H^3\right\} \quad (204)$$

By dividing eq. (204) by M_{el} as given by eq. (33), and by using eqs. (44) and (131), we finally obtain:

$$\frac{M}{M_{el}} = \left\{(1-k_s)[3((\frac{\eta_{cy}}{H})^2 - (\frac{\eta_{ty}}{H})^2 - 4((\frac{\eta_{ty}}{H})^3 + (\frac{\eta_{cy}}{H})^3] - k_s\right\}e + (1-k_s)[\frac{3}{2} - 3((\frac{\eta_{cy}}{H})^2 + (\frac{\eta_{ty}}{H})^2) + 4\zeta((\frac{\eta_{ty}}{H})^3 + (\frac{\eta_{cy}}{H})^3] + k_s\zeta \quad (205)$$

First yield corresponds $\zeta = \varepsilon_{max}/\varepsilon_y = 1$ and $\eta_{cy} = \eta_{ty} = H/2$. Plugging this into eq. (199) will result in:

$$P/P_{pl} = e \quad (206)$$

Plugging the same values into eq. (205) will result in:

$$M/M_{el} = -e + 1 \quad (207)$$

By eliminating e between eqs. (206) and (207), we obtain:

$$\frac{M}{M_{el}} + \frac{P}{P_{pl}} = 1 \quad (208)$$

Equation (208) is identical to eq. (66), and thus as expected eqs. (199) and (205) reduce to the elastic interaction curve when $\eta_{cy} = \eta_{ty} = H/2$ and $\varepsilon_{max}/\varepsilon_y = 1$.

When $k_s = 0$ and $-\eta_{cy} = \eta_{ty}$ we will obtain the fully plastic state for a perfectly plastic material. Plugging this into eq. (199) will give us:

$$P/P_{pl} = 2\eta_{ty}/H \quad (209)$$

Plugging the same values into eq. (205) will give us:

$$\frac{M}{M_{el}} = \frac{3}{2} - 6\left(\frac{\eta_{ty}}{H}\right)^2 \tag{210}$$

By eliminating η_{ty} between eq. (209) and (210), we end up with:

$$\frac{M}{M_{el}} = \frac{3}{2}\left[1 - \left(\frac{P}{P_{pl}}\right)^2\right] \tag{211}$$

Equation (211) is equal to eq. (107), and thus as expected eqs. (199) and (205) reduce to the familiar interaction curve for a perfectly plastic material when $k_s=0$ and $-\eta_{cy}=\eta_{ty}$.

With ζ and e given, we are able to calculate the corresponding values of η_{cy} and η_{ty}. The appropriate relations are obtained from the strain distribution shown in Fig. 14a, from which it follows:

$$\frac{\bar{\eta}}{\varepsilon_a} = \frac{\bar{\eta} + \eta_{cy}}{\varepsilon_y} \tag{212}$$

$$\frac{\varepsilon_y}{\bar{\eta} + \eta_{cy}} = \frac{\varepsilon_{max}}{\bar{\eta} + H/2} \tag{213}$$

Elimination of $\bar{\eta}$ between eqs. (212) and (213) will give us:

$$\eta_{cy} = \frac{\varepsilon_a + \varepsilon_y}{\varepsilon_a - \varepsilon_{max}} \frac{H}{2} \tag{214}$$

By using eqs. (44) and (131) we can now write eq. (214) as:

$$\eta_{cy} = \frac{e - 1}{e - \zeta} \frac{H}{2} \tag{215}$$

or by using eq. (185):

$$\eta_{cy} = \frac{H}{2}(1 - e)/k \tag{216}$$

Obviously the maximum value of η_{cy} is H/2. From Fig. 14a it also follows that:

$$\frac{\varepsilon_y}{\eta_{ty} - \bar{\eta}} = \frac{\varepsilon_{max}}{H/2 + \bar{\eta}} \tag{217}$$

By introducing eqs. (212) and (214) in eq. (217), we will obtain:

$$\eta_{ty} = \frac{\varepsilon_y + \varepsilon_a}{\varepsilon_{max} - \varepsilon_a} \frac{H}{2} \tag{218}$$

By using eqs. (44) and (131) we can now write eq. (218) as:

$$\eta_{ty} = \frac{1 + e}{\zeta - e} \frac{H}{2} \tag{219}$$

Or by using eq. (185):

$$\eta_{ty} = \frac{H}{2}(1 + e)/k \tag{220}$$

Obviously the maximum value of η_{tv} is H/2. By using this value of η_{tv} in eqs. (199) and (205) we will obtain the solutions in the primary plastic regime.

APPROXIMATE MOMENT-CURVATURE RELATIONS

The objective of this chapter is to obtain approximate moment-curvature thrust relations that can be compared with the results form the Shanley model analysis. These approximate relations are important since the exact solution is complicated and cannot be expressed in an explicit form.

When the entire cross-section is elastic, the non-dimensional relation between midsection moment m and curvature k is given by eq. (172). This elastic moment-curvature relation is valid until first yield is reached, as described by eq. (176). The value p corresponding to first yield is p_{el} given by eq. (180). At p equals p_{el}, eq. (176) will give us:

$$k + p_{el} = 1 \tag{221}$$

The elastic moment-curvature relation given by eq. (172) is valid until the limit given by eq. (221) is reached, such that:

$$m = k \quad ; \quad k \leq 1 - p_{el} \tag{222}$$

The axial force-curvature relation up to first yield is given by eq. (174), such that:

$$k = \frac{p/p_c}{1 - p/p_c}\, k_0 \qquad ; \quad k \leq 1 - p_{el} \tag{223}$$

When plastic effects are present (i.e. $k \geq 1 - p_{el}$), the following expression will be investigated:

$$\frac{K}{K_{el}} = m_1 (1 - \frac{m_1}{m_2})^{\gamma} / [1 - \frac{M/M_{el}}{m_2}]^{\gamma} \quad ; \; k \geq 1 - p_{el} \tag{224}$$

Where:

$$m_1 = 1 - \frac{p}{p_{pl}} \tag{225}$$

$$m_2 = \frac{3}{2} [1 - (\frac{p}{p_{pl}})^2] \tag{226}$$

For eq. (224) to give an appropriate moment-curvature relation in the plastic range, firstly when $M/M_{el} = m_1$ we are in the elastic range so that from eq. (222) we should have $M/M_{el} = K/K_{el} = m_1$. By plugging $M/M_{el} = m_1$ into eq. (224) we get the result $K/K_{el} = m_1$, so that the first requirement is satisfied.

Secondly, eq. (226) corresponds to eq. (107) which is the interaction curve for the ultimate capacity for a rectangular cross-section and perfectly-plastic material behavior. The corresponding requirement that eq. (224) must satisfy is that K/K_{el} should approach infinity when $M/M_{el} = m_2$. By plugging $M/M_{el} = m_2$ into eq. (224) we see that also this requirement is satisfied. Eq. (224) can be converted to give M/M_{el} as a function of K/K_{el} with the following result:

$$\frac{M}{M_{el}} = m_2 \, [1 - (m_1 \frac{K_{el}}{K})^{1/\gamma} (1 - \frac{m_1}{m_2})]; \; k \geq 1 - p_{el} \tag{227}$$

The exponent γ is determined by the requirement of continuity of slopes at $K/K_{el} = m_1$, resulting in:

$$\gamma = \frac{m_2}{m_1} - 1 \tag{228}$$

By introducing eqs. (115) and (118), we can now rewrite eq. (227) in the following way:

$$m = m_2 \left[1 - \left(\frac{1}{k}\right)^{1/\gamma} m_3\right] \quad ; \; k \geq 1 - p_{el} \tag{229}$$

Where

$$m_3 = (m_1)^{1/\gamma}\left(1 - \frac{m_1}{m_2}\right) \tag{230}$$

Equation (229) is the final expression for the midsection moment-curvature thrust relation in the plastic range.

The axial force-curvature relation beyond first yield can be obtained by eliminating m between eqs. (120) and (229), with the following result:

$$k = \frac{m_3^{\gamma}}{\left[1 - \frac{p(k + k_0)}{m_2 p_c}\right]^{\gamma}} \quad ; \quad k \geq 1 - p_{el} \tag{231}$$

DISCUSSION

In the previous sections we have derived all the necessary expressions, and these will now be used to do the numerical calculations necessary to evaluate the Shanley model analysis.

Let us start out with comparing the exact moment-curvature thrust relation with the approximate ones.

The most simple case corresponds to pure bending. The exact moment-curvature relation is then given by eqs. (35) and (51) in the elastic and elastic-plastic range respectively. This moment-curvature relation is shown in Fig. 15. The influence of the strain hardening coefficient k_s for a value of $k_s = 1/270$ is also shown. The approximate moment-curvature relations are given by eqs. (222) and (229) in the elastic and the elastic-plastic range respectively. For the bending case eq. (229) will reduce to eq. (51) with $k_s = 0$, such that for this special case the exact and approximate moment-curvature relations will coincide.

When the compressive axial force is present, the situation is more complicated. In order to obtain the exact solution in this case, we must first find the limits that give the transition from the primary plastic to the secondary plastic regime so that the range of validity for a given P/P_{pl} for the governing equiations in the primary plastic to the given P/P_{pl} for the governing equations in the primary plastic and secondary plastic regime can be established. Equation (86) gives us the value of η_{cy} when the transition between primary plastic and secondary plastic behavior occurs.

Now by using eqs. (78), (82), and (85) together with eq. (86), we are able to plot P/P_{pl}, M/M_{el} and K/K_{el} respectively, corresponding to the transition as a function of η_{cy}. This is shown in Fig. 16. For a given P/P_{pl} the value of η_{cy} corresponding to the transition can then be obtained from this figure and then the corresponding values of K/K_{el} and M/M_{el}. For values lower than this limit, we use the expressions for the primary plastic regime, while for values larger than this value we use the expressions for the secondary plastic regime.

The procedure to calculate the exact moment-curvature thrust relations is now to start out with a constant value of P/P_{pl}. We can then determine the extension of the elastic region with respect to

M/M_{el} by eq. (66), and the corresponding elastic moment-curvature relation is given by eq. (67). Between the elastic region and the transition given by Fig. 16, we are in the primary plastic regime, and in this regime we obtain the moment-curvature thrust relations by first inverting eq. (78) to calculate η as a function of η_{cy} for a given P/P_{pl} in the appropriate range as given by Fig. 16. We then use eqs. (82) and (85) to calculate the corresponding values of M/M_{el} and K/K_{el}.

In the secondary plastic regime, we use eqs. (90) and (94) to calculate $\bar{\eta}$ and η_{ty} as a function of η_{cy} for a given P/P_{pl}, corresponding to η_{cy} values in the secondary plastic regime. We then use these values of η_{cy}, η_{ty}, and $\bar{\eta}$ in eqs. (98) and (101) to calculate M/M_{el} and K/K_{el} respectively. The resulting exact moment-curvature thrust relations are plotted in Fig. 17. In Fig. 17 we have also plotted the approximate moment-curvature thrust relations which are obtained by using eqs. (222) and (229). From this figure we can see that, even if the approximate relations are much simpler to use than the exact ones, the accuracy is reasonable and is always within 10% for our case.

In order to be able to do numerical calculations for the Shanley model, certain parameters must be selected. These parameters that we need to know, are ξ, W_o/L, k_s, E/f_y, dk, and L/H.

With the above mentioned parameters given, the calculation procedure for the Shanley model in order to obtain the non-dimensional axial force-axial displacement $p-\delta$ relationship, and the non-dimensional axial force-curvature $p-k$ relationship is to start out using eqs. (181) and (183) to calculate p_c and k_o respectively. With p_c and k_o given we then calculate p_{el}, which is the value of p corresponding to first yield, from eq. (180). We can now use eqs. (174) and (175) to calculate the elastic $p-k$ and $p-\delta$ relationship respectively for values of $p < p_{el}$.

In the elastic plastic range we must use an incremental procedure with increments in dk in order to obtain the $p-k$ and $p-\delta$ relations. The initial values in this incremental procedure correspond to the transition from elastic to plastic behavior, i.e. first yield.

The initial value of p in this incremental procedure corresponds

to p_{el} as given by eq. (180), and the initial values of e and e_R are found from eqs. (171) and (173) respectively. First yield corresponds to $\zeta=1$, and then the initial value of k can be found from eq. (185). With k and e given we can calculate η_{cy} and η_{ty} from eqs. (216) and (220) respectively. The maximum value of η_{cy} and η_{ty} is H/2. With η_{cy} and η_{ty} known, we proceed with calculating $\bar{A}$, $\bar{S}$, and $\bar{I}$ from eqs. (150), (152), and (154) respectively. and then C_1, C_2 and C_3 from equs. (144), (145) and (146). We are now able to calculate the incremental response de, dp, and de_R from eqs. (147), (148), and (169) and (170) respectively. Then finally we can calculate the incremental response $d\delta$ from the incremental version of eq. (166). We then update e, p, e_R, δ, and k by adding the incremental values to the initial, and we have completed one step. After the first step we must go back and calculate η_{cy}, η_{ty} and so on for the updated values.

In order to make this process converge, the increment in curvature dk to be used must be rather small. The first steps are most critical and the value of dk can be increased later on. By trying different values of dk it was found for our cases that dk = 0.01 should be used in the first 50 steps of each Shanley model calculation, and in the following steps a value dk = 0.05 was found to be sufficient.

Let us before we present the p- δ and p-k relations from the Shanley model, show the dependence of $\bar{A}$, $\bar{S}$ and $\bar{I}$ on ζ for k_s = 0 and various values of e. This dependence is shown in Figs. 18, 19, and 20 respectively. We see from Fig. 19 that beyond first yield ($\zeta=1$) $\bar{S}$ is different from zero. Thus from eq. (135) the curvatures produce axial forces, and from eq. (140) the axial strains produce bending moments.

Four different cases are now analyzed. The first case is given by: w_o/L = 0.0015, k_s = 1/270, E/f_y = 2.1 x $10^5/355$ and L/r = 30. The value of L/r = 30 corresponds to L/H = 12.25 for a rectangular cross-section. The p- δ relation for this first case with L/H = 12.25 is shown in Fig. 21, and the corresponding p-k relation is shown in Fig. 22.

The second case is the same as the first one except for L/r which now is equal to 70. This corresponds to L/H = 28.58 for a column of rectangular cross-section. The p-δ relation for this second case with L/H = 28.58 is shown in Fig. 23 and the corresponding p-k relation shown in Fig. 24.

The third case corresponds to $W_o/L = 0.0005$, $k_s = 1/270$, $E/f_y = 638$ and L/r = 49.504. This value of L/r corresponds to L/H = 20.21 for a column of rectangular cross-section. The p-δ relation for this third case with L/H = 20.21 is shown in Fig. 25, and the corresponding p-k relation is shown in Fig. 26. The final case corresponds to the third except for the value of W_o/L which now equals 0.013. The p-δ relation for the final case is for the sake of comparison also plotted in Fig. 25, while the p-k relation is plotted in Fig. 27.

In order to evaluate the results from the Shanley model analysis it is now highly desirable to compare the results from the Shanley model with the exact solutions. The exact solution is however very time consuming to obtain. We can get around this problem by comparing the Shanley model results with the results from the approximate analysis. We can do this because we have already shown that these approximate relations are very close to the exact ones in Fig. 17. The approximate non-dimensional axial force curvature p-k relations are given by eq. (231). The resulting p-k relation corresponding to the cases analyzed by the Shanley model is plotted in Figs. 22, 24, 26, and 27 for comparison. The agreement between these two independent analysis methods is seen to be good.

4. STRENGTHENING CRITERIA

Rational criteria must be developed for the strengthening requirements of Ice-Transiting Vessels. Existing requirements are not always on the conservative side as evidenced by the ice damage to the USNS MAUMEE, and to other Class C strengthened MSC ships such as the TOWLE and WYANDOT. Recently two Canadian ships, one an icebreaker and the other a commercial ice-transiting vessel, suffered extensive hull damage while operating in an ice zone specified by the Canadian Arctic Shipping Pollution Prevention Regulations (CASPRR). It is interesting to note that greater strengthening requirements are imposed by CASPRR than by other regulatory bodies.

A detailed review of the existing strengthening criteria for ice navigation is presented in a recent Ship Structures Committee Report (42). In most cases strengthening requirements are based on Johansson's work (60) who suggested plastic design methods for their determination. The side plating between two adjacent transverse frames was considered as a clamped-clamped beam and the corresponding uniformly distributed collapse pressure was calculated. However, the side shell ship structure consists of a grillage of intersecting beams together with the associated plating. Thus the determination of the collapse pressure should be based in the consideration of all possible collapse mechanisms of the grillage structure. Ice damage records should be evalua ted on the basis of the collapse pressure of the grillage structure to define strengthening criteria for ice navigation.

In the present investigation the ultimate strength of transversely loaded rectangular grids subjected to ice loading is studied. The method described in Ref. 76 is used to obtain the yield point load of rectangular grillages loaded by lateral loads. A grid is considered which consists of two sets of parallel beams at right angles to each other. The grid is loaded by a discrete number of lateral loads which are applied at the nodes of the grillage structure. The lower bound theorem of limit analysis is used to determine a statically admissible distribution of beam moments which nowhere exceed the maximum bending moment (yield moment) of the beam.

A listing of the computer code BEAMPLT was kindly supplied by the senior author of Ref. (76). The code BEAMPLT is a program for finding the yield point load of transversely loaded rectangular grids. The maximum statically admissible multiplier and an associated moment distribution are computed using Linear Programming Techniques.

The necessary modifications have been made to the code BEAMPLT so that the code now interfaces with the M.I.T. computing system facilities. Furthermore, a subroutine has been prepared in order to convert a prescribed ice loading uniformly distributed over a given rectangular region, to equivalent nodal point loads. The output of this subroutine forms the necessary input loading to the BEAMPLT program. The extent and location of the ice loading are independent variables of the problem.

A description of the ICEGRID program (modified BEAMPLT code) is presented in the next section.

4.1 ICEGRID PROGRAM DESCRIPTION

ICEGRID is a FORTRAN computer program that uses plastic methods of analysis to obtain the response of grillages subjected to uniformly distributed transverse loads. Although ICEGRID can be used for many different problems, the specific application discussed in this report is for ship or offshore structures subjected to ice loading.

ICEGRID is a modification of the computer program, BEAMPLT, developed by Tait and Hodge (76), for finding the yield point load of a transversely loaded point, flat, rectangular grillages. BEAMPLT uses the lower bound theorem of limit analysis to find the maximum safety factor of the grillage and the associated bending moment distribution. The maximum safety factor of the grillage is defined as that multiplier of the applied loads such that the grillage will just collapse under the load (PP)$f_{i,j}$ (see Fig. 28) but will support any smaller multiplier of the applied loads. A detailed description of BEAMPLT is provided in Ref. (76).

BEAMPLT solves the problem of grillages subjected to point loads acting at the nodes where two beams intersect. In order to analyze the problem of ice loading against a structure it is desirable to

consider the effect of "patch" and line loads. These loads could be used to simulate the pressure an ice sheet would exert against a structure. The horizontal axes of patch or line loads are parallel with the waterline. Point loads could represent localized regions of high ice pressure loading that might be associated with consolidated (multiyear) pressure ridge interactions (Gerwick (4) and Rojansky and Gerwick (17)).

It is also important to have the option to apply these loads at any location within the grillage and not only at the beam intersections. ICEGRID was developed to provide BEAMPLT with the ability to solve the ice-structure problem.

The problem considered is to find the collapse load for a plated grillage of perpendicular beams subjected to a set of transverse loads. The strength of the plating is accounted for by altering the yield moments due to the beams alone (25). This structural model is valid when plate failure modes are not important. Coburn (43) reports that the U.S. Coast Guard's experience with ice damage has been primarily due to frame failures and no significant failures of plates between frames have been observed.

The applied transverse loads are converted into statically equivalent point loads located at the appropriate intersections of beams by using the lever arm principle. Once the equivalent point loads have been determined ICEGRID follows the same procedure as BEAMPLT for finding the safety factor and the associated moment distribution. Included in Ref. (25) is a detailed description and listing of subroutine GRID which converts the general loads into statically equivalent loads located at beam intersections.

BASIC ASSUMPTIONS

It is assumed that the grid is made of a perfectly plastic material and that deformations are infinitesimal prior to collapse. The torsional strength of the beams is neglected and each beam has a maximum bending moment (yield moment) that can be transmitted across its cross-section. Based on these assumptions the lower bound theorem of limit analysis is used to calculate PP.

It is assumed that the yield moments of the beams in the horizontal direction are all equal, as are those in the vertical direction.

The simulated ice loads are represented as uniformly distributed rectangular patch loads, uniform line loads, or point loads as discussed previously.

The major assumption made is that distributed loads can be adequately modelled as statically equivalent nodal point loads. Clearly the two cases do not provide the same collapse load estimate. A method is presented in Ref. (25) to account for these differences.

INPUT DATA

The input data required by ICEGRID consist of the beam yield moments, the number of nodes along the top and side, the horizontal and vertical spacing between beams, the number of loads, the load data-including load type, magnitude, dimensions and centroid location and the boundary conditions specified along the grillage's boundaries.

GRID SUBROUTINE

Once the load data have been specified ICEGRID branches to subroutine GRID to convert the original loads into statically equivalent loads located at the intersections of beams. GRID finds the location of the load within the grillage and determines the load distribution for each grid. The lever arm principle is then used within each grid to determine the statically equivalent forces at the four corners of the grid. The nodal forces are then summed for nodes that are common to two or more grids which are subjected to loading. The resulting nodal forces are then transferred back to ICEGRID at the appropriate nodal points. A detailed description of GRID is provided in Reference (25).

4.2 PROBLEM FORMULATION

EQUILIBRIUM EQUATIONS

A detailed discussion of the formulation of the equilibrium equation is presented in Reference (76). A brief summary is given below.

The matrix system used to identify the nodes and moments is shown in Fig. 29. The row and column indicating the location of a node is given by i and j respectively. Figure 29 shows a free body diagram of an interior node i,j, and the associated beam lengths, bending moments and shear forces.

Since the torsional moments are neglected, the two horizontal moments $M_{i,j}$ at the nodes are numerically equal, as are the two vertical moments $M_{i,j}$. Moment equilibrium of the beam segment with length ℓ_{j-1} requires that

$$V_2 = V_2 = (M_{i,j} - M_{i,j-1}) / \ell_{j-1} \qquad (232)$$

Similar expressions can be obtained for the other beam segments.

Force equilibrium at the node i,j in Figure 29 is satisfied by

$$V_2 + V_3 + V_6 + V_7 = (PP) f_{i,j} \qquad (233)$$

where PP is the load factor and $f_{i,j}$ is the applied point load at node i,j. Substituting the shear force expressions (equation (232)) into equation (233) gives the governing equation for node i,j which is solved by ICEGRID in terms of the nodal moments and safety factor PP:

$$\frac{Mi,j-Mk,j-1}{\ell_{j-1}} \quad \frac{Mi,j-Mi,j+1}{\ell_j} \quad \frac{^1Mi,j-^1Mi-1,d}{\ell_{i-1}} \quad \frac{^1Mi,j-^1Mi+1,j}{\ell_1}$$

$$= (PP) f_{i,j}$$

This equation satisfies equilibrium for an interior node. For nodes located at, or adjacent to, the grillage boundaries equation (234) may be simplifed depending upon the boundary conditions. The two boundary conditions considered by ICEGRID are the clamped, and simply supported cases. If the boundaries are clamped an unknown moment will exist at each of the boundary nodes, but if the

boundaries are simply supported boundaries.

The yield moments of symmetric beam with at least one axis of symmetry are computed form the material yield stress and the cross-sectional dimensions of the beam.

ICEGRID assumes that all horizontal beam have a yield moment of M_o. The unknown nodal moments must therefore satisfy teh following relations

$$-M_o \leqslant M_{i,j} \leqslant M_o$$
$$-M_o' \leqslant M'_{i,j} \leqslant M_o' \qquad (235)$$

The lower bound theorem of limit analysis is now used to solve the following problem:

"Find a distribution of moments $M_{i,j}$ amd $M'_{i,j}$ which maximizes the load factor PP subject to the conditions given by equation (234) and inequalities (235)."

LINEAR PROGRAMMING PROBLEM

A linear programming procedure is used to solve for the load factor and unknown moments. The formulation of the linear programming problem is discussed in detail in reference (76) and a brief summary is given below. A typical linear programming problem seeks to maximize a scalar objective function ϕ which is defined as

$$\phi = \sum_{j=1}^{n} C_j X_j \qquad (236)$$

where the X_j represent the components of the unknown vector (X_1, X_3... X_n) and C_j are the objective function coefficients. ϕ is linearly dependent upon X_j and must satisfy a set of constraints

$$\sum_{j=1}^{n} a_{i,j} X_j \; (\cdot R_i \cdot) \; b_i \qquad (237)$$

where the symbol (•R•) may stand for any of =, $\leqslant$ or $\geqslant$. The variables b_i must be non-negative. The vector components Xj are also subject to the constraint

$$X_j \geq 0 \tag{238}$$

The linear programming problem may now be stated as:

"Find the vectors X_j which maximize ϕ subject to equations (237) and inequalities (238)."

In order to satisfy the requirement imposed by inequality (238) the horizontal and vertical moments are related to the vector components X_j by

$$X_k = M_{i,j} + M_o \quad \text{(Horizontal)}$$

$$X_\ell = M'_{i,j} + M'_o \quad \text{(Vertical)} \tag{239}$$

so that the inequalities (238) are transformed to

$$0 \leq X_k \leq 2M_o$$

$$0 \leq X_\ell \leq 2M'_o \tag{240}$$

An additional vector component X_z is defined as:

$$PP = X_z \tag{241}$$

Replacing PP by X_z in all of the equations (234) will transform them to the form of equation (237).

The lower bound problem has now been converted to a linear programming problem. After solving for the vector components X_j, the load factor and moments can be obtained from equations (241) and (239).

ICEGRID uses the International Mathematical and Statistical Library (IMSL) subroutine ZX3LP to solve the linear programming problem. A detailed discussion of ZX3LP including a simple example showing how ICEGRID arranges the input data for ZX3LP is given in Reference (25).

4.3 DISCUSSION

Several problems are solved using the ICEGRID program to study the effect of adding frames and/or stringers to a square plate subjected to a uniformly distributed patch load. The safety factors of two loading conditionsare plotted n Figures 30 and 31 for several grillages. The loading for both cases is assumed to be symetrically located between the main deck and inner bottom and to extend across the entire width of the grillage structure. The grillage length and height are taken to be equal to one as are the horizontal and vertical yield moments (any consistent set of units may be used). The forces per unit area of the patch load is also equal to one. Figures 30 and 31 show the results obtained for the cases of the vertical extent of the load (=ice thickness) being equal to .2 and .3 times the vertical dimensions of th plate respectively.

It is interesting to note that the grillages having three intermediate longitudinal stringers apparently have a lower safety factor than grillages with only two longitudinal stiffeners. This is due to the geometry of the problem and the conversion of the distributed load to statically equivalent loads acting at beam intersections. The grillage containing two longitudinals has the patch load centered between the stringers with each carrying half the load. The grillage having three stringers has the load centerd upon the middle stringer which supports most of the load. Thus the force supported by the middle stringer is greater than the force shared by the two adjacent longitudinal stringers and a smaller safety factor is calculated for the grillage containing three intermediate stringers. Once the ICEGRID program is modified to allow the formation of intermediate plastic hinges between beams it should be possible to correct this descrepancy.

A close look at the results shown in Figures 30 and 31 reveals that non-symmetric collapse mechanisms are obtained for the 5x5, 6x5, and 5x6 grillages. Since the grillages are symmetrically loaded and a symmetric solution must exist this implies that the solution is not unique. The possilibity of multiple solutions is discussed by Tait and Hodge (76). The lack of uniqueness explains the fact that in may cases yield moments are obtained that are not yield hinges. In general there will be at least as many excess yield moments as there

are degrees of indeterminancy.

The results of Johansson are also plotted in Figures 30 and 31. Johansson did not consider longitudinal stringers in his model and his results therefore do not change when additional stringers are added. The ICEGRID program allows various collapse mechanisms to form and the prediction of the collapse load is therefore expected to be lower than the collapse load predicted by Johansson who considered only one collapse mechanism. However, from the results plotted in Figures 30 and 31 it appears that Johansson's values are more conservative. The primary reason for this is that the ICEGRID program in its present state of development only allows plastic hinges to form at beam intersections. When ICEGRID is modified to allow the formation of intermediate plastic hinges between beams it is expected that the results will be more conservative than Johansson's.

Another plot showing the effect of increasing the number of intermediate frames and stiffeners is shown in Figure 32. This figure plots the ratio of the safety factor of a particular grillage (PP) to the safety factor of a grillage with only one intermediate frame (PP_1) versus the number of intermediate frames. It appears that these ratios remain constant for the loading conditions previously described as long as the loading height does not extend beyond the top or bottom of the grid it is centered in.

It must be re-emphasized that the results given here should only be used when the applied loads are acting at the nodal points of the grillage structure since the ICEGRID program does not allow the formation of intermediate plastic hinges and therefore does not allow many potential collapse mechanisms to occur. When the program is modified to allow intermediate hinges to form between beams then many of the shortcomings of the ICEGRID program could probably be resolved.

5. CONCLUSIONS

The present report very briefly summarizes existing methods to predict the maximum ice pressure exerted on the walls of the side shell structure of an Ice-Transiting Vessel. Furthermore methods are developed to define stiffness and strengthening criteria for the structural design of Ice-Transiting Vessels.

Methods to obtain structural criteria for ice navigation are given for the basic structural elements of the side structure: plates, stringers, frames and the grillage assembly. Plate criteria were suggested in References 41 , 62 , and 63 . These give very useful practical suggestions for plate damage due to ice loading.

First-yield structural criteria for stringers and transverse frames are given in section 3.1 and Reference 82 . Ultimate plastic strength criteria for stringers and transverse frames are given in section 4 and References 25 , and 26 . Elastic-plastic buckling criteria for transverse frames are given in sections 3.2 and Reference 84 .

Structural buckling criteria for transverse frames are very important since as reported in Reference 41 structural damage due to ice loading has always been associated with frame buckling or crippling of its web. As reported in Reference 39 these elastic-plastic frame buckling criteria are valid when the web depth to thickness ratio for flatbar sections is lower than about $0.4\sqrt{E/f_y}$ where E is the Young's modulus and f_y is the yield stress in compression. For higher values of this ratio web crippling is likely to occur and the method presented in Reference (67) is applicable.

Structural criteria for the grillage assembly can be obtained using the methods reported in section 4. We adopted to ice loading the limit analysis method presented in Reference (76). The listing of the resulting computer program is given in Reference (25).

More details of the work done on this project are reported in the following References: (14), (22), (25), (26), (36), (38), (40), (44), (83) and (84). In section 8.2 a bibliography search on torsional buckling and tripping is included.

6. RECOMMENDATIONS

There are two important aspects of the strengthening criteria problem that should be further investigated. The first one is the coupling of local frame buckling modes with the grillage mechanisms of collapse. The second one is the development of fracture-tearing criteria for the stiffened panel assembly.

The coupling of local modes to grillage mechanisms should be considered. One should check if this coupling results in lower collapse loads than the ones predicted without considering this effect. One way to develop this method is to incorporate into the grillage code presented in section 4 the numerical buckling method presented in section 3.2. Alternatively one may want to use the approximate method presented in section 3.2.

Another important area for further work from the practical viewpoint is the development of fracture-tearing criteria for the stiffened panel assembly. The photographs of ice damage included in Reference 42 show an example of such a mode of failure.

7. ACKNOWLEDGEMENTS

The authors are indebted to the American Bureau of Shipping and to the M.I.T. Sea Grant Office for their support of this project. In particular the authors appreciate the comments received by Dr. D. Liu, Dr. Y. N. Chen and Mr. A. Chen of the American Bureau of Shipping and by Professor C. Chryssostomidis of the Department of Ocean Engineering of M.I.T. The authors wish to express their appreciation to Professor P. G. Hodge of the University of Minnesota for providing a listing and description of the computer program BEAMPLT developed by himself and P. Tait for work under contract with the Office of Naval Research for allowing the use of the BEAMPLT program in this project.

8. REFERENCES

The list of references is given below, in alphabetical order by the authors' name.

8.1 REFERENCES RELATED TO LOCAL ICE RESPONSE

1. A. Assur, "Composition of Sea Ice and its Tensile Strength," U.S. Snow, Ice and Permafrost Research Establishment, Research Report 44,1960.

2. C.G. Daley, J.W. St. John and F. Seibold, "Analysis of Extreme Ice Loads Measured on USCGC Polar Sea," Trans. SNAME, November 1984.

3. G. Frankenstein and R. Garner, "Equations for Determining theBrine Volume of Sea Ice from -0.5° to -22.9° C," Journal of Glaciology, Vol. 6, No. 48, 1967, pp. 943-944.

4. B.C. Gerwick, Jr., R.W. Litton, and R.B. Reimer, "Resistance of Concrete Loads to High Concentrated Ice Loads,: OTC 4111, Vol. III, Houston, Texas, May 1981, pp. 425-436.

5. M. Hetenyi, "Beams on Elastic Foundation," The University of Michigan Press, Ann Arbor, 1946, pp. 1-255.

6. A.D. Kerr, "On the Detemination of Horizontal Forces a Floating Ice Plate Exerts on a Structure," Journal of Glaciology, Vol. 20. No. 82, 1978.

7. A.D. Kerr, "On the Buckling Force of Floating Ice Plates," IUTAM Symposium, Physics and Mechanics of Ice, Ed. Per Tryde, 1979.

8. K.N. Korzhavin, "Action of Ice on Engineering Structures," U.S.S.R. Academy of Science, Siberian Branch, 1962. Draft translation by U.S. Army CRREL, 1971.

9. J.R. Kreider, "Determining Local Pressure Area Curves for Design," Workshop on Breaking Process of Ice Plates," M.I.T Department of Ocean Engineering, Cambridge, Massachusett November, 1984.

10. P.R. Kry, "A Statistical Prediction of Effective Ice Crushing Stresses on Wide Structures," IAHR Ice Symposium, Lulea, Sweden, 1978.

11. J.W. St. John and C. Daley, "Shipboard Measurement of Ice Pressures in the Bering, Chukchi and Beaufort Seas," ASME Conference ETCE 1984, New Orleans, February, 1984.

12. R.A. Major, D.M. Berenger and C.J.R. Lawrie, "A Model to Predict Hull-Ice Impact Loads in the St. Lawrence," SNAME Ice Tech Symposium, Montreal, Canada, April 1975.

13. B. Michel and R. Ramseier, "Classification of river and lake ice," Canadian Geotech. Journal, Vol. 8, No. 1, 1971, pp. 38-45.

14. A. Muina, "Design Proposals for Ice Pressures including Hull-Structure Interaction Effects," M.Sc. Thesis in Ocean Engineering, M.I.T., May 1983.

15. Y.N. Popov, O.V. Faddeyev, D.Y. Kheysin, and A.A. Yakovlev, "Strength of Ships Sailing in Ice," USSR Leningrad 1967, U.S. Army Material Command Techn. Transl., 1969, pp. 1-228.

16. A.Y. Rivlin, D.Y. Kheisin, "Investigation of Ships in Ice," Sudostroyeniye Publish House, Leningrad, 1980.

17. M. Rojansky and B.C. Gerwick, "Failure Modes and Forces of Pressure Ridges Acting on Cylindrical Towers," POAC 81, Quebec City, Canada, 1981, Vol. II, pp. 663-673.

18. J. Schwarz, "Engineering Properties of Sea Ice," Journal of Glaciology, Vol. 19, No. 81, 1977, pp. 499-531.

19. D.S. Sodhi and H.E. Hamza, "Buckling Analysis of a Semi-Infinite Ice Sheet," 4th International Conf. on Port and Ocean Engineering under Arctic Conditions, Sept. 1977, pp. 593-604.

20. P. Varsta, "Modelling of Impact Between Ship Hull and Ice," Proc. POAC 83, Helsinki, Finland, Vol. 2, 1983, pp. 760-777.

21. K.D. Vaudrey, "Ice Engineering-Study of Related Properties of Floating Sea-Ice Sheets and Summary of Elastic and Viscoelastic Analyses," Civil Engineering Laboratory, Technical Report R860, Port Hueneme, California, 1977.

22. P.C. Xirouchakis, T. Wierzbicki, "Plastic Failure of Floating Ice Beams," Third OMAE Symposium, New Orleans, Louisiana, Feb. 1984, pp. 166-172.

23. T. Watanabe, K. Yammamoto,N. Yoshimura, "Interaction Between Ice and Stiffened Panel," Proc. POAC 83, Helsinki, Finland, Vol. 3, 1983, pp. 458-467.

24. W.F. Weeks and A. Assur, "The Mechanical Properties of Sea Ice," CRREL Cold Regions Science and Engineering Monograph II-C3, Hanover, New Hampshire, 1967.

8.2. REFERENCES RELATED TO STRENGTHENING CRITERIA

25. G.L. Abbott, "Strengthening Criteria for Grillages Subjected to Ice Loads," Ocean Engineer and M.Sc. Thesis in Ocean Engineering, M.I.T., Feb. 1982.

26. G.L. Abbott, P.C. Xirouchakis, "On the Rational Selection of Strengthening Criteria for Navigation in Ice," Draft Final Report for First Year of Work on American Bureau of Shipping/Sea Grant Project, Feb. 1982, p.72.

27. J.C. Adamchak, "Design Equations for Tripping of Stiffeners Under In-Plane and Lateral Loads," David W. Taylor NSRDC-79/064, October 1979.

28. W.A. Alwis, T.Usami, "Elastic Lateral Torsional Buckling of Unbraced and Brace Planar Frames," Comput. Struct. Vol. 10, No. 3, June 1979, pp. 517-529.

29. American Bureau of Shipping, Rules for Building and Classing, Steel Vessels, 1980.

30. Atsuta, T. and Chen, W.F., Theory of Beam Columns, McGraw-Hill, 1976.

31. M.M. Attard, "Determining Experimental Lateral Buckling Loads by Extrapolation Techniques," UNICIV Rep. Ser. R. Uni. NSW Sch. Civ. Eng. 202, Mar 1982, p.16.

32. B.H. Barber, L.M. Baez, and G.J. North, "Structural Considerations in the Design of the POLAR class of Coast Guard Icebreakers," Paper C, SSC Symposium '75 Washington D.C. 1975..

33. D. Bartels, C.A.M. Bos, "Investigation of the Effect of the Boundary Conditions on the Lateral Buckling Phenomenon, Taking Account of Cross Sectional Deformation," Heron Vol. 19. No. 1,

1973, pp. 3-26.

34. C.M. Bender and S.A. Orszag, "Advanced Mathematical Methods for Scientists and Engineers," McGraw-Hill, New York, 1978.

35. F.S.K. Bijlaard, "The Design of Transverse and Longitudinal Stiffeners for Stiffened Plate Panels", Inst. for Building Materials and Building Structures, Heron Vol. 27, No. 4, 1982, p. 91.

36. G.P. Bore, "A Simplified Computer Program for the Analysis of Flat Rectangular Grillages," Ocean Engineer and M. Sc. Thesis in Naval Arch. and Marine Eng., M.I.T., August 1984..

37. T.G. Brown, "Lateral-Torsional Buckling of Tapered I-Beams," ASCE J. Struct. Div. Vol.. 107, No. 4, Apr. 1981, pp. 689-697.

38. R. Cancino, "Ultimate Strength of Rectangular Stiffened Plates Under Uniaxial Compression," Ocean Engineer and M. Sc. Thesis in Naval Arch. and Marine Eng., M.I.T., Aug. 1984.

39. C.A. Carlsen, W.J. Shao and S. Fredheim, "Experimental and Theoretical Analysis of Post-Buckling Strength of Flatbar Stiffeners Subjected to Tripping," Det norske Veritas, Technical Report 80-0149, February 1980.

40. C.F. Chen, "Design Proposals for Ship Grillages Subjected to Ice Loading," M. Sc. Thesis in Naval Arch. and Marine Eng., M.I.T., Dec. 1983.

41. R. Chiu, E. Hacicki and P.. Hirsimaki, "Application of Plastic Analysis to U.S. Coast Guard Icebreaker Shell Plating," Trans. SNAME, Vol. 89, November 1981, pp. 249-274.

42. J.L. Coburn, F.W. DeBord, J.B. Montgomery, A. Nawwar, D.W. Czimmek, and K.E., Dane, "A Rational Basis for the Selection of

Ice Strengthening Criteria for Ships," Ship Structures Committee Report 309, 1981.

43. J. L. Coburn "A Rational Basis for Hull Ice-Strengthening Criteria,: Spring Meeting of the Society of Naval Architects and Marine Engineers, Ottawa, Canada, June 17-18, 1981.

44. S.L. Coulter, "Design Proposals for Torsional Buckling of Stiffeners," Ocean Engineer and M. Sc. Thesis in Mech. Eng., M.I.T., June 1984.

45. P.F. Dux, S. Kitipornchai, "Buckling Approximations for Laterally Continous Elastic I Beams," Res. Rep. Ser. Uni. Queens Dep. Civ. Eng. No. CE11, April 1980.

46. M. Epstein, D.W. Murray, "Three-Dimensional Large Deformaton Analysis of Thin-Walled Beams," Int. J. Solids Struct. Vol. 12, No. 12, 1976, pp. 867-876.

47. J.H. Evans, "Ship Structural Design Concepts," 1975 and Second Cycle 1983, Cornell Maritime Press.

48. Y. Fukumoto, Y. Itoh, M. Kubo, "Strength Variation of Laterally Unsupported Beams," ASCE J. Struct. Div. Vol. 106, No. 1, Jan. 1980, pp.165-181.

49. Y. Fukumoto, Y. Itoh, "Statistical Study of Experiments on Welded Beams," ASCE J. Struct. Div. Vol. 107, No. 1, Jan. 1981, pp. 89-103.

50. Y. Fukumoto, M. Kubo, Ultimate Bending Strength of Plate Girders with Longitudinal Stiffeners Failed by Lateral Instability," Stahlbou, Vol. 46, No. 12, Dec. 1977, pp. 365-371.

51. Y. Fukumoto, M. Kubo, "Experimental Review of Lateral Buckling of Beams and Girders, Int. Colloq. on Stab. of Struct. Under Static and Dyn. Loads. Proc. Washington, D.C., May 1977, Publ. by ASCE, New York, NY, 1977, pp. 541-562.

52. M.K. Hakala, "A Non-linear Finite Element Analysis of an Ice-Strengthened Ship Shell Structure," Proc. Intern. Conf. on Eng. Application of the ?FEM, Vol. 2, Hovik, Norway, May 1979.

53. H.S. Harung, M.A. Millar, "Laterally Restrained Beam Columns with Uniform Biaxial Loading," Int. J. Mech. Sci. Vol. 15, No. 9, Sep. 1973, pp. 765-773.

54. M.R. Horne, R. Narayanan, "Design of Axially Loaded Stiffened Plates," ASCE J. Struct. Div., Vol. 103, No. 11, Nov. 1977, pp. 2243-2257.

55. O. Hughes, "Ship Structural Design: A Rotationally-Based, Computer-Aided, Optimization Approach," 1983, Johng Wiley and Sons, New York.

56. S. Karve and C.P. Manoudakis, "Structural Design Criteria for Ice capable Tankers," Ship Structure Symposium '84, SSC and SNAME, October 1984.

57. J.B. Kennedy, M.K.S. madugula, "Buckling of Angles: State of the Art," ASCE J. Struct. Div., Vol. 108, No. ST-9, 1982, pp. 1967-1980.

58. S. Kitipornchai, N.S. Trahair, "Buckling of Inelastic I-Beams Under Moment Gradient," ASCE J. Struct. Div., Vol. 101, No. 5, May 1975, pp. 991-1004.

59. S. Kitiporhchai, N.S. Trahair, "Inelastic Buckling of Simply Supported Steel I-Beams," ASCE J. Struct. Div., Vol. 101, No. 7,

July 1975, pp. 1333-1347.

60. B.M. Johansson, "On the Ice-Strengthening of Ship Hulls," International Shipbuilding Progress," 1967.

61. B.M. Johansson, A.J. Keinonen and B. Mercer, "Technical Development of an Environmentally Safe Arctic Tanker," SNAME Spring Meeting/Star Symposium, Ottawa, Ontario, June 1981.

62. N. Jones, "Plastic Behavior of Ship Structures," Trans. SNAME, Vol. 84, 1976, pp. 115-145.

63. N. Jones, "Damage Estimates for Plating of Ships and Marine Vehicles," International Symposium on Practical Design in Shipbuilding, SNA Japan, Tokyo, October 1977.

64. C. Matsui, S. Morino, J. Kimura, "An Experimental Study on Inelastic Lateral-Torsional Buckling of H-Shaped Beam-Columns Permited to Sway," Mem. Fac. Eng. Kyushu Univ. Vol. 43, No. 1, Mar. 1983, pp. 69-85.

65. C.R. Michaelides, A.N. Koundadis, "Lateral Buckling of Elastically Restrained I Beams,: Epistem Phylla Anotates Sch. Polit. Mech. EMP, Vol. 4, No. 3 Jul-Sep. 1980, pp. 25-38.

66. S.P. Morchi, E.G. Lovell, "Lateral Buckling of Intersecting Connected Beams," ASCE J. Eng. Mech. Div. Vol. 104, No. 2, Apr. 1978, pp. 367-381.

67. N.W. Murray, "Buckling of Stiffened Panels Loaded Axially and In Bending," The Structural Engineer, Vol. 51, No. 8, August 1973, pp. 285-301.

68. D.A. Nethercot, "Buckling of Welded Hybrid Steel I-Beams," ASCE J. Struct. Div. Vol. 102, No. 3, Mar. 1976, pp. 461-474.

69. D.A. Nethercot, N.S. Trahir, "Design Rules for the Lateral Buckling of Steel Beams," Natl. Conf. Publ. Inst. Eng. Aust. N. 76/11 1976, Met. Struct. Conf., Prep. of Pap., Adelaide, Aust., Nov. 1976, pp. 20-23.

70. D.A. Peters, "Effect of Principal Bending Curvature on the Lateral Buckling of Uniform Slender Beams," ASME Pap. No. 77-APM-22 for Meet. Jun 1977, p. 6.

71. D.A. Peters, "Effect of Principal Bending Curvature on the Lateral Buckling of Uniform Slender Beams," J. Appl. Mech. Trans. ASME, Vol. 44, Ser. E, No. 2, Jun. 1977, pp. 311-316.

72. C.H. Popelar, "Optimal Design of Strucures Agains Buckling: A Complementary Energy Approach," J. Struct. Mech., Vol. 5, No. 1, 1977, pp. 45-66.

73. A.J. Reis, F.A. Branco, "Lateral and Local Stability of

Thin-Walled Sections under Eccentric Loading," Thin-Walled Strcut. Recent Tech. Adv. and Trends in Des. Res. and Constr. Int. Conf. Univ. of Strathclyde, Glasgow, Scott, Apr. 1979, Halsted Press, New York NY, 1980, pp. 705-717.

74. Shanley, F.R., Inelastic Column Theory, Journal of teh Aeronautical Sciences, Vol. 14, No. 5, May 1947.

75. C. Szymczak, "Buckling and Initial Post-Buckling Behavior of Thin-Walled I Columns," Comput. Struct. Vol. 11, No. 6, June 1980,pp 481-487.

76. P. Tait and P.G. Hodge, BEAMPLT: A Program for Finding the Yield-Point Load of Trnasversely Loaded Rectangular Grids, Report AEM-H1-26, Department of Aerospace Engineering and Mechanics, University of Minnesota, Minneapolis, January 1981.

77. T. Tarnai, "Lateral Buckling of Elastic Beams with Initial Stresses and Initial Deformations," Acta. Tech. Budapest, Vol. 87, No. 1-2, 1978, pp. 187-192.

78. A.L. Tunik, "Strength Standard for Arctic Ships," Proc. POAC '83, Helsinki, Finland, Vol. 2, April 1983, pp. 664-676.

79. P. Vacharajittiphan, S.T. Woolcock, N.S. Trahair, "Effect of In-Plane Deformation on Lateral Buckling," J. Struct. Mech. Vol. 3, No. 1, 1974, pp. 29-60.

80. P. Vacharajittiphan, N.S. Trahair, "Analysis of Lateral Buckling in Plane Frames," ASCE J. Struct. Div. Vol. 101, No. 7, July 1975, pp. 1497-1516.

81. P. Varsta, I.V. Droumev and M. Hakala, "On Plastic Design of an Ice-Strengthened Frame," WNRB Research Report No. 27, Finland 1978.

82. P.C. Xirouchakis, and R. Strotstrom, "On the Structural Analysis of Ice-Transiting Vessels," SNAME Spring Meeting/STAR Symposium, ICE TECH '81, paper No. 11, Ottawa, Ontario, June 1981, pp. 133-143.

83. P.C. Xirouchakis, "Arctic Technology II, Introduction," Arctic Technology and Policy, Proc. Second Annual MIT Sea Grant College Program Lecture and Seminar Series MIT, Cambridge, Massachusetts, March 1983.

84. J. Yanai, "An Elastic-Plastic Analysis of a Column with an Ideal I Cross-Section," M.Sc. Thesis in Naval Arch. and Marine Eng., MIT, August 1984.

85. H. Yoshida, Y. Imoto, "Inelastic Lateral Buckling of Restrained Beams," ASCE J. Eng. Mech. Div. Vol. 99, No. EM2, April 1973, Paper 9666, pp. 343-366.

APPENDIX A

NOMENCLATURE OF ICE TERMS

FLOATING ICE: Any form of ice found floating in water. This term includes ice that is stranded or grounded.

SEA ICE: Any form of ice found at sea which has originated from the freezing of sea water.

FIRST YEAR ICE: Sea ice of not more than one winter's growth. Thickness, 30 cm to 2m. (12" to 6').

OLD ICE: Sea ice which has survived at least one summer's melt.

OPEN WATER: A large area of freely navigable water in which sea ice is present in concentration less than 1/10.

ICE FREE: No sea ice present. There may be some ice of land origin (icebergs, growlers) present however.

FLOE: Any relatively flat piece of sea ice (65') or more across.

FLOEBERG: A massive piece of sea ice composed of a hummock or a group of hummocks frozen together and separated from any surrounding ice. It may float up to 5m (16') above sea level.

BRASH ICE: Accumulations of floating ice made up of fragments not more than 2m (6') across, the wreckage of other forms of ice.

APPENDIX A (cont.)

ICEBERG: A massive piece of land formed ice of greatly varying shape and size, showing more than 5m (16') above sea level. Icebergs in heights above sea level of 450' have been sighted in Canadian and Greenland Arctic waters.

MULTI YEAR ICE: Old ice up to 3m (10') or more thick which has survived at least two summers' melt.

PACK ICE: Any accumulation of Sea Ice other than fast ice, no matter what form it takes or how disposed.

ICE COVER: The ratio of an area of ice of any concentration to the total area of sea surface within some large geographic locale.

CONCEN-TRATION: The ratio in tenths of the sea surface actually covered by ice to the total area of sea surface, both ice covered and ice free, at a specific location or over a defined area.

COMPACT PACK ICE: Pack ice in which the concentration is 10/10 and no water is visible.

CONSOLIDATED PACK ICE: Pack ice in which the concentration is 10/10 and the floes are frozen together.

OPEN PACK ICE: Pack ice in which the concentration is 4/10 to 6/10 with many leads and polynyas, and floes are generally not in contact with one another.

BERGY BIT: A large piece of floating glacier ice, generally showing less than 5m (16') above sea level, but more than 1m (3') and of 100 sq. to 300 sq. metres (109 to 328 sq. yds.) in area.

APPENDIX A (cont.)

GROWLER: Smaller piece of ice than a Bergy Bit or FLOEBERG, extending less than 1m (3') above the sea surface and with an area of about 20 sq. metres (65 sq. ft.).

ICE UNDER PRESSURE: Ice in which deformation processes are actually occurring and hence a potential impediment or danger to shipping.

HUMMOCKING: The pressure process by which sea ice is forced into hummocks. When the floes rotate in the process it is termed screwing.

RIDGING The pressure process by which sea ice is forced into ridges.

RAFTING: The pressure process by which sea ice is forced into ridges.

FRACTURE: Any break or rupture through very close pack ice, consolidated pack ice, fast ice, or a single floe, resulting from deformation processes. Fractures may contain brash ice.

CRACK: A fracture that has not parted.

LEVEL ICE: Sea ice which is unaffected by deformation.

DEFORMED ICE: General term for ice which has been squeezed together and forced upwards or downwards, e.g., rafted ice, ridged ice, hummocked ice.

RIDGE: A line or wall of broken ice forced up by pressure. The submerged volume of broken ice under a ridge, forced downward by pressure, is known as Ice Keel.

HUMMOCK: A hillock of broken ice which has been forced upward by pressure. The submerged volume of broken ice under the hummock, forced downward by pressure, is known as a Hummock.

APPENDIX B

TRANSVERSE FRAME FOUNDATION MODULUS PREDICTION

The derivation of equation (17) is presented in this Appendix.

The deflection v_s at the midlength of the longitudinal stringer in way of ice loading length L, subjected to uniformly distributed ice loading of magnitude q per unit length is

$$v_S = 5qL^4/384EI_L \tag{B.1}$$

for simply supported boundary conditions, where E is the Young modulus of the hull structural material and I_L is the longitudinal stringer cross-sectional moment of inertia. For fixed ends the deflection v_F is

$$v_F = qL^4/384EI_L \tag{B.2}$$

In reality the ends of the longitudinal stringer are elastically restrained. An estimate of the resulting longitudinal stringer deflection v is made by taking the geometric mean of v_S and v_F

$$v = 0.005823qL^4/EI_L \tag{B.3}$$

For closely spaced longitudinal stringers the discrete elastic supports can be replaced by an imaginary continuous elastic foundation with elastic modulus

$$K_L = qL/vs_L = 171.73EI_L/s_L L^3 \tag{B.4}$$

where s_L is the longitudinal stringer spacing. The above condition is satisfied if s_L satisfies the inequality provided by (18).

9. TITLES OF FIGURES

Figure 1. Stress-strain rate curve for uniaxial compression and indentation of S2 ice at -10°C.

Figure 2. Maximum ice pressure as a function of ice thickness; vertical sided structures; I = 1, m = 1, K = $1/\sqrt{2}$, σ_c = 1958kPa (284 p.s.i.), τ_s = 296 kPa (43 p.s.i.), ρg = 1000 kg/m^3 (62.4 lb/ft^3), E_I = 3.9*10^{5}kPa (5.7*10^4 p.s.i.), ν_I = 0.34 and n = 1.

Figure 3. Ice sheet forces (sloping structure).

Figure 4. Geometry of the side shell structure.

Figure 5. Beam of rectangular cross-section subjected to pure bending.

Figure 6. Bilinear stress-strain relation.

Figure 7. Bending deformation of beam segment.

Figure 8. Stress distribution in the elastic-plastic range in the pure bending case.

Figure 9. Stress distribution in the elastic region when both bending moment and axial compression are considered.

Figure 10. Elastic-plastic stress distributions when both bending moment and axial compression are considered, a) Primary plastic, b) secondary plastic, c) fully plastic.

Figure 11. Generalized Shanley model.

Figure 12. Relation between curvature and rotation of the spring.

Figure 13. Displacement u_3 due to change in geometry.

9. TITLES OF FIGURES (cont.)

Figure 14. Stress and strain distibution in secondary plastic regime when strain hardening is included.

Figure 15. Moment-curvature relation in pure bending.

Figure 16. Moment-curvature thrust coordinates in the transition state between primary plastic and secondary plastic behavior.

Figure 17. Moment-curvature thrust relations.

Figure 18. Reduction of sectional area parameter $\overline{A}$ with extent of partial yielding.

Figure 19. Reduction of sectional area parameter $\overline{S}$ with extent of partial yielding.

Figure 20. Reduction of sectional area parameter $\overline{I}$ with extent of partial yielding.

Figure 21. Non-dimensional axial force versus axial displacement variation for Shanley model with L/H = 12.25.

Figure 22. Non-dimensional axial force versus axial displacement variation for Shanley model with L/H = 28.58.

9. TITLES OF FIGURES (cont.)

Figure 23. Grillage problem solved by: a) BEAMPLT, b) ICEGRID.

Figure 24. Free body diagram of an interior node.

Figure 25. Collapse load of grillages; load height/grillage height = 0.2.

Figure 26. Collapse load of grillages; load height/grillage height = 0.3.

Figure 27. Non-dimensional collapse load of grillages.

Figure 28. Ice pressure versus contact area from Reference (9).

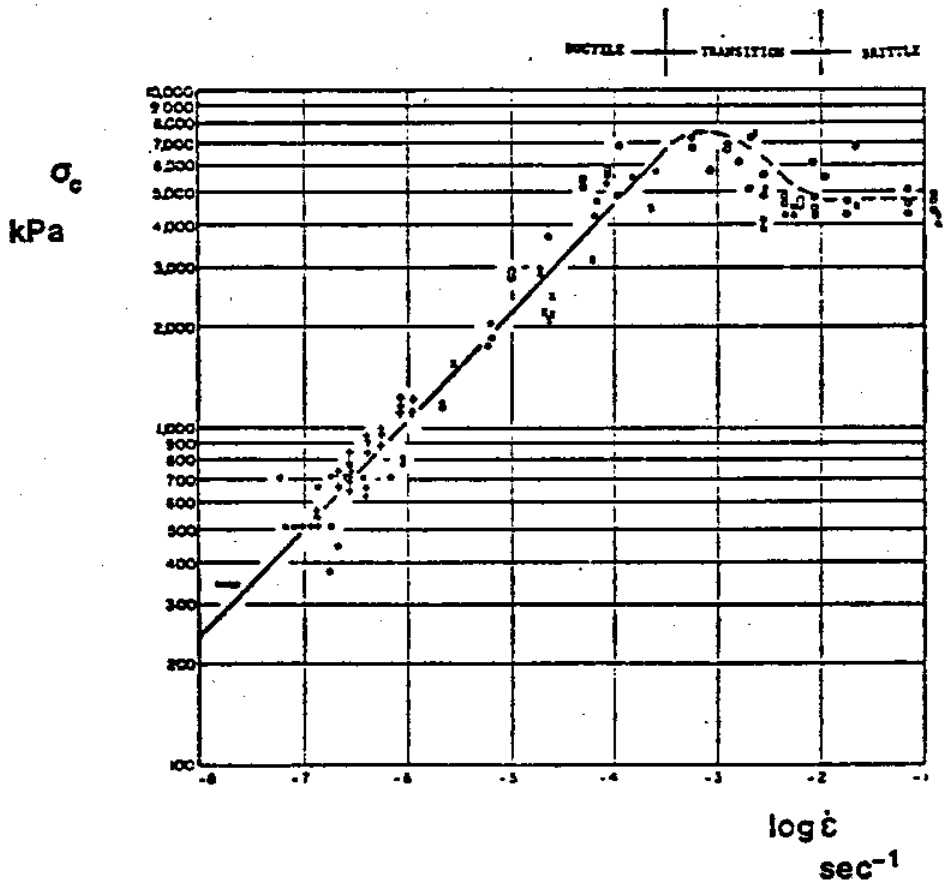
DUCTILE
TRANSITION
BRITTLE
σ_c
kPa
log $\dot{\varepsilon}$
sec^{-1}

FIGURE 1

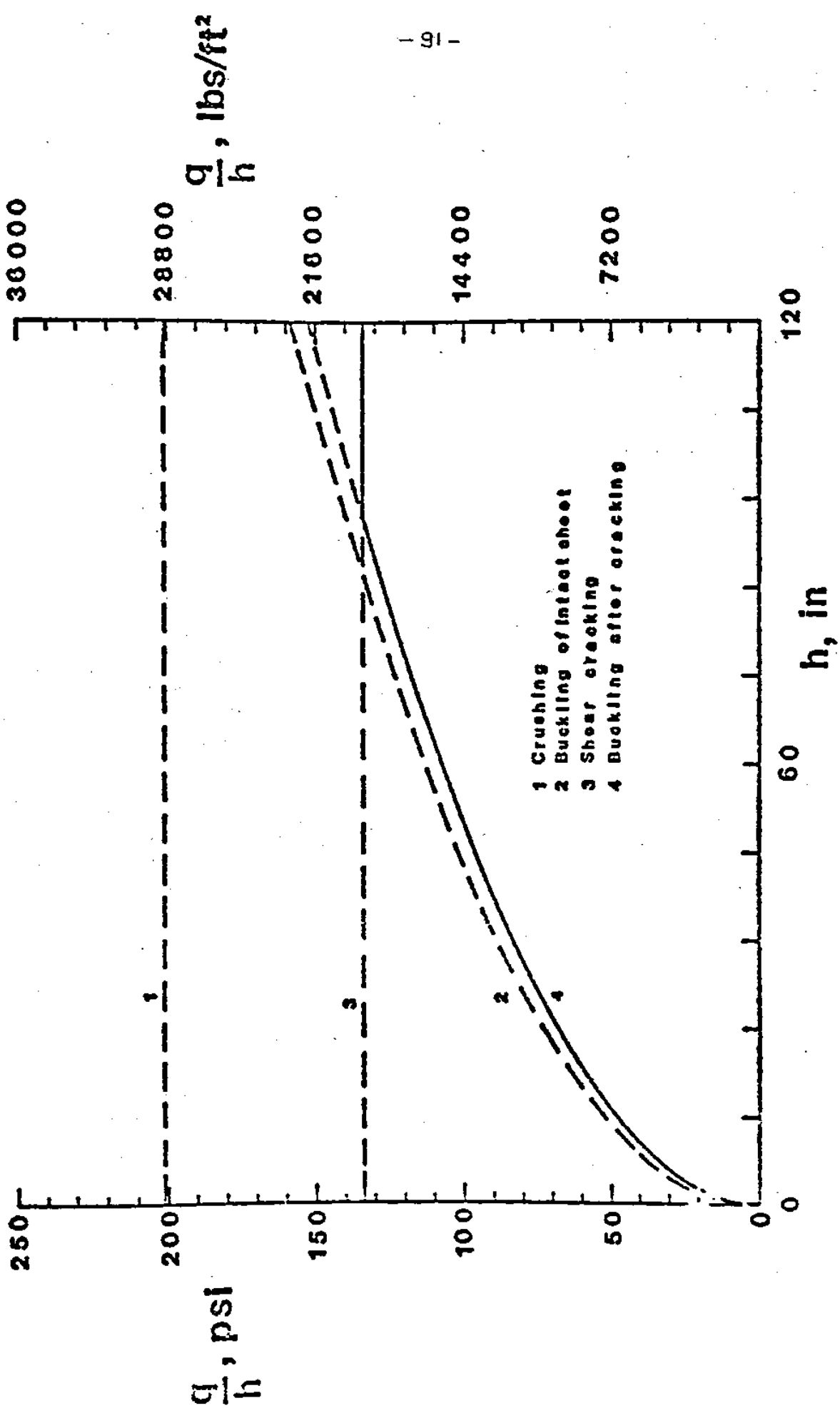
q/h, psi
250
200
150
100
50
0
0
60
120
h, in
q/h, lbs/ft²
36000
28800
21600
14400
7200
1 Crushing
2 Buckling of intact sheet
3 Shear cracking
4 Buckling after cracking
1
2
3
4

FIGURE 2

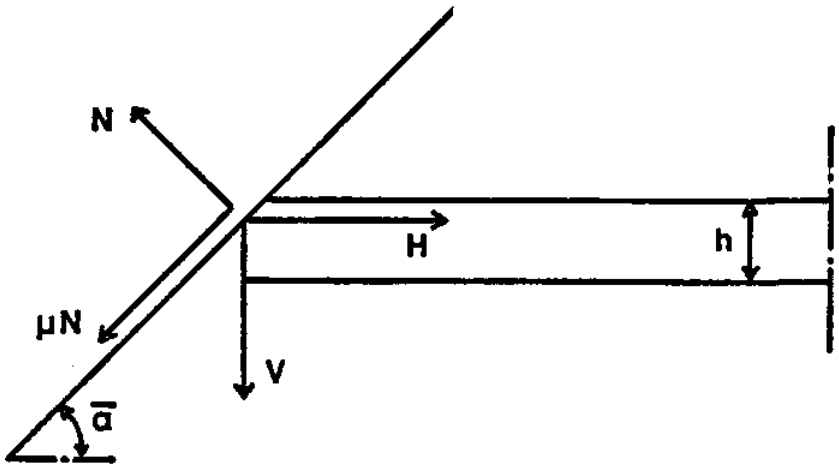

FIGURE 3

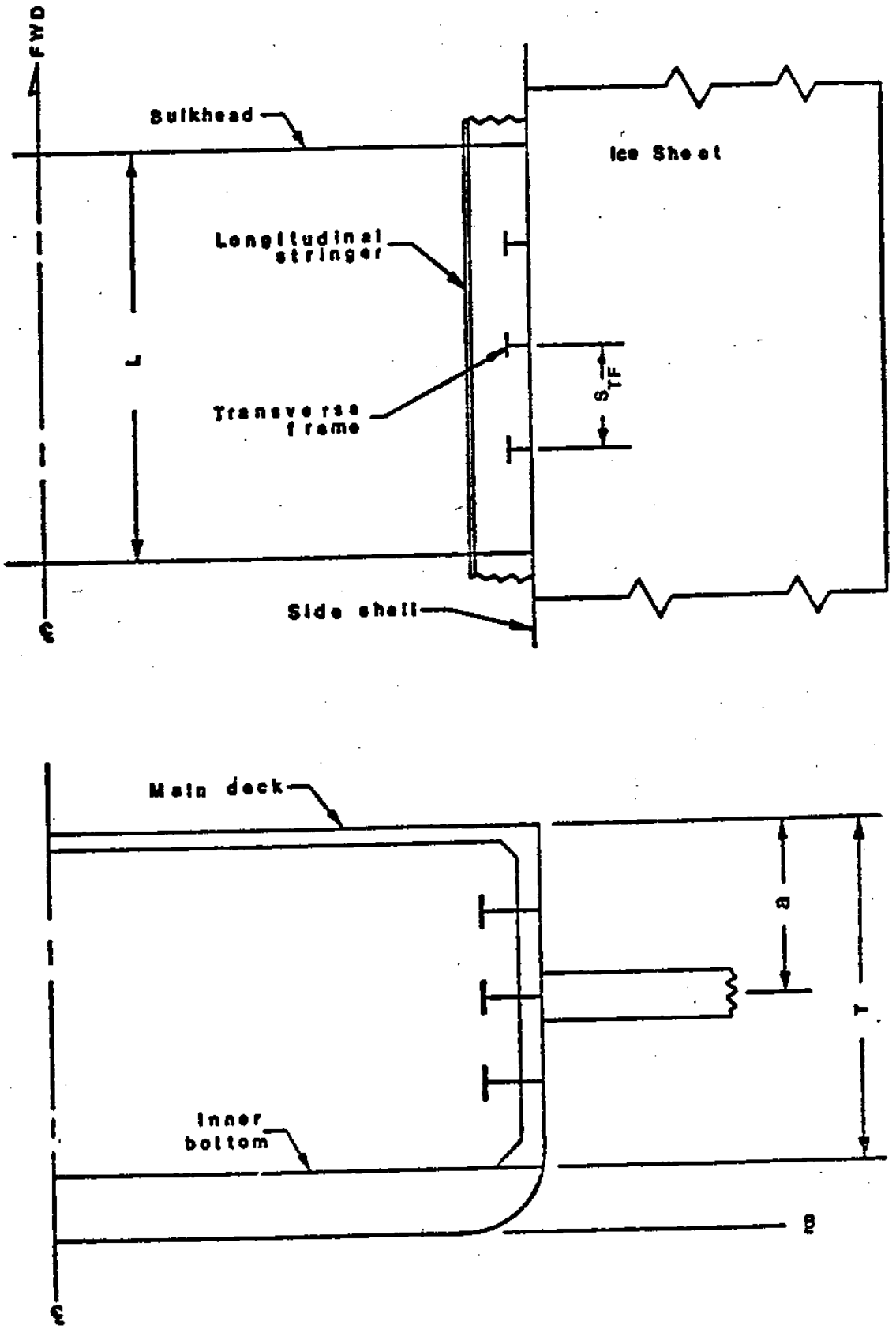
FWD
Bulkhead
Ice Sheet
Longitudinal stringer
L
Transverse frame
S_{TF}
Side shell
℄
Main deck
a
T
Inner bottom
B
℄

FIGURE 4

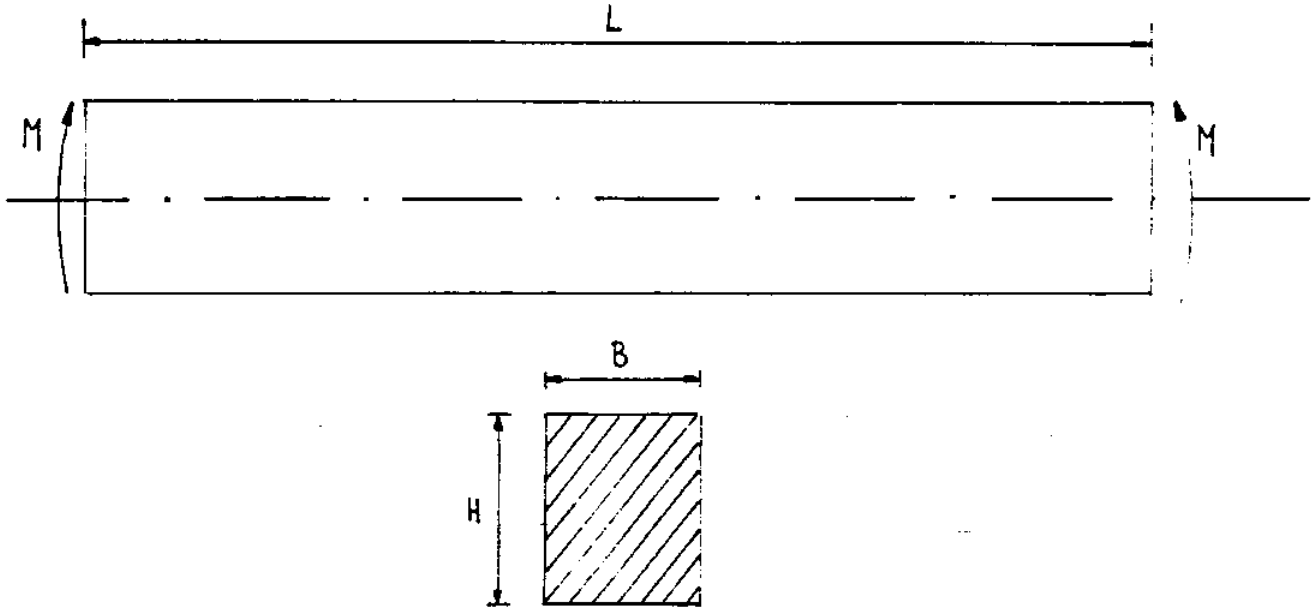

FIGURE 5

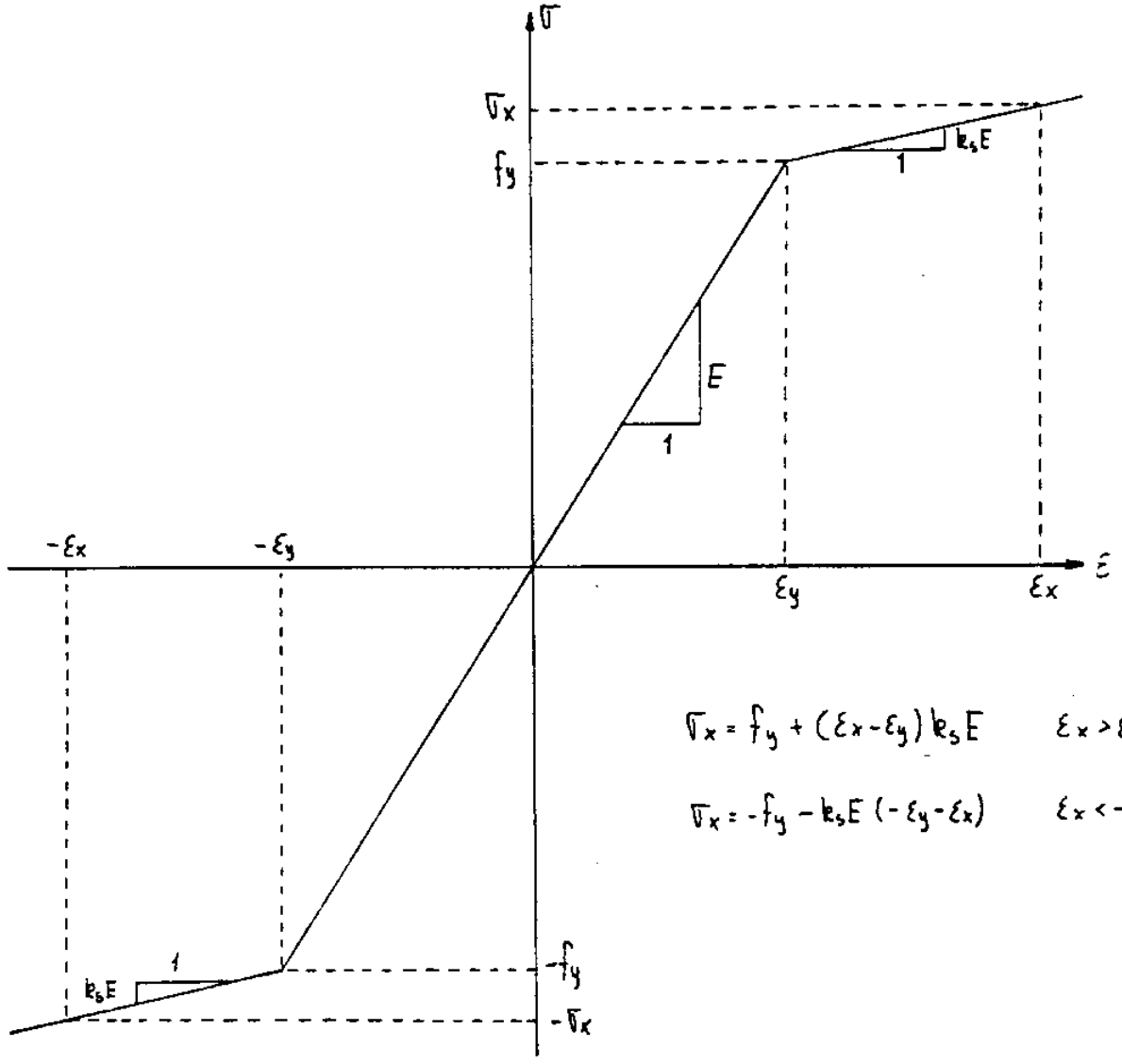

$$\sigma_x = f_y + (\varepsilon_x - \varepsilon_y)\, k_s E \qquad \varepsilon_x > \varepsilon_y$$

$$\sigma_x = -f_y - k_s E\,(-\varepsilon_y - \varepsilon_x) \qquad \varepsilon_x < -\varepsilon_y$$

FIGURE 6

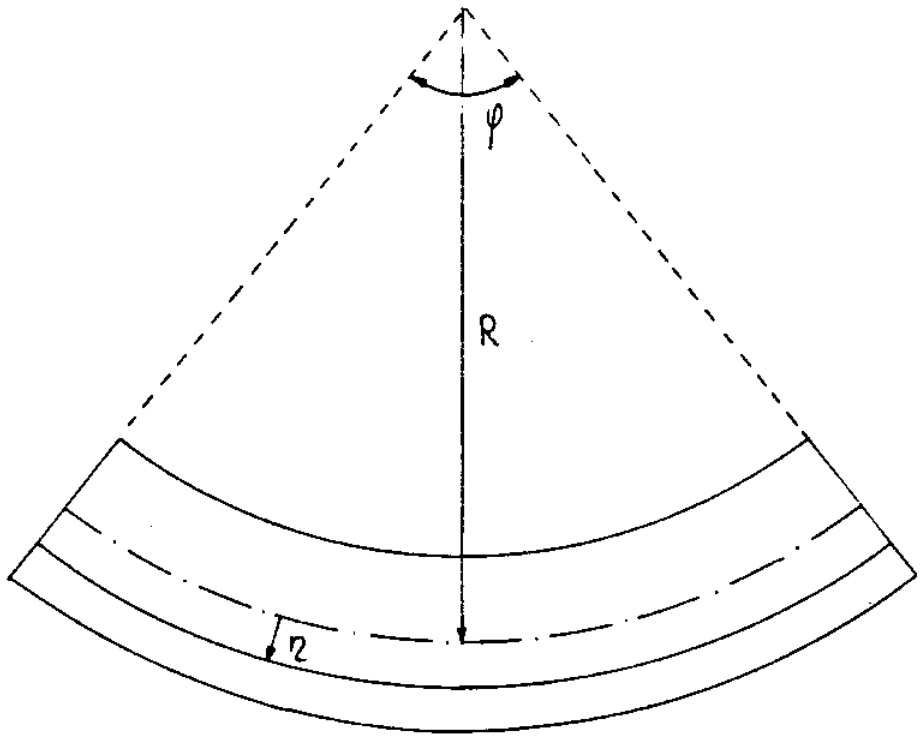

FIGURE 7

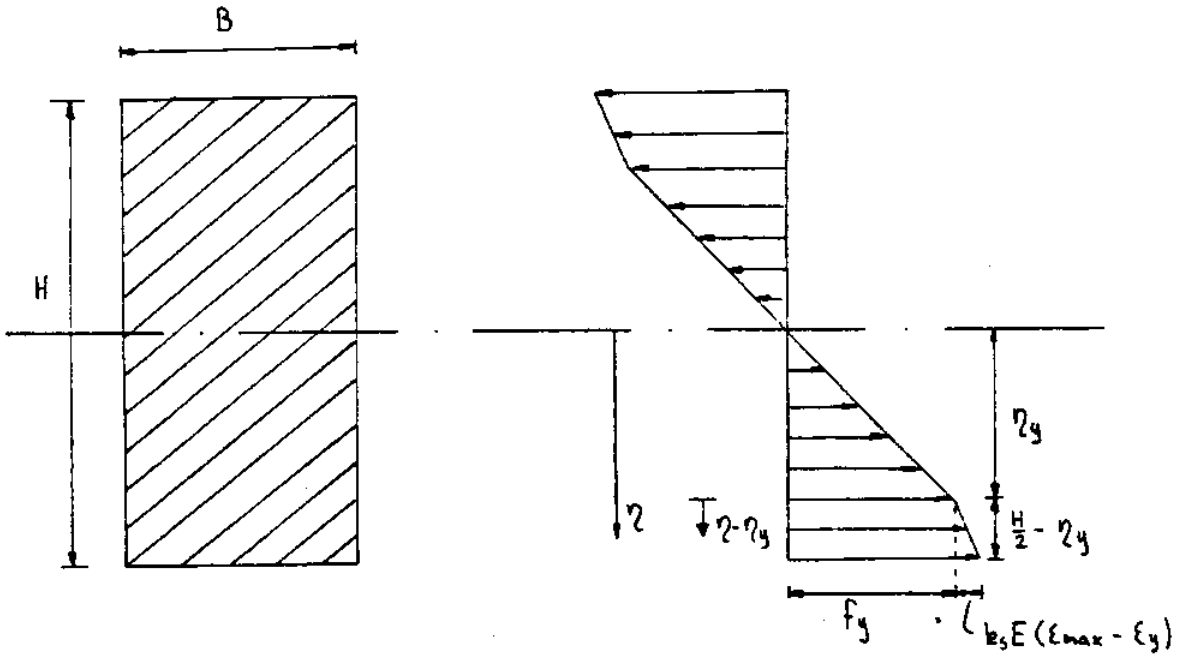

FIGURE 8

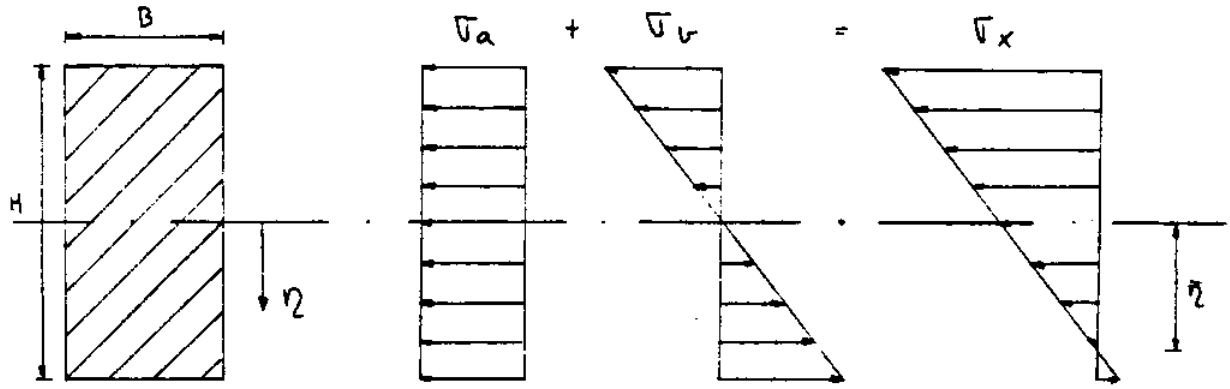

FIGURE 9

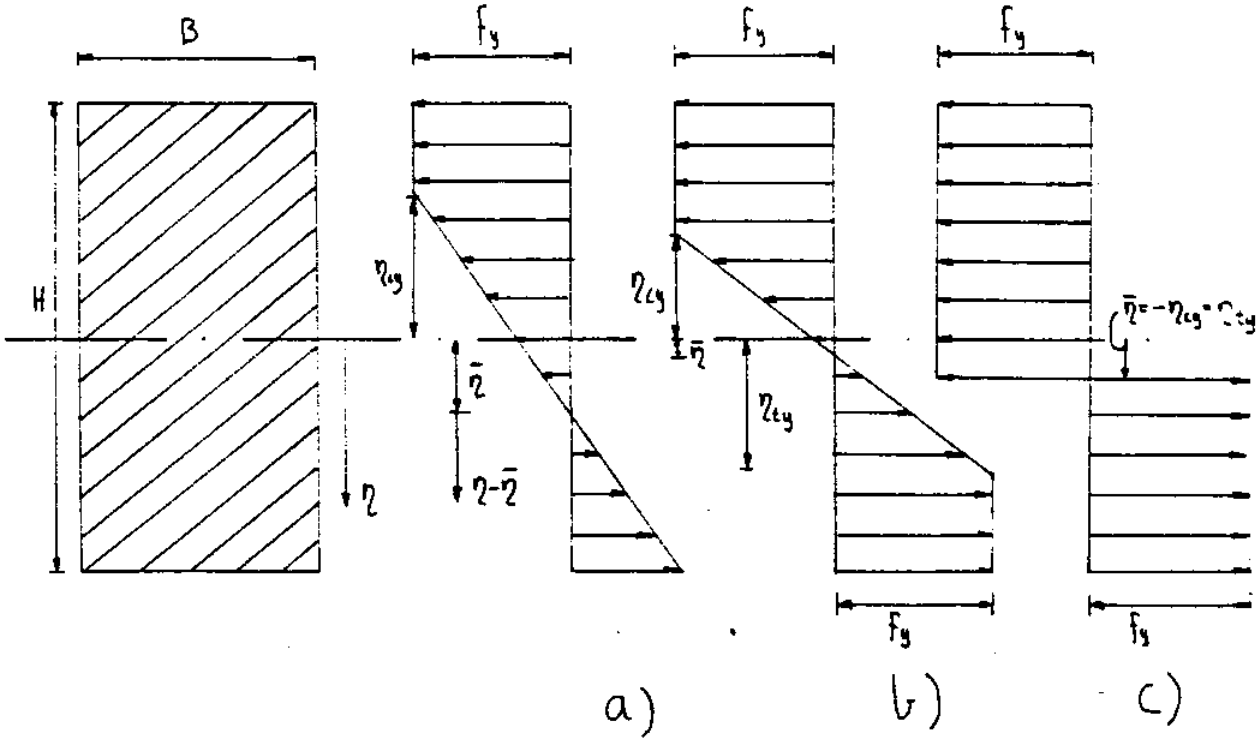

FIGURE 10

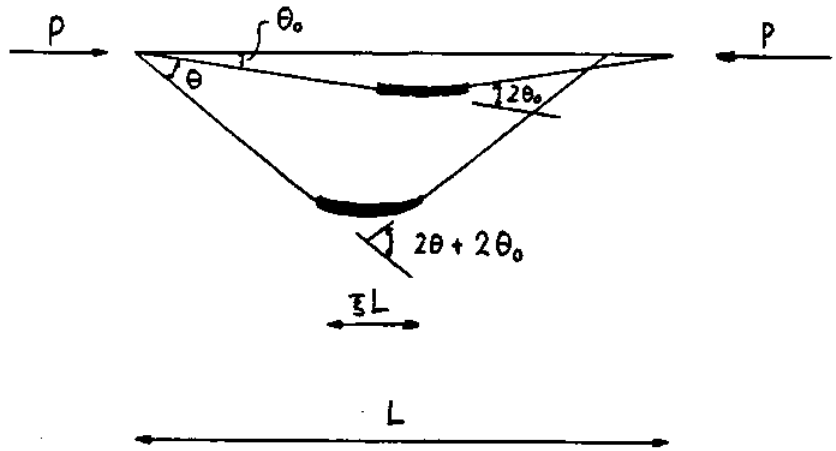

FIGURE 11

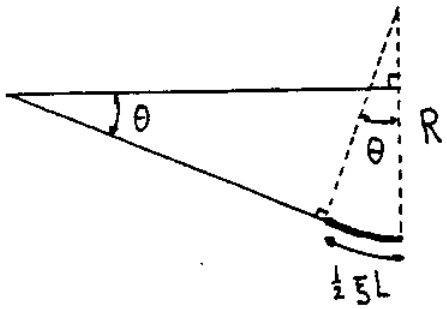

$$K = \frac{1}{R}$$

$$\theta = \tfrac{1}{2}\xi L \tfrac{1}{R} = \tfrac{1}{2}\xi L K$$

$$2\theta = \xi L K$$

FIGURE 12

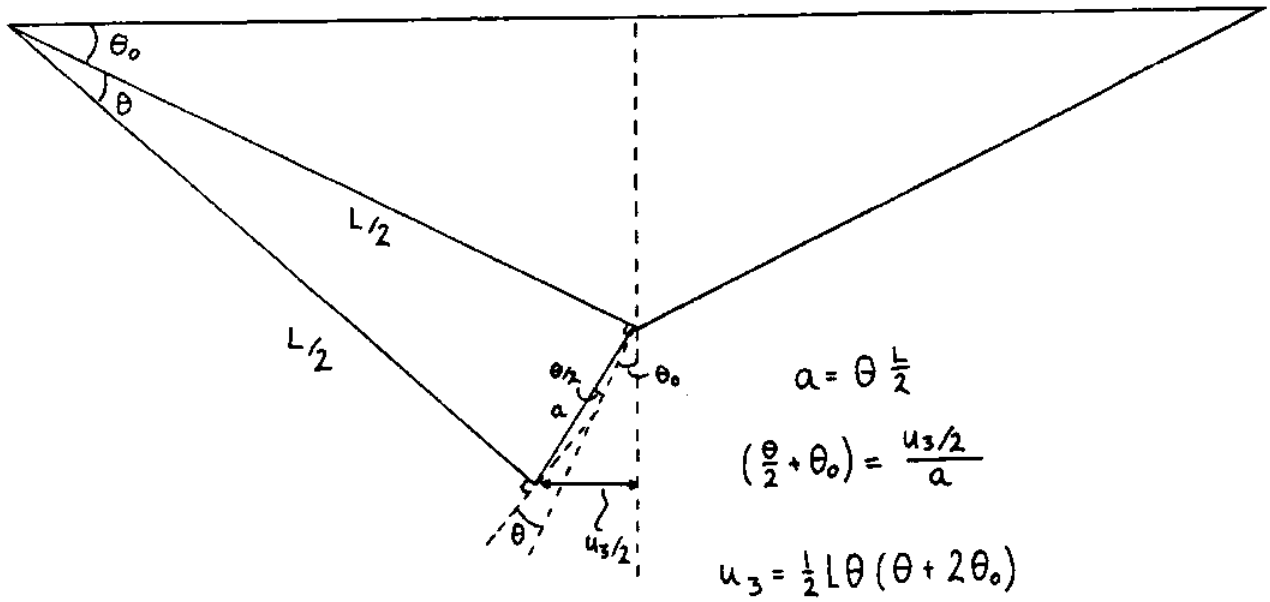

FIGURE 13

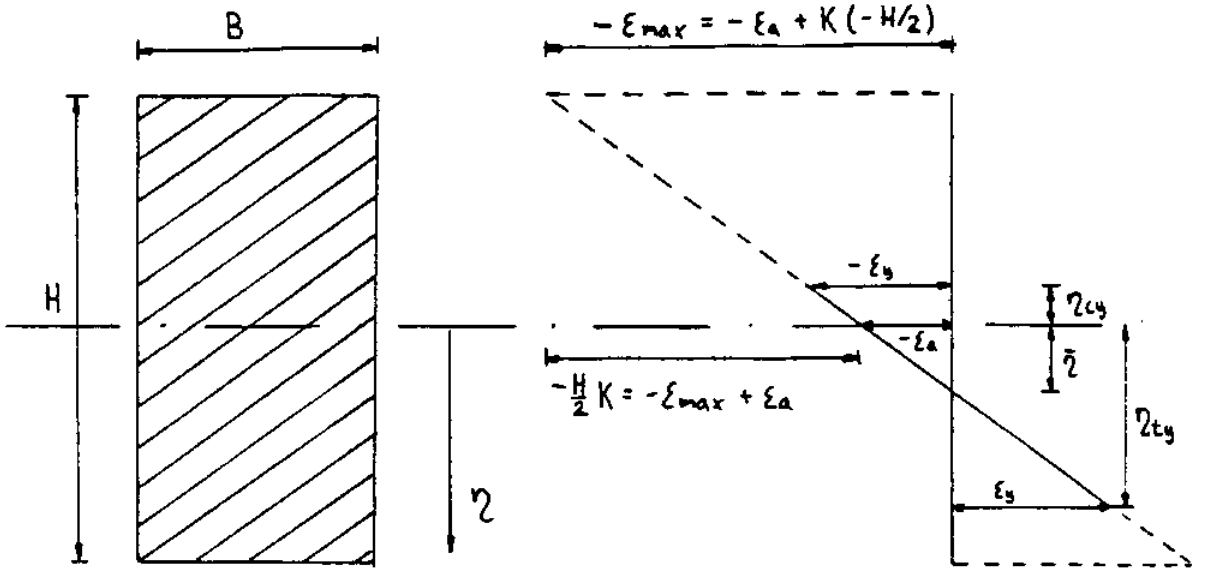

a) Strain

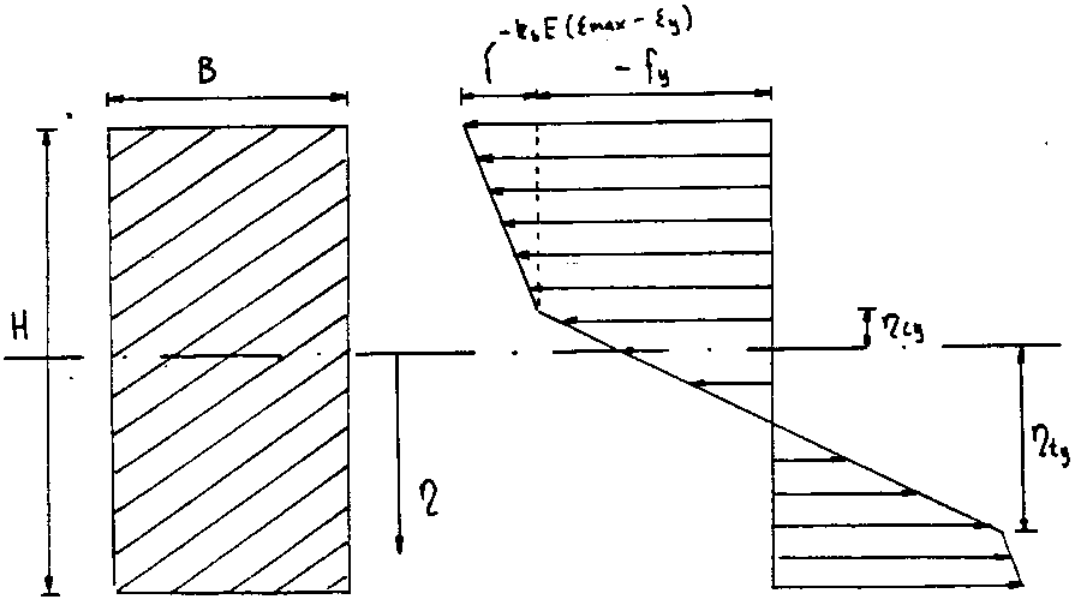

b) Stress

FIGURE 14

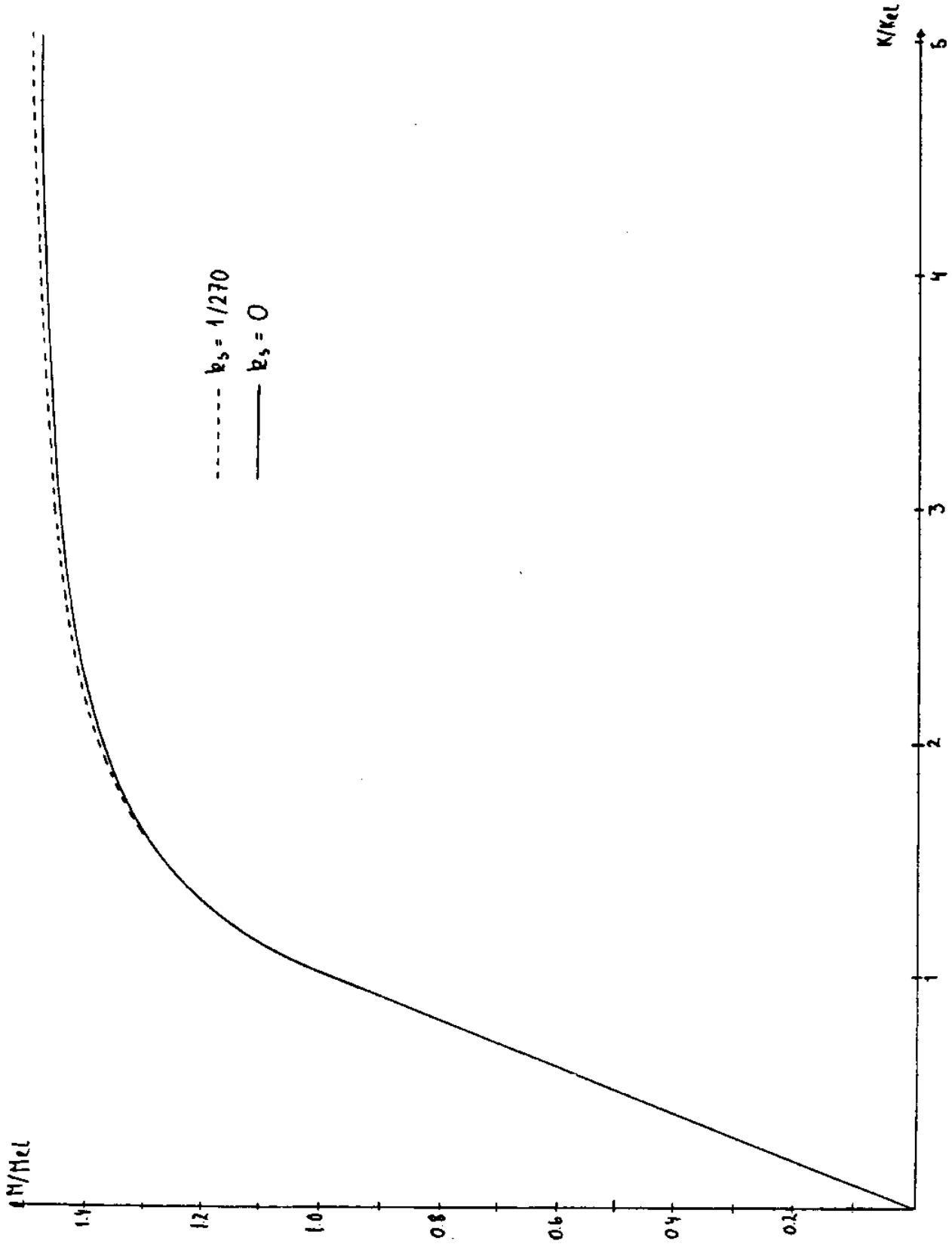

FIGURE 15

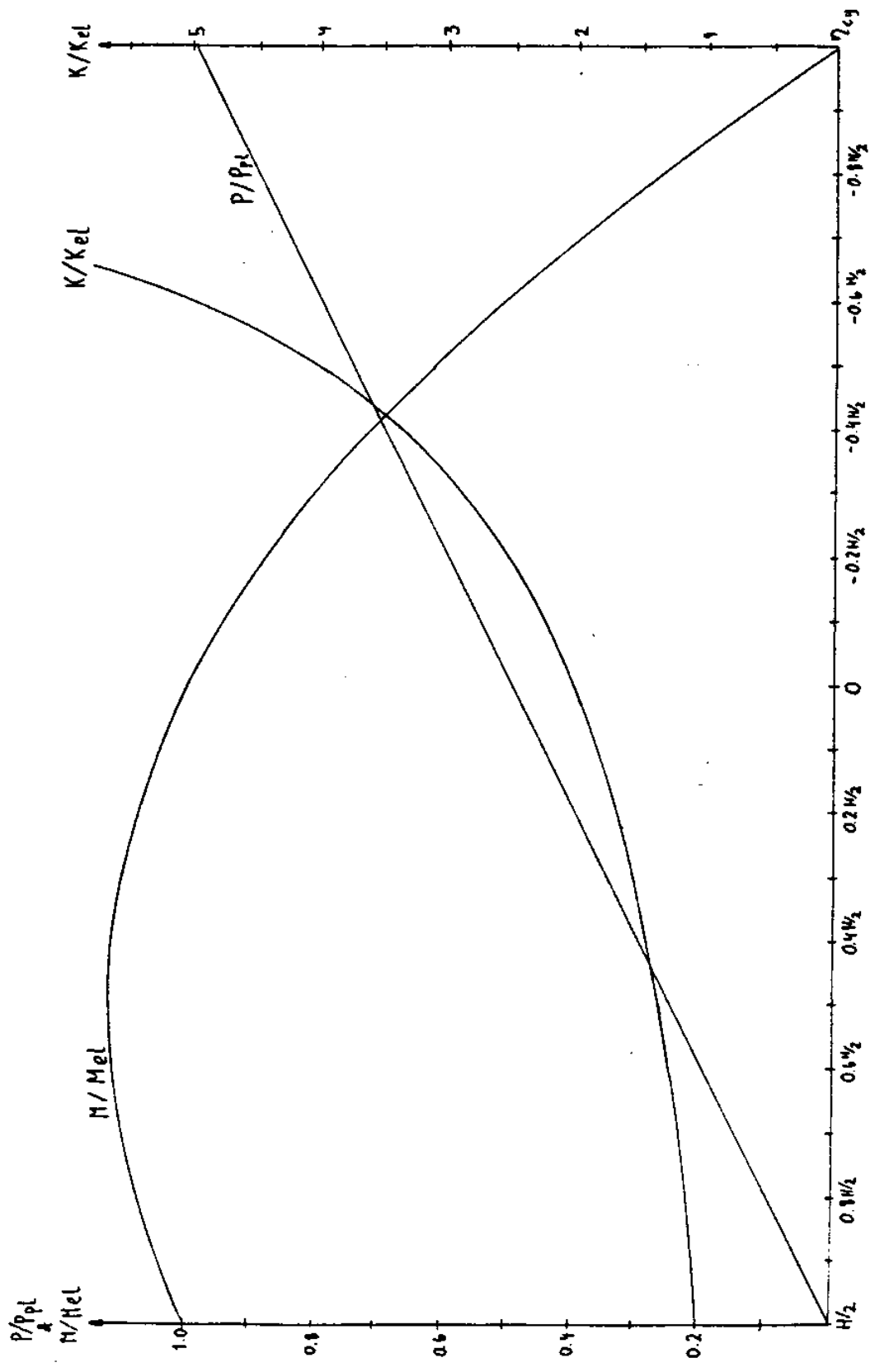
K/Kel
5
4
3
2
1
η_{cg}
K/Kel
P/Ppl
M/Mel
P/Ppl
&
M/Mel
1.0
0.8
0.6
0.4
0.2
H/2
0.1H/2
0.2H/2
0.4H/2
0.6H/2
0.8H/2
0
-0.1H/2
-0.2H/2
-0.4H/2
-0.6H/2
-0.8H/2

FIGURE 16

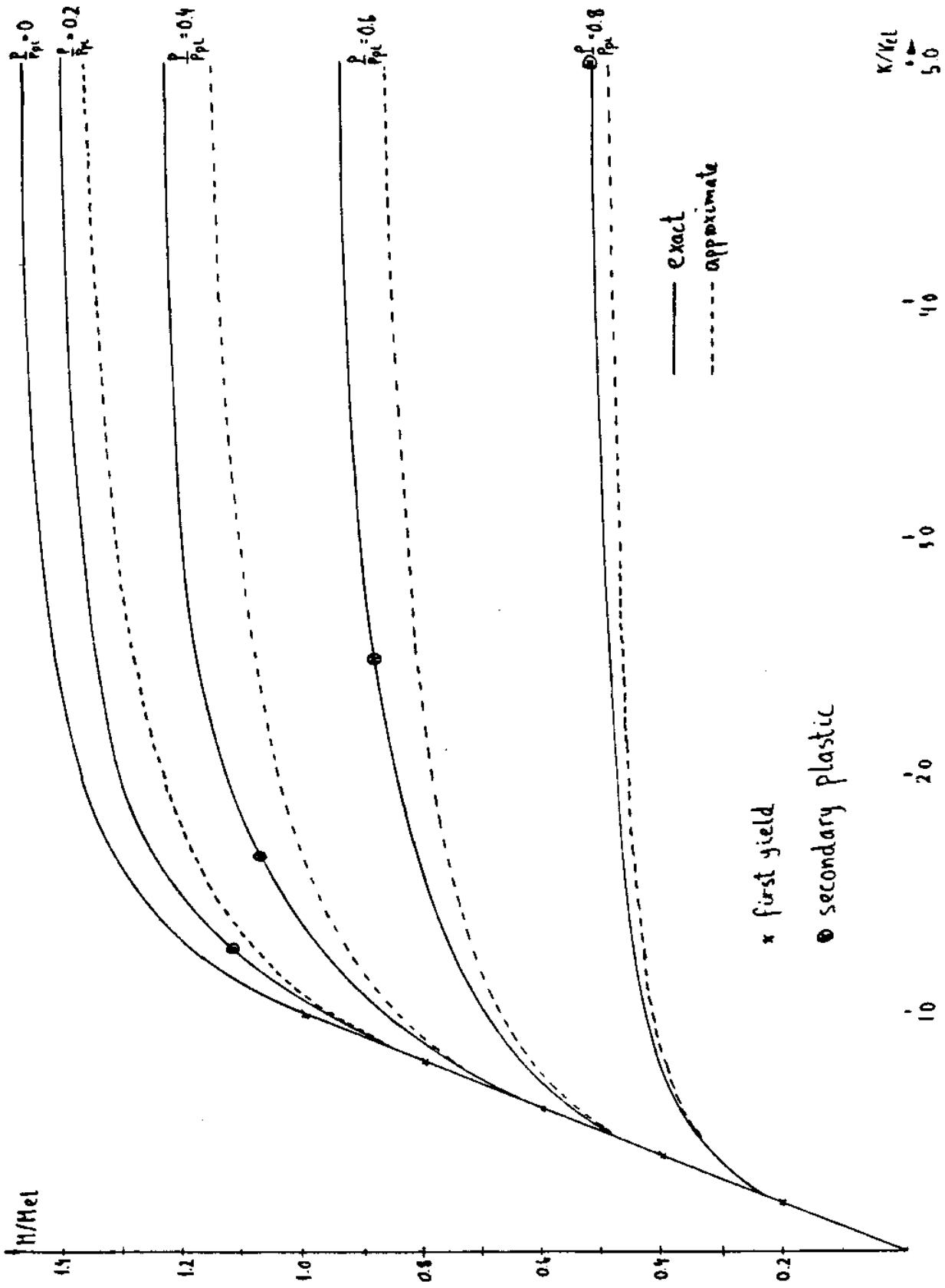
H/Hel
1.4
1.2
1.0
0.8
0.6
0.4
0.2
1/10
1/5.0
1/2.0
1/1.0
K/Kel
P/Ppl = 0
P/Ppl = 0.2
P/Ppl = 0.4
P/Ppl = 0.6
P/Ppl = 0.8
exact
approximate
× first yield
● secondary plastic

FIGURE 17

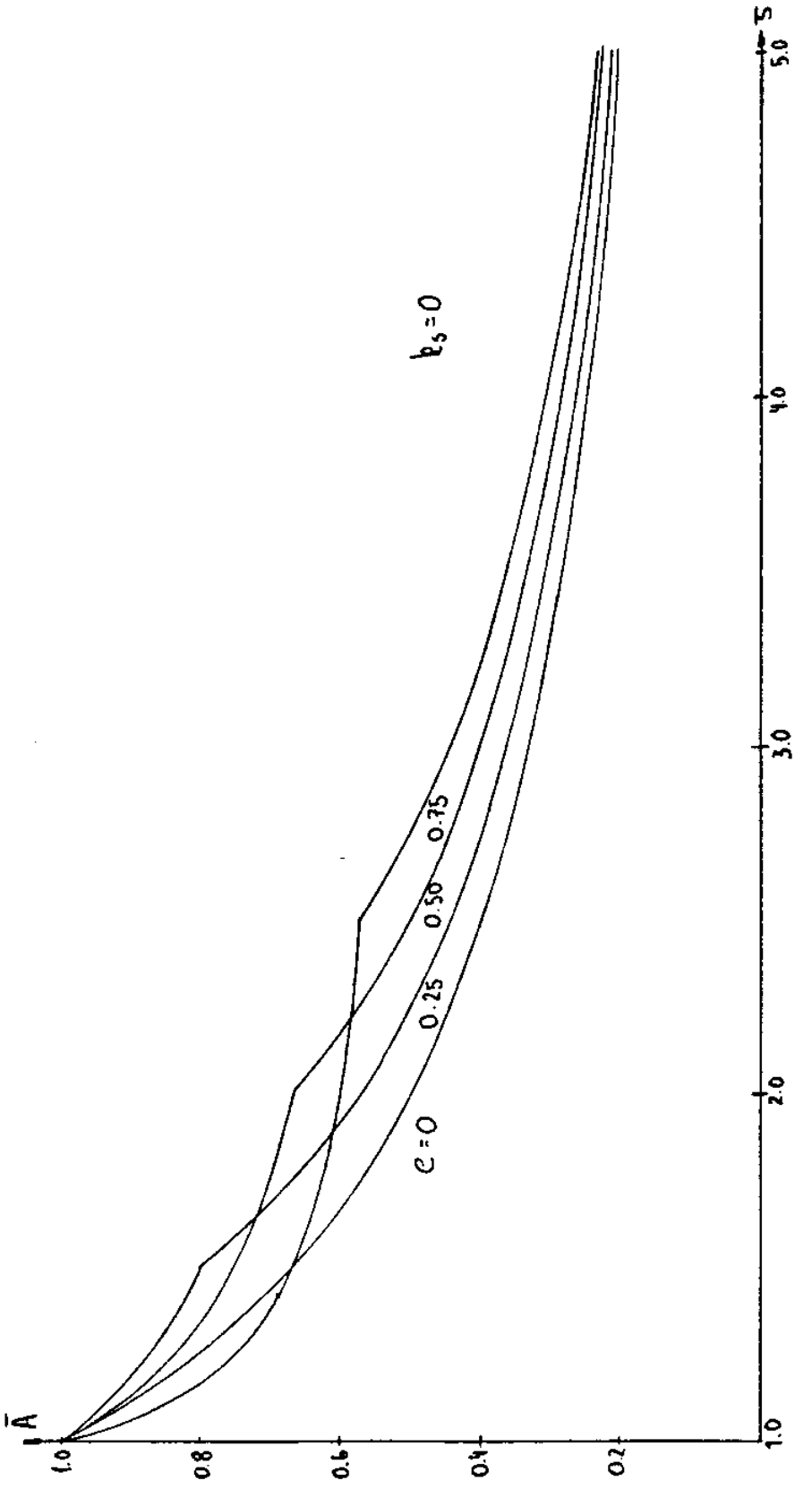

FIGURE 18

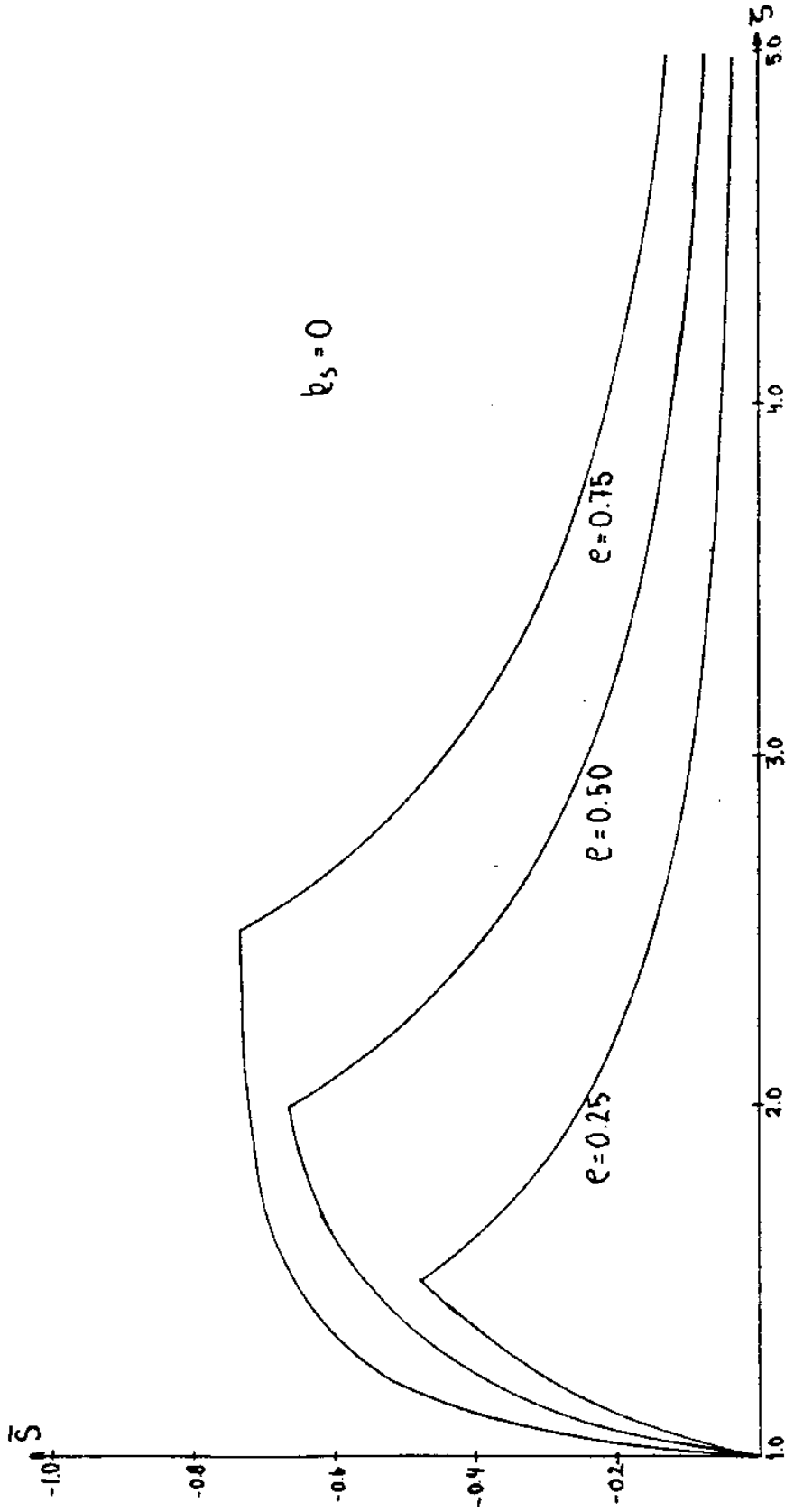

FIGURE 19

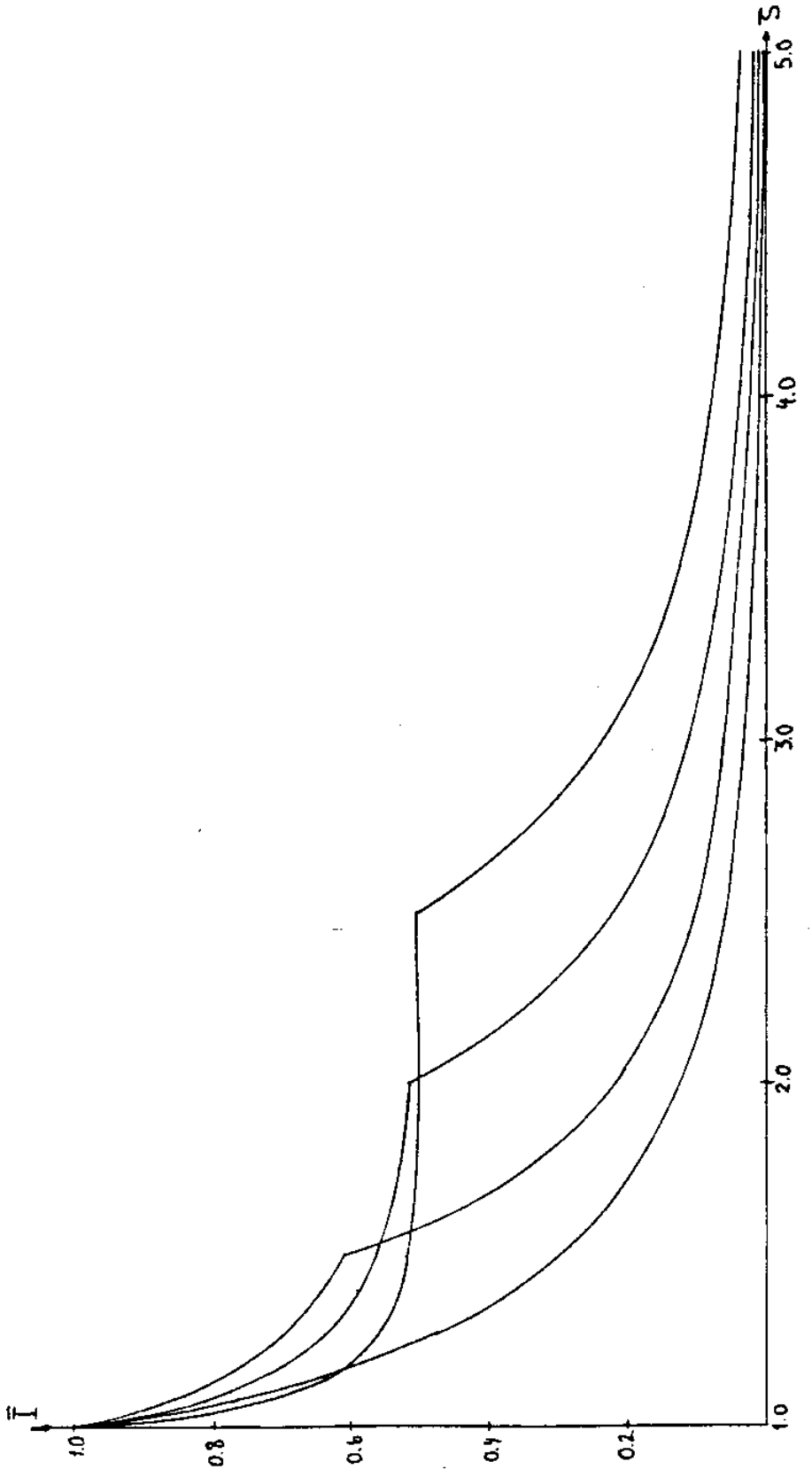

FIGURE 20

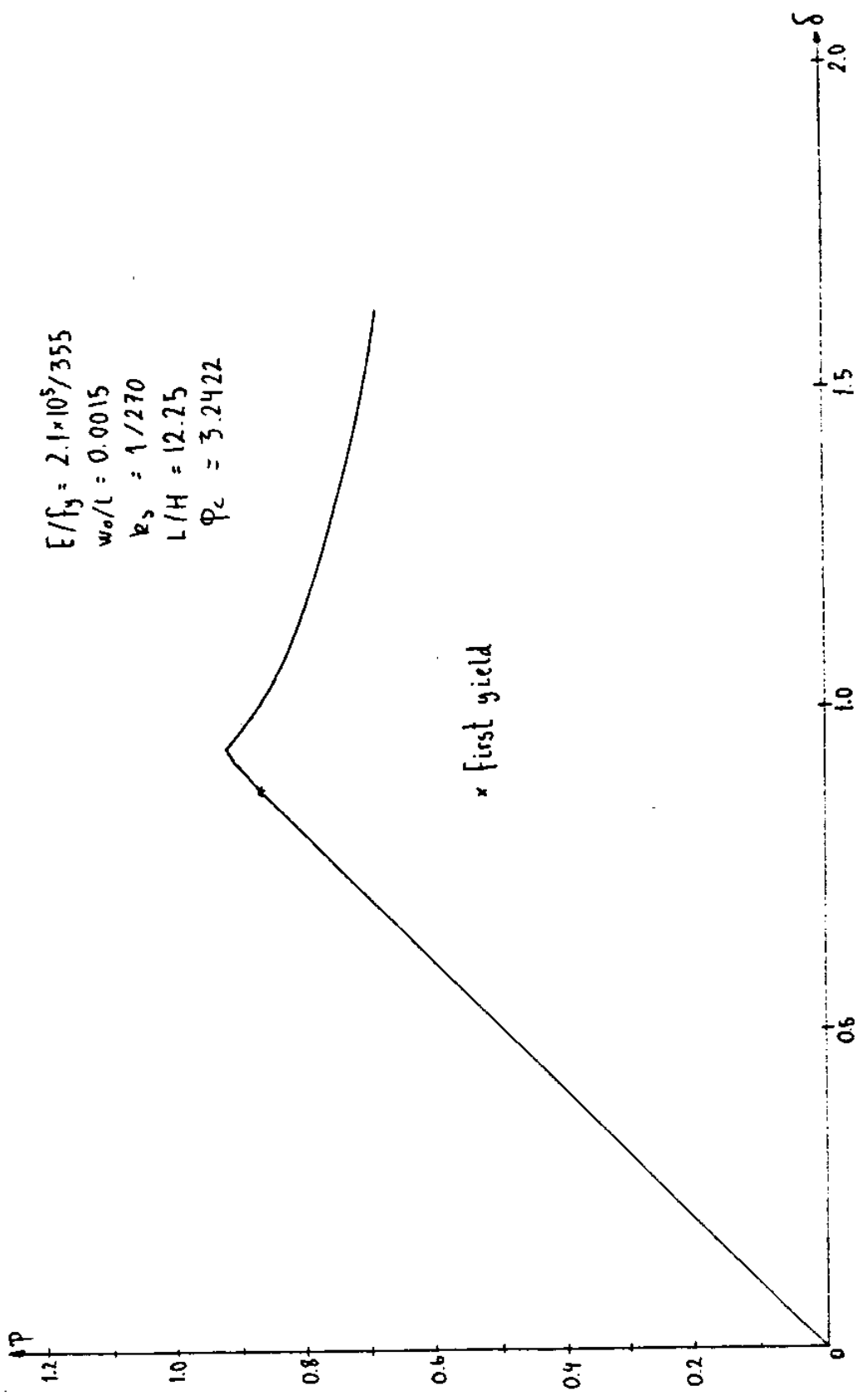
P
1.2
1.0
0.8
0.6
0.4
0.2
0
0.6
1.0
1.5
2.0
δ
E/fy = 2.1×10⁵/355
wo/L = 0.0015
εs = 1/270
L/H = 12.25
φc = 3.2422
× First yield

FIGURE 21

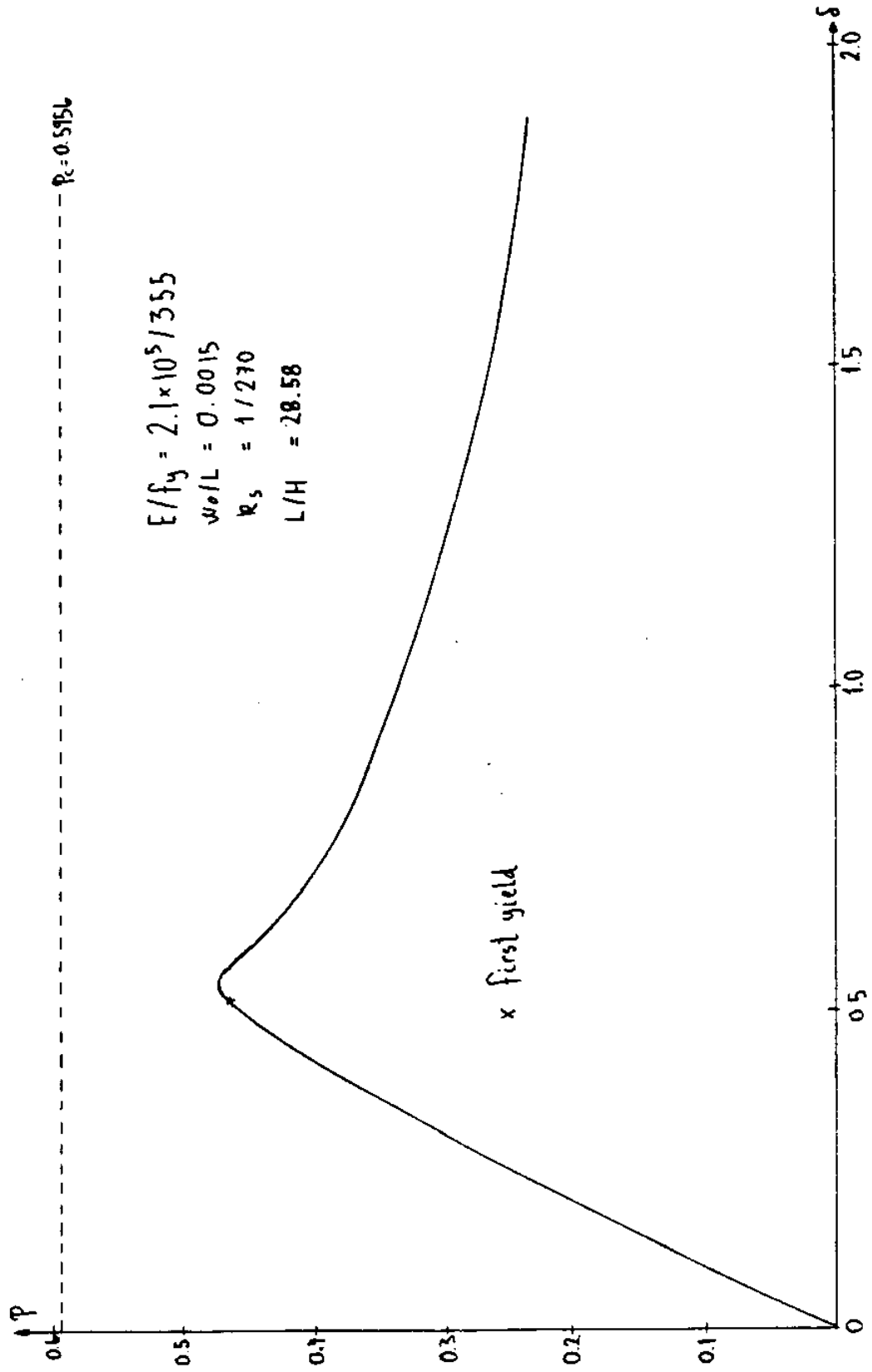
P
P_c=0.515L
$E/f_y = 2.1\times10^5/355$
w_o/L = 0.0015
R_s = 1/270
L/H = 28.58
× first yield
0.4
0.5
0.4
0.3
0.2
0.1
0
0.5
1.0
1.5
2.0
δ

FIGURE 22

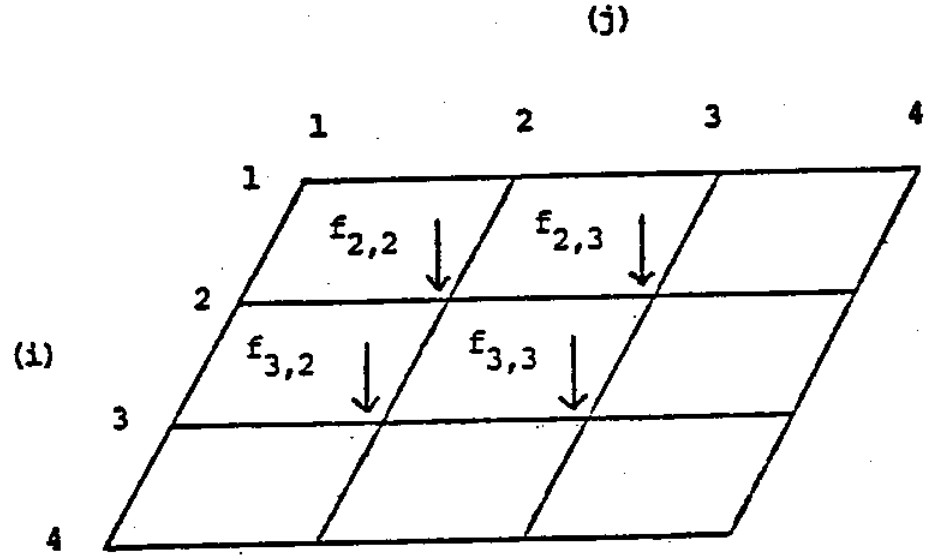

(a)

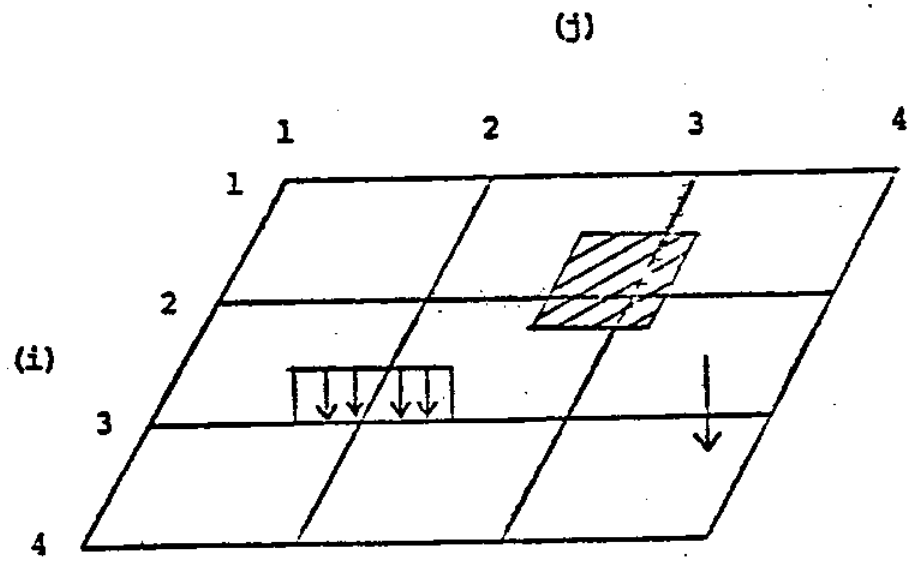

(b)

FIGURE 23

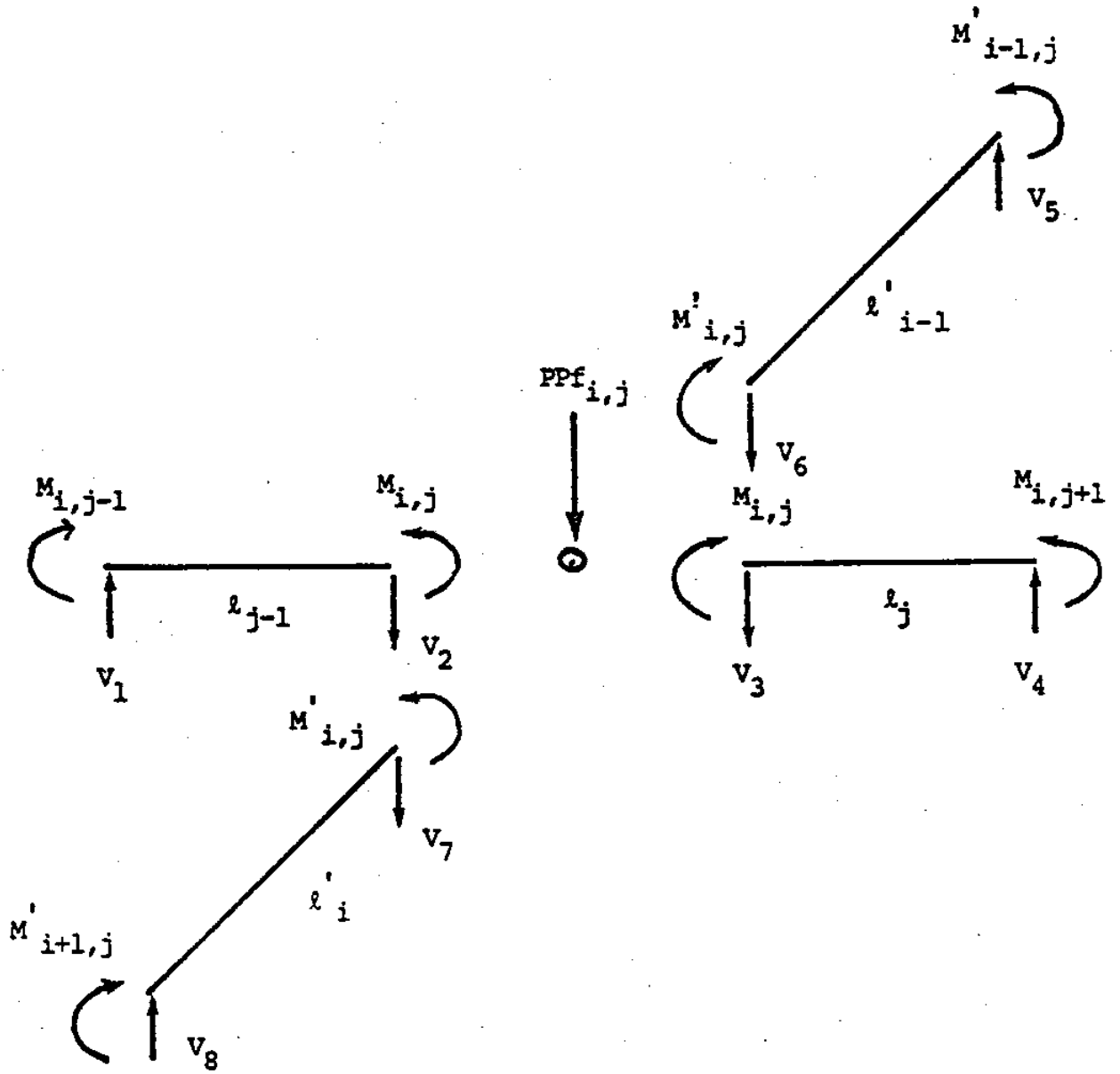
M'i-1,j
V5
M'i,j
ℓ'i-1
PPfi,j
V6
Mi,j-1
Mi,j
Mi,j
Mi,j+1
ℓj-1
ℓj
V1
V2
V3
V4
M'i,j
V7
ℓ'i
M'i+1,j
V8

FIGURE 24

600
500
400
300
200
100
0
Collapse Load
1
2
3
4
5
6
Number of Intermediate Frames
J
x
o
+
*
(*)
(+)
Y=.2
1.0
1.0
Loading distribution on a grillage having one intermediate frame and one longitudinal stringer
J - Johansson
x - 1 Longitudinal Stringer
o - 2 Longitudinal Stringers
+ - 3 Longitudinal Stringers
* - 4 Longitudinal Stringers
( ) - Non-Symmetric Collapse Mechanism
(Ice Thickness = .2 X Plate Height)

FIGURE 25

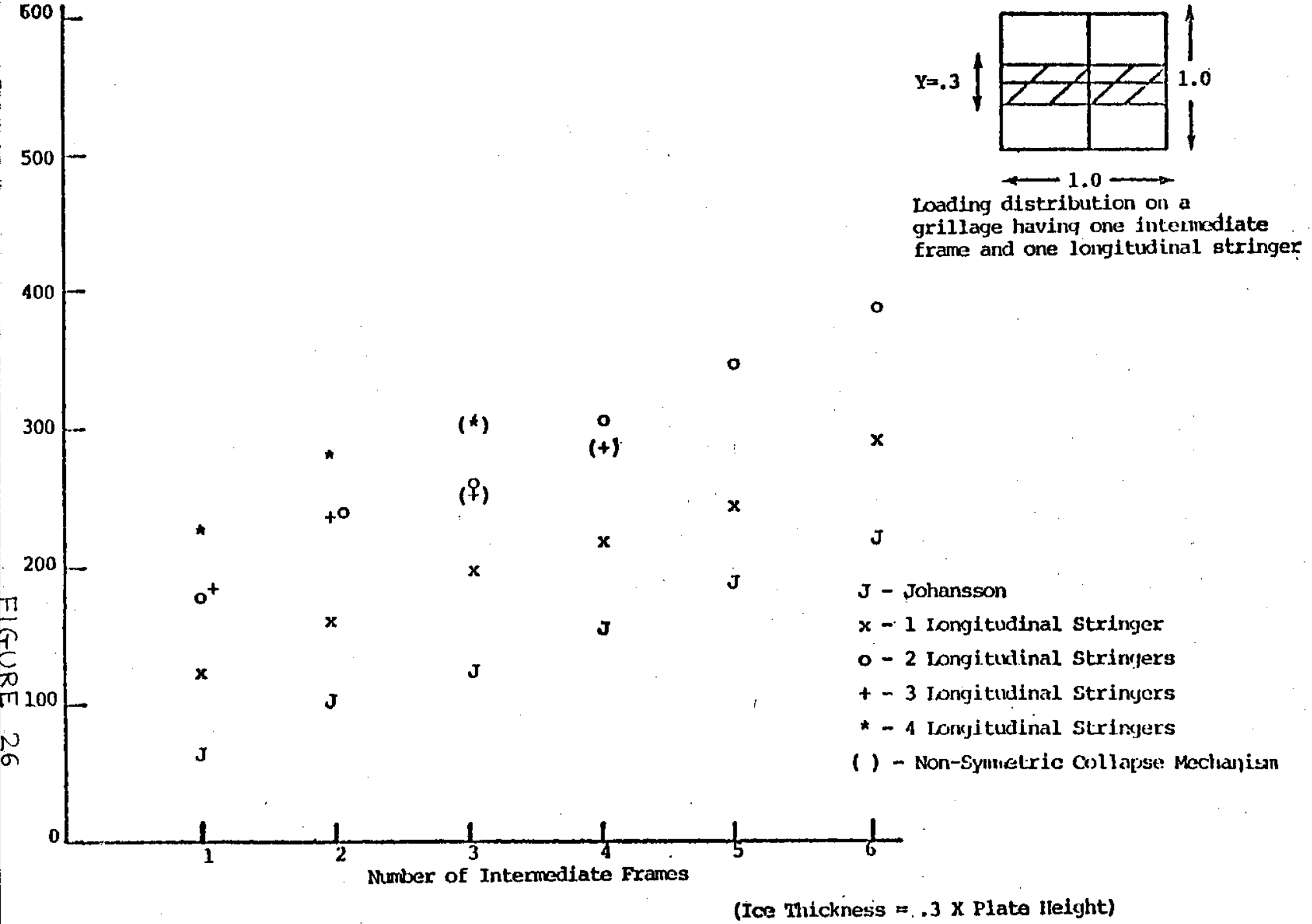
600
500
400
300
200
100
0
1
2
3
4
5
6
Number of Intermediate Frames
Y=.3
1.0
1.0
Loading distribution on a grillage having one intermediate frame and one longitudinal stringer
J - Johansson
x - 1 Longitudinal Stringer
o - 2 Longitudinal Stringers
+ - 3 Longitudinal Stringers
* - 4 Longitudinal Stringers
( ) - Non-Symmetric Collapse Mechanism
(Ice Thickness = .3 X Plate Height)

FIGURE 26

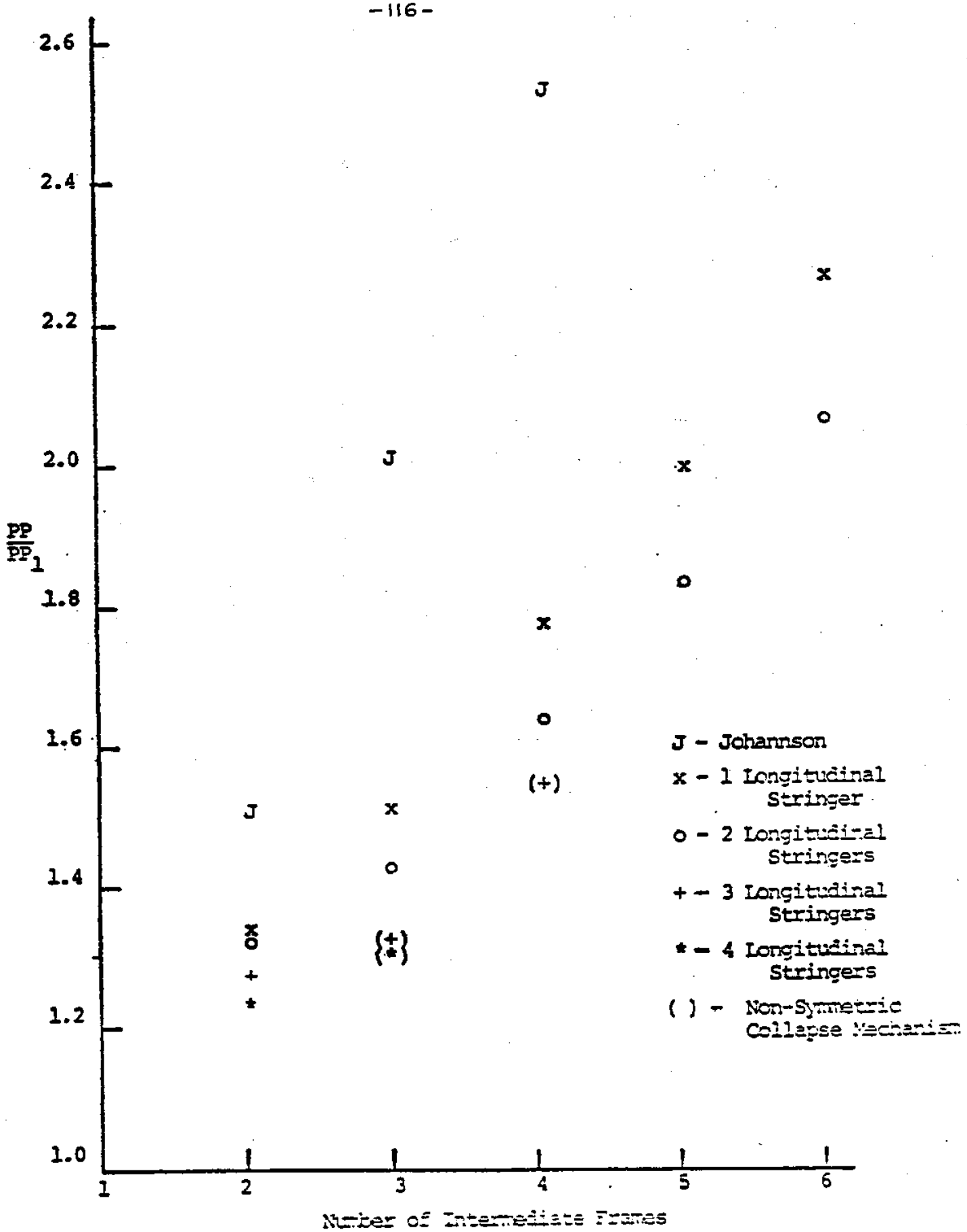
2.6
2.4
2.2
2.0
1.8
1.6
1.4
1.2
1.0
PP/PP1
1
2
3
4
5
6
Number of Intermediate Frames
J - Johannson
x - 1 Longitudinal Stringer
o - 2 Longitudinal Stringers
+ - 3 Longitudinal Stringers
* - 4 Longitudinal Stringers
( ) - Non-Symmetric Collapse Mechanism

FIGURE 27

LOCAL CONTACT PRESSURE MEASUREMENTS REF [9]

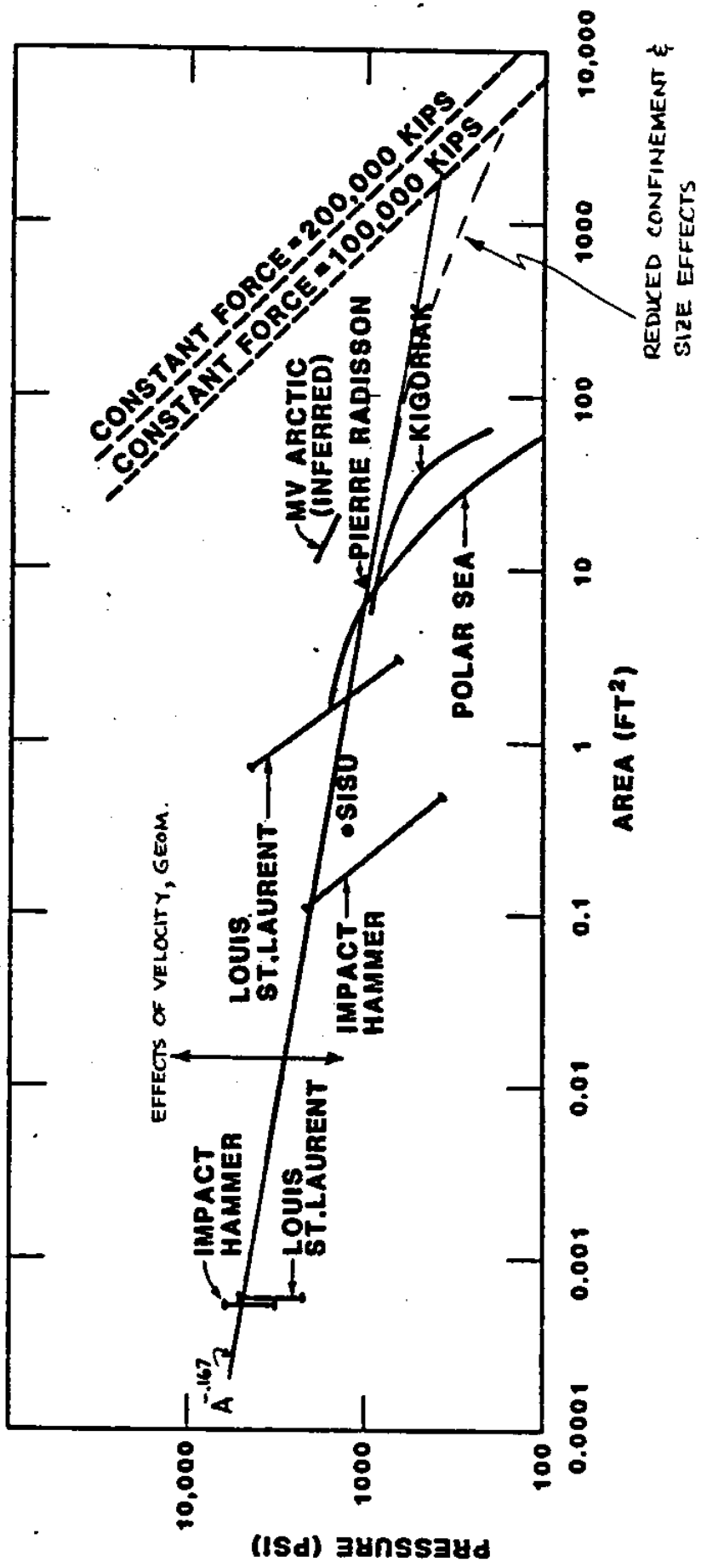

FIGURE 28

The second case is the same as the first one except for L/r which now is equal to 70. This corresponds to L/H = 28.58 for a column of rectangular cross-section. The p-δ relation for this second case with L/H = 28.58 is shown in Fig. 23 and the corresponding p-k relation shown in Fig. 24.

The third case corresponds to $W_o/L = 0.0005$, $k_s = 1/270$, $E/f_y = 638$ and L/r = 49.504. This value of L/r corresponds to L/H = 20.21 for a column of rectangular cross-section. The p-δ relation for this third case with L/H = 20.21 is shown in Fig. 25, and the corresponding p-k relation is shown in Fig. 26. The final case corresponds to the third except for the value of W_o/L which now equals 0.013. The p-δ relation for the final case is for the sake of comparison also plotted in Fig. 25, while the p-k relation is plotted in Fig. 27.

In order to evaluate the results from the Shanley model analysis it is now highly desirable to compare the results from the Shanley model with the exact solutions. The exact solution is however very time consuming to obtain. We can get around this problem by comparing the Shanley model results with the results from the approximate analysis. We can do this because we have already shown that these approximate relations are very close to the exact ones in Fig. 17. The approximate non-dimensional axial force curvature p-k relations are given by eq. (231). The resulting p-k relation corresponding to the cases analyzed by the Shanley model is plotted in Figs. 22, 24, 26, and 27 for comparison. The agreement between these two independent analysis methods is seen to be good.